ISSN 0009-3084
CPLIA 88 (1) 1–82

CPL

CHEMISTRY AND PHYSICS OF LIPIDS

VOL. 88 NO. 1 AUGUST 8th 1997

ELSEVIER

CHEMISTRY AND PHYSICS OF LIPIDS

SCOPE OF THE JOURNAL

Chemistry and Physics of Lipids publishes research papers and review articles in the field of molecular biology which emphasise chemical and physical aspects of lipids. Accordingly, the journal covers: advances in synthetic and analytical lipid methodology; chemical and physical characterisation of isolated structures; thermodynamics, phase behaviour, topology and dynamics of lipid assemblies; physicochemical studies into lipid-lipid and lipid-protein interactions in lipoproteins and in natural and model membranes; movement of lipids within, across and between membranes; intracellular lipid transfer; structure-function relationships and the nature of lipid-derived second messengers; chemical, physical and functional alterations of lipids induced by free radicals; and the role of lipids in the regulation of membrane-dependent biological processes. Reviews, full articles and short communications will be considered for publication in each issue. Special Issues will consist of invited contributions organized and edited to cover specific themes.

Publication information: *Chemistry and Physics of Lipids* 0009-3084. For 1997 volumes 86–90 are scheduled for publication. Subscription prices are available upon request from the publisher. Subscriptions are accepted on a prepaid basis only and are entered on a caldendar year basis. Issues are sent by surface mail except to the following countries where Air delivery via SAL mail is ensured: Argentina, Australia, Brazil, Canada, Hong Kong, India, Israel, Japan, Malaysia, Mexico, New Zealand, Pakistan, PR China, Singapore, South Africa, South Korea, Taiwan, Thailand, USA. For all other countries airmail rates are available upon request. Claims for missing issues should be made within six months of our publication (mailing) date.

Orders, claims and product enquiries: please contact the Customer Support Department at the Regional Sales Office nearest you:

New York
Elsevier Science
P.O. Box 945
New York, NY 10159-0945
USA
Tel. (+ 1)212-633-3730
[Toll free number for North American customers: 1-888-4ES-INFO (437-4636)]
Fax (+ 1)212-633-3680
e-mail usinfo-f@elsevier.com

Amsterdam
Elsevier Science
P.O. Box 211
1000 AE Amsterdam
The Netherlands
Tel. (+ 31)20-4853757
Fax (+ 31)20-4853432
e-mail nlinfo-f@elsevier.nl

Tokyo
Elsevier Science
9-15 Higashi-Azabu 1-chome
Minato-ku, Tokyo 106
Japan
Tel. (+ 81)3-5561-5033
Fax (+ 81)3-5561-5047
e-mail kyf04035@niftyserve.or.jp

Singapore
Elsevier Science
No. 1 Temasek Avenue
17-01 Millenia Tower
Singapore 039192
Tel. (+ 65)434-3727
Fax (+ 65)337-2230
e-mail asiainfo@elsevier.com.sg

Submission of a paper to Chemistry and Physics of Lipids is understood to imply that it is not being considered for publication elsewhere and that the author's permission to publish his/her article(s) in this journal implies the exclusive authorisation of the publisher to deal with all issues concerning copyright therein.

Submission of multi-authored manuscripts implies the consent of *each* of the authors. The publisher will assume that the senior or corresponding author has specifically obtained the approval of all other co-authors to submit the manuscript to this journal.

Periodicals postage paid at Rahway, New Jersey. Chemistry and Physics of Lipids (ISSN 0009-3084) is published monthly, except June and December, by Elsevier Science Ireland Ltd., Bay 15, Shannon Industrial Estate, Shannon, Co. Clare. The annual subscription in the USA is $1422. Chemistry and Physics of Lipids is distributed by Virgin Mailing and Distribution, 10 Camptown Road, Irvington, New Jersey 07111-1105. POSTMASTER: Please send address corrections to Chemistry and Physics of Lipids, c/o Elsevier Science Regional Sales Office, Customer Support Department, 655 Avenue of the Americas, New York, NY 10010.

CHEMISTRY AND PHYSICS OF LIPIDS

Volume 88/1 (1997)

CHEMISTRY AND PHYSICS OF LIPIDS

VOLUME 88 (1997)

ELSEVIER

Amsterdam — Lausanne — London — New York — Shannon — Tokyo

ELSEVIER

Chemistry and Physics of Lipids
88 (1997) 1–13

CPL
CHEMISTRY AND
PHYSICS OF LIPIDS

Lipid microdomains in dimyristoylphosphatidylcholine–ceramide liposomes

Juha M. Holopainen, Jukka Y.A. Lehtonen [1], Paavo K.J. Kinnunen *

Department of Medical Chemistry, Institute of Biomedicine, University of Helsinki, P.O. Box 8 (Siltavuorenpenger 10a) Helsinki, FIN-00014, Finland

Received 5 March 1997; received in revised form 6 May 1997; accepted 4 June 1997

Abstract

Binary membranes composed of dimyristoylphosphatidylcholine (DMPC) and natural ceramide (up to a mole fraction $X_{cer} = 0.25$) were investigated by measuring the excimer:monomer fluorescence emission intensity ratio I_E:I_M for the pyrene labeled phospholipid probe 1-palmitoyl-2[(pyren-1-yl)]decanoyl-*sn*-glycero-3-phosphocholine (PPDPC), by monitoring fluorescence polarization of diphenylhexatriene (DPH), as well as using differential scanning calorimetry (DSC). Increasing $X_{cer} > 0.10$ both below and above the main transition temperature T_m increased I_E:I_M for PPDPC maximally approximately 1.6-fold at $X_{cer} = 0.25$. Above T_m, and when X_{cer} approaches 0.10, fluorescence polarization P for DPH increases steeply, reflecting an overall decrease in acyl chain motions. At $X_{cer} = 0.10$ there is a discontinuity in P and upon further increase in the content of ceramide a smaller, yet significant increase in P is evident. DSC revealed ceramide to increase the pretransition temperature until at X_{cer} exceeding 0.07 this transition was no longer evident. Simultaneously, increasing X_{cer} up to 0.05 increased T_m from 23.9 to 24.6°C. Total enthalpy ΔH_m of the main transition diminished progressively upon increase in X_{cer} up to ≈ 0.10. Above this concentration of ceramide a new endotherm became evident at 22.5°C, and exceeding $X_{cer} = 0.14$ this endotherm became dominant. Our results indicate an enrichment of the pyrene labeled phospholipid analog into microdomains concomitant with the formation of a distinct ceramide-enriched phase at $X_{cer} > 0.10$. © 1997 Elsevier Science Ireland Ltd.

Keywords: Ceramide; Domain formation; Differential scanning calorimetry; Pyrene labeled lipids

Abbreviations: Cer, ceramide; DMPC, dimyristoylphosphatidylcholine; DPH, 1,6-diphenyl-1,3,5-hexatriene; I_E, excimer fluorescence intensity at 470 nm; I_M, monomer fluorescence intensity at 380 nm; LUVs, large unilamellar vesicles; MLVs, multilamellar vesicles; P, steady-state fluorescence emission polarization; PPDPC, 1-palmitoyl-2[(pyren-1-yl)]decanoyl-*sn*-glycero-3-phosphocholine; T_m, main phase transition temperature; T_p, pretransition temperature; $\Delta T_{1/2}$, main transition peak width; $\Delta T_{p1/2}$, pretransition peak width; ΔH_m, main transition enthalpy; ΔH_p, pretransition enthalpy.

* Correspondence author. Tel.: +358 9 1918237; fax: +358 9 1918276; e-mail: Paavo.Kinnunen@Helsinki.Fi

[1] Present address: Department of Medicine, Brigham and Women's Hospital, Harvard Medical School, Boston, MA, USA.

PII S0009-3084(97)00040-6

1. Introduction

Although ceramides are ubiquitous components of eukaryotic cells in abundance these lipids are found only in the stratum corneum of the skin (Schurer and Elias, 1991). This tissue consists of multiple layers of lamellar membrane sheets occupying the intercellular space between corneocytes. These lamellae are currently believed to provide the structures yielding the water impermeability of skin (Elias and Menon, 1991). The lipid composition of these sheets is unusual and consists mainly of specific skin ceramides, cholesterol, and free fatty acids (McIntosh et al., 1996). The ceramides in the membrane lamellae vary in their chain length, acyl hydroxylation, and unsaturation (Schurer and Elias, 1991). The amide group of ceramide which serves as a link between the hydrocarbon chains is of importance to the conformation of the entire molecule (Pascher, 1976). The rigid head group, which comprises six atoms in a planar conformation, adopts a perpendicular orientation with respect to the axes of the hydrocarbon chains. A conical overall shape of ceramide in both biological and membrane lipids was proposed (Pascher, 1976). The detailed structural arrangement of the stratum corneum lipids is, however, not well understood (Bouwstra et al., 1991).

In addition to the functional significance of ceramide for stratum corneum recent cell biological studies have revealed ceramide to be involved also as a second messenger in cellular signalling cascades for growth and differentiation (Hannun, 1994), induction of apoptosis (Quintans et al., 1994; Cifone et al., 1994), and causing cell damage (Quintans et al., 1994; Strum et al., 1994; Haimovitz-Friedman et al., 1994). Ceramide may also have a role in cell senescence (Jayadev et al., 1995). The molecular level mechanisms of action of ceramide in these processes are being intensively investigated. The involved enzymatic interconversions have been conceptualized as the sphingomyelin cycle (Hannun, 1994). Accordingly, in various cell lines several extracellular agents and agonists cause the activation of a neutral sphingomyelinase which results in the generation of ceramide and phosphocholine (Hannun, 1994). The addition of 1α,25-dihydroxyvitamin D3, for instance, to HL-60 human leukemia cells causes early and reversible hydrolysis of sphingomyelin and the concomitant generation of ceramide (Okazaki et al., 1989, 1994). Similar effects have been observed for tumor necrosis factor-α, γ-interferon (Kim et al., 1991; Mathias et al., 1991; Dressler et al., 1992; Okazaki et al., 1994), interleukin-1 (Ballou et al., 1992; Mathias et al., 1993), dexamethasone (Ramachandran et al., 1990), and complement components (Niculescu et al., 1993). Completion of the sphingomyelin cycle occurs with the resynthesis of sphingomyelin, presumably by the transfer of the choline phosphate headgroup from phosphatidylcholine to ceramide (Hannun, 1994). Interestingly, formation of ceramide has been shown to be compartmentalized in the cell surface and a possible role for this molecule in the formation of caveolae has been suggested (Liu and Anderson, 1995). Several recent reviews summarize these highly intriguing and important biological effects of ceramide (Ballou, 1992; Chao, 1995; Hannun, 1994, 1996; Hannun and Obeid, 1995; Michell and Wakelam, 1994; Obeid and Hannun, 1995; Saba et al., 1996; Schütze et al., 1994).

As the physicochemical effects of ceramide on lipid bilayers have remained poorly understood we undertook an investigation of the thermal phase behaviour of binary alloys of dimyristoylphosphatidylcholine and ceramide as revealed by fluorescence spectroscopy and DSC.

2. Experimental procedures

2.1. Materials

Hepes, EDTA, and DMPC were from Sigma and ceramide (According to the manufacturer approximately 46.8% of the total fatty acids of this lipid were hydroxy fatty acids, the fatty acid composition was specified as follows: C16:0 (0.3%), C18:0 (4%), C18:0 (2-OH) (15.4%), C20:0 (0.7%), C20:0 (2-OH) (0.7%), C22:0 (4.1%), C22:0 (2-OH) (6%), C23:0 (2.3%), C23:0 (2-OH) (4.5%), C24:0 (10.4%), C24:0 (2-OH)) (17.1%), C24:1 (15.3%), C25:0(8.5%), C25:0 (2-OH) (3.1%), C25:1 (1.2%, C26:0 (1.7%), C26:1 (1.2%), C27:0 (2%), C27:1 (2%)) from Matreya, (Pleasant Gap, PA). PPDPC was from K&V Bioware (Espoo, Finland), and DPH from EGA Chemie (Steinheim, Germany).

The purity of the above lipids was checked by thin-layer chromatography on silicic acid coated plates (Merck, Darmstadt, Germany) using chloroform–methanol–water (65:25:4 v/v/v) for the phospholipid and 1,2-dichloroethane–methanol–water (90:20:0.5 v/v/v) solvent system for ceramide. Examination of the plates after iodine staining or, when appropriate by fluorescence illumination revealed no impurities. The concentrations of PPDPC and DPH were determined spectrophotometrically using 42 000 cm^{-1} at 342 nm and 91 000 cm^{-1} at 354 nm as the respective molar extinction coefficients. Phospholipid concentrations were determined by the phosphorus assay (Bartlett, 1959) and those of ceramide gravimetrically. The concentration for ceramide was determined using an average molecular weight of 565.

2.2. Liposome preparation

Multilamellar vesicles (MLVs) were prepared by first mixing appropriate amounts of lipid stock solutions in chloroform to obtain the desired compositions.The resulting mixtures were then evaporated to dryness under a stream of nitrogen and any traces of solvent subsequently removed by evaporation under reduced pressure for 2 h. The dry residue was stored at $-20°C$ until it was used. The samples were hydrated at 50°C in 5 mM Hepes and 0.1 mM EDTA, pH = 7.4. To obtain unilamellar vesicles (LUVs) multilamellar vesicles were first made as above. These were first maintained at 50°C for 30 min and thereafter sonicated for 2 min in a bath type ultrasonicator (NEY Ultrasonik 104H, Yucaipa, CA). These dispersions (at a lipid concentration of 0.750 mM) were extruded through a stack of two Millipore (Bedford, MA) 0.1 μm pore size polycarbonate filters using a Liposofast low pressure homogenizer (Avestin, Ottawa, Canada) essentially as described (Olson et al., 1979; MacDonald et al., 1991).

2.3. Fluorescence measurements

A monomeric excited state pyrene may relax to ground state by emitting photons with a maximum wavelength of $\approx$ 380 nm (I_M), the exact peak energy and spectral fine structure depending on the solvent polarity. During its lifetime, the excited state pyrene may also form a characteristic short-lived complex, excimer (excited dimer) with a ground state pyrene. This complex relaxes back to two ground state pyrenes by emitting quanta as a broad and featureless band centered at $\approx$ 480 nm (I_E). In the absence of possible quantum mechanical effects (Kinnunen et al., 1987) and the formation of superlattices the excimer to monomer fluorescence intensity ratio (I_E:I_M) depends on the rate of collision between pyrenes (Förster, 1969). Consequently, for a pyrene containing phospholipid analog such as PPDPC the value for I_E:I_M reflects the lateral mobility (Galla and Sackmann, 1974; Galla et al., 1979) as well as the local concentration of the fluorophore in the membrane (Galla and Hartmann, 1980; Somerharju et al., 1985; Hresko et al., 1986; Eklund et al., 1988). Two recent reviews describing the use of pyrene-labeled lipids in research on the properties of biomembranes and membrane models are available (Kinnunen et al., 1993; Duportail and Lianos, 1996).

Fluorescence emission spectra were recorded with a Perkin-Elmer LS50B spectrofluorometer equipped with a magnetically stirred, thermostated cuvette compartment. Excitation wavelength was 344 nm and the excitation and emission bandwidths were 4 nm. 2 ml Of liposome solution (60 nmol of lipid) in a four-window quartz cuvette was used in each measurement.

2.4. Fluorescence polarization of DPH

DPH was included in liposomes to yield a lipid:DPH molar ratio of approximately 1000:1 (Lakowicz et al., 1979a,b; Prendergast et al., 1981). Polarized emission was measured with SLM 4800S spectrofluorometer in T-format using Glan-Thompson calcite prisms. Excitation at 360 nm and emission at 450 nm were selected with monochromators, with respective bandwidths of 1 and 16 nm. Emission was also monitored with a long pass filter (430–455 nm). Values of steady state fluorescence polarization P were calculated by the following equation (Lakowicz, 1983):

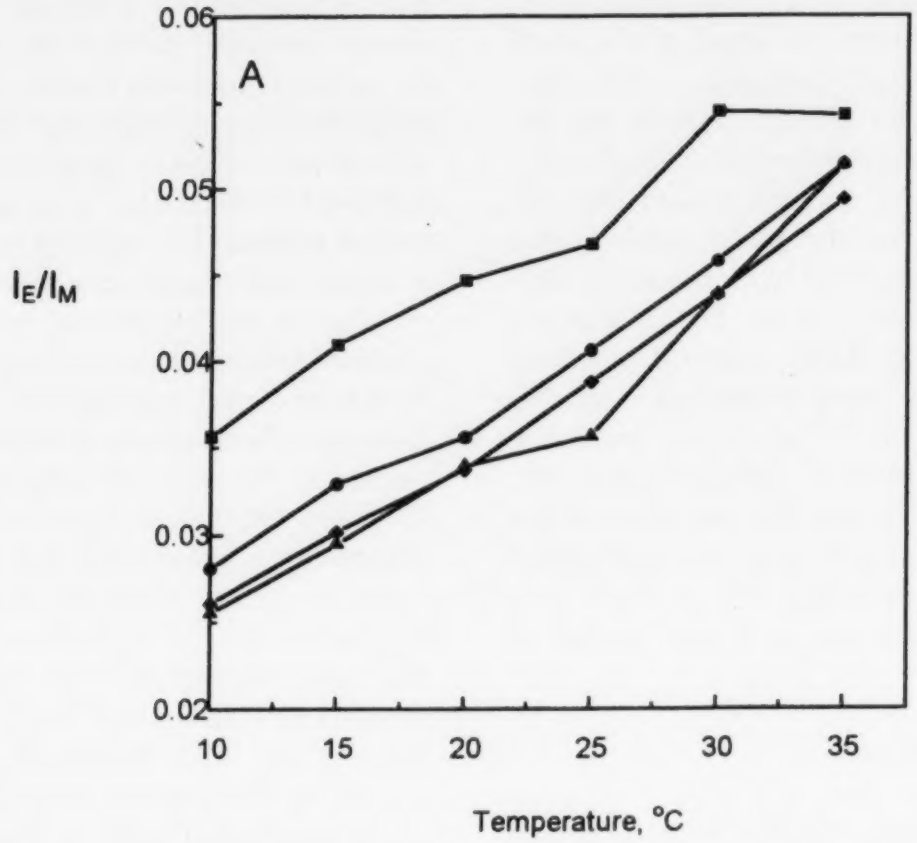

Fig. 1. I_E:I_M for PPDPC ($X = 0.01$) in LUVs and at increasing temperatures is illustrated for X_{cer} of 0 (▲), 0.05 (◆), 0.10 (●), and 0.20 (■) (panel A). I_E:I_M for PPDPC residing in LUVs composed of DMPC with increasing X_{cer} and at 20 (▲) and 30 (■) °C is depicted in panel B. The error measured was typically < 5% and for the sake of clarity is not shown.

$$P = \frac{I_{\parallel} - I_{\perp}}{I_{\parallel} + I_{\perp}}$$

2.5. Differential scanning calorimetry (DSC)

Heat capacity scans for MLVs were recorded using a high-sensitivity adiabatic differential scanning calorimeter DASM-4 (Biopribor, Pushchino, Russia) at a heating rate of 0.5°C/min. The instrument was calibrated using the internal electric power signal as a reference. Prior to DSC samples were maintained on ice for ~24 h and were thereafter loaded into precooled calorimeter cuvettes. The instrument output is recorded via an analog/digital converter board (EZ-01, Data Translation, Marlboro, MA) into a 486-computer. Transition enthalpies were determined using routines of the Origin software (Microcal Software, Northampton, MA).

3. Results

3.1. Intermolecular I_e:I_m as a function of X_{cer}

For fluorescent probes such as PPDPC containing a single pyrene moiety I_E:I_M depends on the rate of intermolecular collisions between pyrene moieties. Accordingly, this parameter can be used to observe phase separation and changes in the dynamics of bilayers upon phospholipid phase transition for instance (Kinnunen et al., 1993; Duportail and Lianos, 1996). Unlike dipalmitoylphosphatidylcholine (Somerharju et al., 1985) no lateral segregation for osmotically non-stressed vesicles of PPDPC in DMPC was observed below T_m (Lehtonen and Kinnunen, 1995). Lack of separation of PPDPC is evident also in the temperature scans for I_E:I_M shown in Fig. 1A. In brief, at this resolution our data reveal no discontinuities, thus indicating lack of major temperature-dependent changes in the dynamics of the probe. These data are also depicted as I_E:I_M versus X_{cer} (Fig. 1B). Above T_m at 30°C increasing X_{cer} up to 0.075 had little effect on I_E:I_M. Yet, increasing X_{cer} further caused I_E:I_M to increase, and at $X_{cer} = 0.25$ approximately 1.6-fold higher values were recorded compared to control bilayers lacking ceramide. Essentially similar behaviour was evident also below T_m at 20°C. In addition, similar behaviour for PPDPC was also observed when substituting the unsaturated lipid 1-palmitoyl-2-oleoyl-phosphatidylcholine for DMPC (data not shown).

3.2. DPH polarization as a function of X_{cer}

The augmented I_E:I_M for PPDPC described above could result from two mutually nonexclusive mechanisms, lateral enrichment of the probe into microdomains or increase in the rate of its lateral diffusion. To resolve between these two possibilities and to obtain further insight into the effects of ceramide on membrane properties we measured fluorescence polarization P for DPH as a function of X_{cer} (Fig. 2).

Below T_m the chain motions of DMPC are hindered compared to the liquid crystalline state and the values for P are high, in keeping with a high order prevailing in the membrane. Upon raising the temperature above T_m the lipids undergo a phase transition into the liquid crystalline

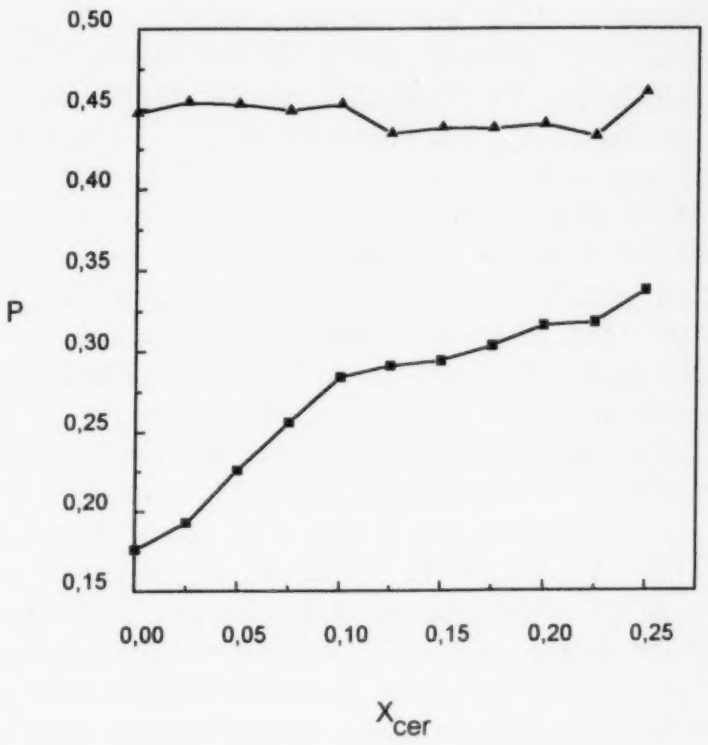

Fig. 2. P for DPH ($X = 0.0013$) residing in DMPC–ceramide binary LUV alloys shown as a function of X_{cer} and measured at 20 (▲) and 30 (■) °C. Typical error measured was < 5% and for the sake of clarity is not depicted.

state with a sharp decrement in P (Silvius, 1982). Below T_m increasing X_{cer} up to 0.10 had little effect on P. However, upon exceeding this content of ceramide in LUVs caused a small, yet clearly distinguishable, decrease in P. Above T_m and upon increasing X_{cer} from zero to 0.25 there was an increase in P from 0.18 to 0.34, indicating increased microviscosity and/or augmented acyl chain order (Jähnig, 1979). Interestingly, the increase in P occurred in two stages. First increment is evident upon increasing X_{cer} from 0 to 0.10. Thereafter, increasing X_{cer} further, from 0.1 to 0.23 causes a significant, yet smaller additional increase in P.

3.3. DSC

In order to obtain further information on the changes in the membrane underlying the above alteration in the signals from the two fluorescent probes we used DSC to characterize the thermal phase behaviour of the binary ceramide–DMPC alloys. The thermal transitions of the latter lipid have been extensively studied. In brief, neat DMPC exhibits two transitions, pretransition at approx. 8–16°C and the main transition at approx. 24°C (Silvius, 1982). Representative DSC endotherms for DMPC–ceramide MLVs as a function of X_{cer} are illustrated in Fig. 3A and B. Increasing X_{cer} from 0 to 0.07 caused the pretransition temperature T_p to increase from 16.0 to 18.5°C (Fig. 4A). Concomitantly, the pretransition enthalpy ΔH_p decreased approximately linearly (Fig. 4B) with simultaneous broadening of the peak (Fig. 4C). At X^3_{cer} 0.08 pretransition could no longer be resolved with certainty.

For the main transition there was first at low contents of ceramide ($X_{cer} \leq 0.05$) an increase in T_m from 23.9 to 24.6°C (Fig. 4D). In the range of $0.05 < X_{cer} < 0.14$ the value for T_m remained at ~ 24.6°C whereafter upon X_{cer} approaching 0.2 a sharp decrease of ~ 2°C is seen. Simultaneously, the temperature width at half-maximum ($\Delta T_{1/2}$) increased and the transition peak became slightly asymmetric (Fig. 4F). At $X_{cer} = 0.10$ a new endotherm emerged at $\sim 2°$ below T_m (Fig. 3B). This peak increased in enthalpy as X_{cer} increased and became the dominant peak at $X_{cer} = 0.16$

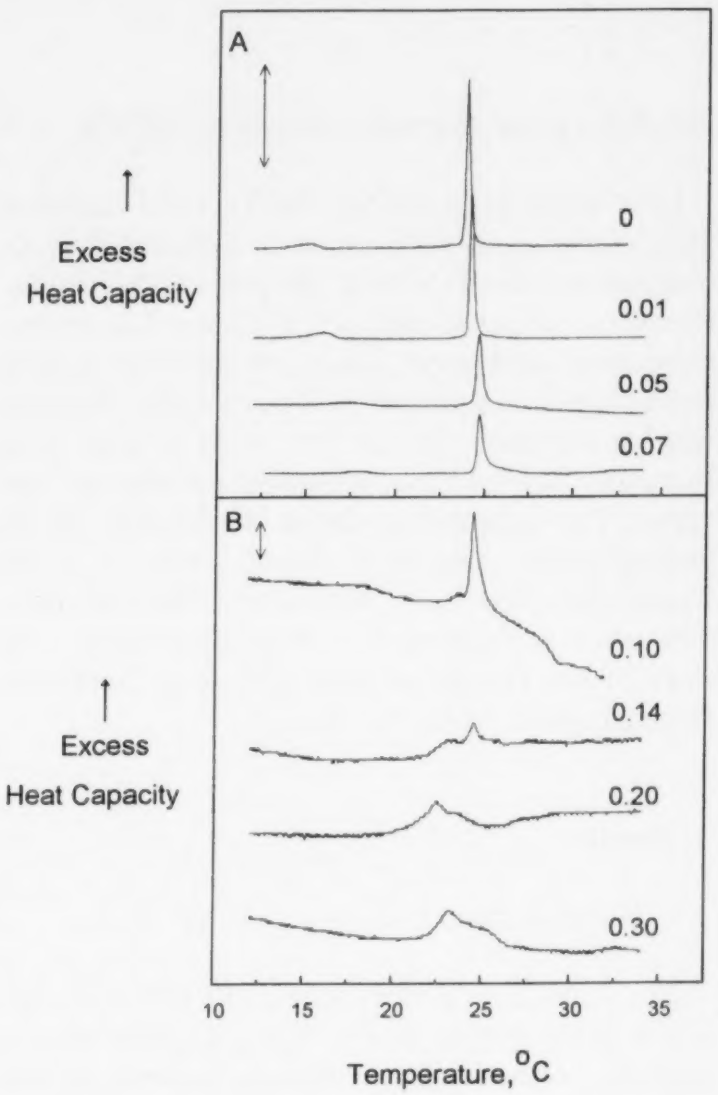

Fig. 3. DSC traces for DMPC MLVs with increasing contents of ceramide. In panel A, from top to bottom, X_{Cer} was 0, 0.01, 0.05, and 0.07; panel B, 0.10, 0.14, 0.20, and 0.30. The calibration bars in these panels correspond to 0.5 and 0.05 kJ/mol/°C, respectively. Total concentration of the lipids was 0.68 mM in 5 mM Hepes, 0.1 mM EDTA buffer, pH 7.4.

(Fig. 4D). At $X_{cer} > 0.2$ two endotherms were evident at ~ 22.5°C and at ~ 23.6°C, possibly indicating the presence of two phases, one likely being enriched in DMPC and the other in ceramide. Increasing contents of ceramide further in DMPC MLVs induce a progressive decrease in the enthalpy of the main transition peak, Fig. 4E. As X_{cer} is increased to 0.3 the enthalpy of the lower temperature endotherm increased further but no new endothems were detected at higher temperatures. Due to extensive aggregation MLVs with higher contents of ceramide ($X_{cer} > 0.30$) could not be investigated. Studies on physical

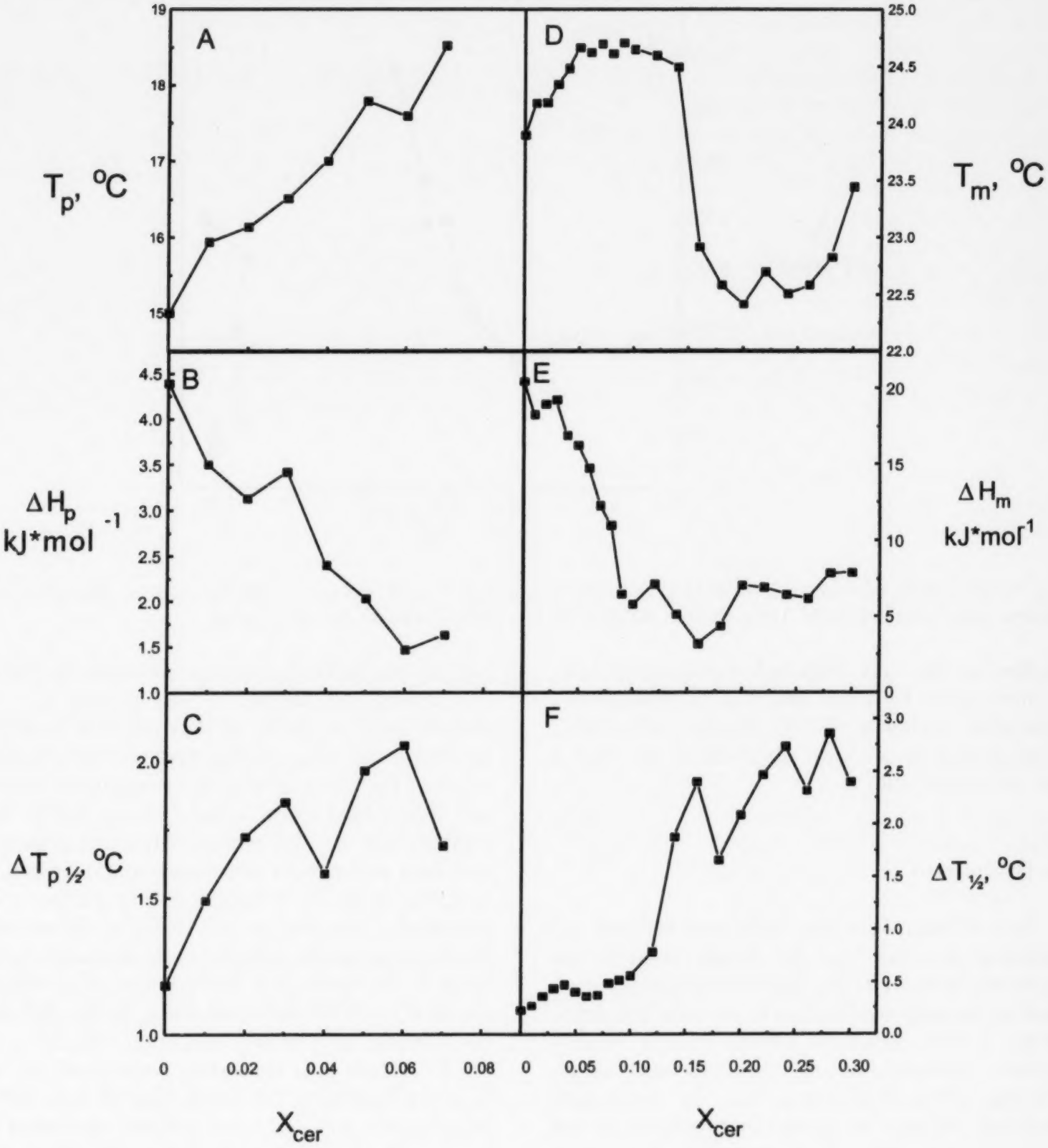

Fig. 4. Pretransition temperature T_p, enthalpy, and peak width (panels A, B and C), as a function of X_{cer} in binary MLVs with DMPC. Corresponding data for the main transition are compiled in the panels on the right depicting T_m, enthalpy, and peak width (panels D, E and F).

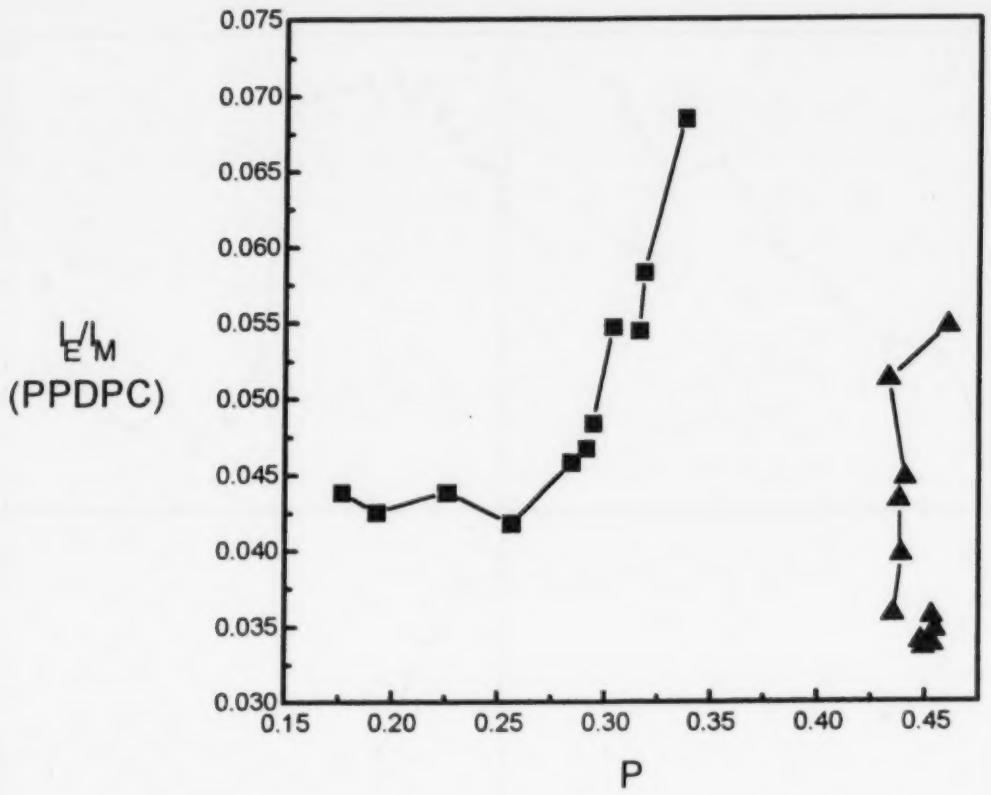

Fig. 5. Relationship between I_E:I_M for PPDPC and DPH polarization P at 20 (▲) and 30 (■) °C. Data are taken from the measurements illustrated in Fig. 1BFig. 2. For both data sets X_{cer} increases with an increase in I_E:I_M.

properties for fully hydrated non-hydroxy fatty acid-ceramide have revealed that an endothermic transition occurs at 72.7°C (Shah et al., 1995). This endotherm was not observed in our studies on the binary alloys.

4. Discussion

Free volume V_f is the difference between the effective and the van der Waals volumes per molecule. For a phospholipid membrane V_f arises due to thermal motion as well as from the short-lived, mobile structural defects due to *trans*→*gauche* isomerization of the lipid acyl chains (Xiang, 1993). Our recent data on osmotically induced changes in LUVs lend support to the concept of membrane free volume determining the rate of lipid lateral diffusion as reflected in the intermolecular I_E:I_M for PPDPC (Lehtonen and Kinnunen, 1994). Fluorescence polarization relates to the average angular displacement of the fluorophore which occurs between the absorption and subsequent emission of a photon and thus depends on the rate and extent of rotational diffusion during the lifetime of the excited state of probes such as DPH (Lakowicz, 1983). DPH molecules lie deep in the lipid bilayer, mostly oriented parallel to the lipid hydrocarbon chains and detect lipid chain order (Jähnig, 1979). Yet caution must be used when interpreting polarization data as the exact orientation and distribution of DPH in the lipid bilayer is not known with precision (Lakowicz et al., 1979a,b). Membrane free volume can be expected to be inversely correlated to P. Increasing the content of ceramide above $X_{cer} \rightarrow 0.07$ enhanced the I_E:I_M for PPDPC both below and above the main transition of DMPC. These data are further emphasized in Fig. 5. which illustrates the correlation between DPH polarization and I_E:I_M for PPDPC measured at varying X_{cer} both below and above T_m. Below T_m when $X_{cer} > 0.125$ polarization P decreases slightly indicating a decrement in lateral ordering. Concomitantly, a rapid increase in I_E:I_M is seen. Increasing X_{cer} above T_m causes an increase in P. This could be due to headgroup interactions between ceramide and DMPC or restriction of acyl

chain movement which would restrain the motion of DPH molecules. With increasing P the rate of lateral diffusion should decrease, which in turn should result in a decrease in I_E:I_M. In contrast, the opposite is observed. Accordingly, lateral enrichment of PPDPC into microdomains must take place when $X_{cer} > 0.10$ at 30°C.

Studies on the phase behaviour and phase transition of lipids in different model systems have provided a wealth of data on the physical properties of various types of membrane alloys and these complex temperature-dependent phenomena are now known to involve both the hydrocarbon phase and the interfacial water (Kinnunen and Laggner, 1991). DSC has been widely utilized to observe phase transitions and in combination with other techniques it allows to establish structural properties and phase preference of bilayers and their perturbation by molecules of interest (Mabrey-Gaud, 1981; McElhaney, 1982). Of the model compounds utilized one of the best characterized is DMPC. Below T_m the two homologous saturated acyl chains of this type of phospholipid are mostly in an all-*trans* configuration and the bilayer is in a well-ordered gel state. Upon increasing temperature a lamellar-to-undulated-lamellar phase transition, pretransition is observed. This endotherm reflects rotational transitions of the hydrocarbon chains and headgroups as well as enhanced lipid hydration (Cevc and Marsh, 1987). Further increase in temperature causes the subsequent main phase transition at T_m during which *trans-gauche* rotational isomerization of the chains is augmented, thus resulting in lateral expansion and decrease in bilayer thickness (Mabrey-Gaud, 1981). T_m depends on fatty acid chain lengths, degree of unsaturation, chain branching, structure of the polar headgroup, as well as on water activity.

Inclusion of ceramide into DMPC strongly influences the phase behaviour of the latter as revealed by DSC. In brief, incorporation of ceramide (up to $X_{cer} = 0.07$) into DMPC LUVs progressively decreases the pretransition enthalpy while T_p increases. Simultaneously, T_m increases by ~ 0.7°C while the main transition enthalphy decreases and peak width increases. Thereafter, increasing X_{cer} further up to 0.16 decreases both ΔH_m and T_m. Unfortunately, our attempts to obtain liposomes at $X_{cer} > 0.30$ were not successful. Accordingly, a complete phase diagram could not be constructed, thus impeding interpretation of the DSC data.

Comparison of the above effects of ceramide to those exerted by sphingosine is of interest. Kõiv et al. (1993) showed increasing concentrations of sphingosine in DMPC liposomes to increase T_p, similarly to ceramide. However, for increasing concentrations of sphingosine T_m also increases, in contrast to what is seen when X_{cer} exceeds 0.16. The effects of sphingosine were discussed in terms of electrostatic interactions and hydrogen bonding with PCs and may additionally involve changes in hydration (Kõiv et al., 1993; Lopez-Garcia et al., 1994). Tight packing of ceramides could further be promoted by hydrogen bonding between the head groups of this lipid.

Hydrophobic mismatch was first introduced on a theoretical basis to provide a mechanism for integral proteins to attract lipids of appropriate chain length (Mouritsen and Bloom, 1984). This mechanism is supported by recent experimental evidence (Lehtonen and Kinnunen, 1997). Likewise, there is evidence for hydrophobic mismatch being important in lipid–lipid interactions (McMullen et al., 1993; McMullen and McElhaney, 1995; Lehtonen et al., 1996). For lipid bilayers with large differences in the hydrophobic thickness of their constituents non-random lateral organization has been demonstrated (Lehtonen et al., 1996). The average chain length of the natural ceramide greatly exceeds that in DMPC. It is plausible to consider the possibility that due to its considerably longer hydrocarbon chain lengths ceramide in binary alloys with DMPC would also be driven into microdomains, the driving force being due to a hydrophobic matching condition. Chain–chain interactions in ceramide-enriched microdomains can readily be expected to be perturbed by the bulky pyrene moiety of PPDPC. As a consequence the latter lipid should be expelled from the former more tightly packed domains, analogously to what is observed in PPDPC–dipalmitoylphosphatidylcholine alloys below the T_m (Somerharju et al., 1985). Likewise, removal of water from the hydration shell of DMPC diminishes the effective size of the headgroup, thus enhancing lipid packing and causing PPDPC to

be expelled into the microdomains (Lehtonen and Kinnunen, 1995).

Long chain length alcohols and monocarboxylic acids have been shown to increase the T_m for DPPC (Eliasz et al., 1976). Incorporating the high melting ceramide with long chains into DMPC bilayers should increase T_m as observed when $X_{cer} < 0.05$. Simultaneously, increased anisotropy of DPH due to increase in X_{cer} should be evident, as illustrated in Fig. 2.

Interdigitation in sphingomyelins have been shown to be involved when the *N*-acyl chain within the same molecule exceeds markedly from the sphingosine chain (Levin et al., 1985; Maulik et al., 1986). There is no a priori reason why this would not occur also in ceramide–DMPC alloys. Interdigitation should decrease lateral diffusion and increase P, as observed. Additionally, T_m should be reduced if the thickness of the interdigitated bilayer is smaller than for DMPC alone. Hence, decrease in T_m is observed when $X_{cer} > 0.14$. Unfortunately, such data as described in the present communication does not allow for the elucidation of the molecular level events underlying the observed segregation of the fluorescent lipid. For this structural information studies such as X-ray scattering are required. Efforts along these lines are currently in progress.

The present study provides evidence for the lateral enrichment of the probe PPDPC into microdomains to result from the introduction of ceramide into binary alloys with DMPC. Phase separation and domain formation have been postulated to be of functional significance to biomembranes (Sackmann, 1980; Kinnunen, 1991; Knoll et al., 1991). In sarcoplasmic reticulum vesicles, for instance, phase separation of phospholipids has been correlated to changes in the conformation as well as function of Ca^{2+}-ATPase (Asturias et al., 1990). Peripheral interactions of proteins such as phospholipase A_2 (Grainger et al., 1990; Burack et al., 1993; Maloney et al., 1995), lipases (Smaby et al., 1994), and cytochrome *c* (Mustonen et al., 1987) with membrane surfaces can be modulated by the lateral distribution of phospholipids. Caveolae are 50–100 nm diameter invaginations of the plasma membrane that represent a specific domain enriched in ceramide (Liu and Anderson, 1995). These membrane domains contain G-protein-coupled receptors and a possible role in signal transduction has been suggested (Lisanti et al., 1994). There is evidence for interleukin-1β binding to a sphingomyelin-rich plasma membrane domain with the characteristics of caveolae (Liu and Anderson, 1995). Hormone binding yielded first diacylglycerol from phospholipids together with an almost concomitant hydrolysis of sphingomyelin to ceramide (Liu and Anderson, 1995). These authors concluded ceramide production to be highly compartmentalized in the cell surface. Egg yolk sphingomyelin incorporated into DMPC has been reported not to segregate into domains (McKeone et al., 1986). Our results suggest the possibility of removing the phosphocholine headgroup by sphingomyelinase to result in lateral phase separation of the generated ceramide. Intriguingly, in stimulated cells contents of ceramide approaches the content of $X_{cer} = 0.10$ to total phospholipid (Hannun, 1996). Exceeding this proportion of ceramide is interpreted here to form microdomains.

Phase separation could be of importance also in membrane fusion (Hoekstra, 1982) and this process has been postulated to play an important role in the budding–fission–fusion sequence in cells (Sackmann and Feder, 1995). In view of this idea, considering effective molecular shapes, there is a resemblance between ceramide and diacylglycerols. In DPPC bilayers already low contents of diglycerol ($X_{DG} \approx 0.06$–0.12) become separated into microdomains (Ortiz et al., 1988). Interestingly, it has been recently shown that in vesicle fusion and aggregation diacylglycerols and ceramides have different effects (Ruiz-Argüello et al., 1996). Diacylglycerols induce vesicle aggregation followed by fusion. In contrast, ceramide promotes aggregation and leakage whereas fusion is not observed. These effects were explained in terms of the formation of non-lamellar structures and increased stability of ceramide-containing LUVs. A recent study has shown the elimination of pretransition to be predictive of fusogenity of binary DPPC–amphiphile bilayers (Lentz et al., 1996). However, as ceramide does not promote fusion it is possible that an increase in T_p would correlate with events preceding fusion, such as close apposition and adherence of vesicles. To this

end, an increase in T_p is promoted by dehydration of the bilayers (Cevc, 1991). This would be in agreement with the observations by Lentz et al. (1996).

Acknowledgements

The authors wish to thank Birgitta Rantala for tecnical assistance. This study was supported by the Finnish State Medical Research Council, Biocentrum Helsinki, and by the Finnish Medical foundation (JYAL). JMH and JYAL are supported by the MD/PhD program of the University of Helsinki.

References

Asturias, F.J., Pascolini, D., Blasie, J.K., 1990. Evidence that lipid lateral phase separation induces functionally significant structural changes in the Ca^{2+}-ATPase of the sarcoplasmic reticulum. Biophys. J. 58, 205–217.

Ballou, L.R., 1992. Sphingolipids and cell function. Immunol. Today 13, 339–341.

Ballou, L.R., Chao, C.P., Holness, M.A., Barker, S.C., Raghow, R., 1992. Interleukin-1-mediated PGE_2 production and sphingomyelin metabolism. J. Biol. Chem. 267, 20044–20050.

Bartlett, G.R., 1959. Phosphorus assay in column chromatography. J. Biol. Chem. 234, 466–468.

Bouwstra, J.A., Gooris, G.S., Van Der Spek, J.A., Bras, W., 1991. Structural investigations of human stratum corneum by small angle X-ray scattering. J. Invest. Dermatol. 97, 1005–1012.

Burack, R.W., Yuan, Q., Biltonen, R.L., 1993. Role of lateral phase separation in the modulation of phospholipase A_2 activity. Biochemistry. 32, 583–589.

Cevc, G., 1991. Polymorphism of the bilayer membranes in the ordered phase and the molecular origin of the lipid pretransition and rippled lamellae. Biochim. Biophys. Acta 1062, 59–69.

Cevc, G., Marsh, D., 1987. In: Phospholipd Bilayers. Physical Principles and Models. Wiley, New York, pp. 231–269.

Chao, M.V., 1995. Ceramide: a potential second messenger in the nervous system. Mol. Cell. Neurosci. 6, 91–96.

Cifone, M.G., De Maria, R., Roncaioli, P., et al., 1994. Apoptotic signalling through CD95 (Fas/Apo-1) activates an acidic sphingomyelinase. J. Exp. Med. 180, 1547–1552.

Dressler, K.A., Mathias, S., Kolesnick, R.N., 1992. Tumor necrosis factor-α activates the sphingomyelin signal transduction pathway in a cell-free system. Science 255, 1715–1718.

Duportail, G., Lianos, P., 1996. In: Rosoff, M. (Ed.), Vesicles. Marcel Decker, New York, pp. 295–372.

Eklund, K., Vuorinen, J., Mikkola, J., Virtanen, J.A., Kinnunen, P.K.J., 1988. Ca^{2+}-induced lateral phase separation in phosphatidic acid/phosphatidylcholine monolayers as revealed by fluorescence microscopy. Biochemistry. 27, 3433–3437.

Elias, P.M., Menon, G.K., 1991. Structural and lipid biochemical correlates of the epidermal permeability barrier. Adv. Lipid Res. 23, 753–758.

Eliasz, A.W., Chapman, D., Ewing, D.F., 1976. Phospholipid phase transitions. Effects of n-alcohols, n-monocarboxylic acids, phenylalkyl alcohols and quaternaty ammonium compounds. Biochim. Biophys. Acta 448, 220–233.

Förster, T., 1969. Excimers. Angew. Chem. Int. Ed. 8, 333–343.

Galla, H.-J., Hartmann, W., 1980. Excimer-forming lipids in membrane research. Chem. Phys. Lipids 27, 199–219.

Galla, H.-J., Hartmann, W., Theilen, U., Sackmann, E., 1979. On two-dimensional passive random walk in lipid bilayers and fluid pathways in biomembranes. J. Membr. Biol. 48, 215–236.

Galla, H.-J., Sackmann, E., 1974. Lateral diffusion in the hydrophobic region of membranes: use of pyrene excimer as optical probes. Biochim. Biophys. Acta 339, 103–115.

Grainger, D.W., Reichert, A., Ringsdorf, H., Salesse, C., 1990. Hydrolytic action of phospholipase A_2 in monolayers in the phase transition region: direct observation of enzyme domain formation using fluorescence microscopy. Biochim. Biophys. Acta 1023, 365–379.

Haimovitz-Friedman, A., Kan, C.-C., Ehleiter, D., et al., 1994. Ionizing radiation acts on cellular membranes to generate ceramide and initiate apoptosis. J. Exp. Med. 180, 525–535.

Hannun, Y.A., 1994. The sphingomyelin cycle and the second messenger function of ceramide. J. Biol. Chem. 269, 3125–3128.

Hannun, Y.A., 1996. Functions of ceramide in coordinating cellular responses to stress. Science 274, 1855–1859.

Hannun, Y.A., Obeid, L.M., 1995. Ceramide: an intracellular signal for apoptosis. TIBS 20, 73–77.

Hoekstra, D., 1982. Fluorescence method for measuring the kinetics of Ca^{2+}-induced phase separations in phosphatidylserine-containing lipid vesicles. Biochemistry 21, 1055–1061.

Hresko, R.C., Sugár, I.P., Barenholz, Y., Thompson, T.E., 1986. Lateral disatribution of a pyrene-labeled phosphatidylcholine in phosphatidylcholine bilayers: fluores cence phase and modulation study. Biochemistry 25, 3813–3823.

Jayadev, S., Liu, B., Bielawska, A.E., et al., 1995. Role for ceramide in cell cycle arrest. J. Biol. Chem. 270, 2047–2052.

Jähnig, F., 1979. Structural order of lipids and proteins in membranes: evaluation of fluorescence anisotropy data. Proc. Natl. Acad. Sci. USA 76, 6361–6365.

Kim, M.-Y., Linardic, C., Obeid, L., Hannun, Y.A., 1991. Identification of sphingomyelin turnover as an effector mechanism for the action of tumor necrosis factor α and γ-interferon. J. Biol. Chem. 266, 484–489.

Kinnunen, P.K.J., Tulkki, A.-P., Lemmetyinen, H., Paakkola, J., Virtanen, J.A., 1987. Characteristics of excimer formation in Langmuir-Blodgett assemblies of 1-palmitoyl-2-pyrenedecanoylphosphatidylcholine and dipalmitoylphosphatidylcholine. Chem. Phys. Lett. 136, 539–545.

Kinnunen, P.K.J., 1991. On the principles of functional ordering in biological membranes. Chem. Phys. Lipids 57, 375–399.

Kinnunen, P.K.J., Laggner, P., 1991. Phospholipid phase transitions. Chem. Phys. Lipids 57, 109–408.

Kinnunen, P.K.J., Kõiv, A., Mustonen, P., 1993. Pyrene-labeled lipids as fluorescent probes in studies on biomembranes and membrane models. In: O.S. Wolfbeis (Ed.), Fluorescence Spectroscopy. Springer, Berlin. pp. 159–169.

Knoll, W., Schmidt, G., Rötzer, H., et al., 1991. Lateral order in binary lipid alloys and its coupling to membrane functions. Chem. Phys. Lipids. 57, 363–374.

Kõiv, A., Mustonen, P., Kinnunen, P.K.J., 1993. Influence of sphingosine on the thermal phase behaviour of neutral and acidic phospholipid liposomes. Chem. Phys. Lipids 66, 123–134.

Lakowicz, J.R., 1983. Fluorescence polarization. In: Principles of Fluorescence Spectroscopy. Plenum, New York. pp. 111–151.

Lakowicz, J.R., Prendergast, F.G., Hogen, D., 1979a. Differential polarized phase fluorometric investigations of diphenylhexatriene in lipid bilayers quantitation of hindered depolarizing rotations. Biochemistry 18, 508–519.

Lakowicz, J.R., Prendergast, F.G., Hogen, D., 1979b. Fluorescence anisotropy measurements under oxygen quenching conditions as a method to quantify the depolarizing rotations of fluorophores. Application to diphenylhexatriene in isotropic solvents and in lipid bilayers. Biochemistry 18, 520–527.

Lehtonen, J.Y.A., Kinnunen, P.K.J., 1994. Changes in the lipid dynamic of liposomal membranes induced by poly(ethylene glycol). Free volume alterations revealed by inter- and intramolecular excimer forming phospholipid analogs. Biophys. J. 66, 1981–1990.

Lehtonen, J.Y.A., Kinnunen, P.K.J., 1995. Phospholipase A_2 as a mechanosensor. Biophys. J. 68, 1888–1894.

Lehtonen, J.Y.A., Kinnunen, P.K.J., 1997. Evidence for phospholipid microdomain formation in liquid crystalline liposomes reconstituted with Escherichia coli lactose permease. Biophys. J. 72, 1247–1257.

Lehtonen, J.Y.A., Holopainen, J.M., Kinnunen, P.K.J., 1996. Evidence for the formation of microdomains in liquid crystalline large unilamellar vesicles caused by hydrophobic mismatch of the constituent phospholipids. Biophys. J. 70, 1753–1760.

Lentz, B.R., Wu, J.R., Zheng, L., Prevrátil, J., 1996. The interfacial region of dipalmitoylphosphatidylcholine bilayers is perturbed by fusogenic amphipaths. Biophys. J. 71, 3302–3310.

Levin, I.W., Thompson, T.E., Barenholz, Y., Huang, C., 1985. Two types of hydrocarbon chain interdigitation in sphingomyelin bilayers. Biochemistry 24, 6282–6286.

Lisanti, M.P., Scherer, P.E., Tang, Z., Sargiacomo, M., 1994. Caveolae, caveolin and caveolin-rich membrane domains: a signalling hypothesis. Trends Cell Biol. 4, 231–235.

Liu, P., Anderson, G.W., 1995. Compartmentalized production of ceramide at the cell surface. J. Biol. Chem. 270, 27179–27185.

Lopez-Garcia, F., Villain, J., Gomez-Fernandez, J.C., 1994. A phase behaviour study of mixtures of sphingosine with zwitterionic phospholipids. Biochim. Biophys. Acta 1194, 281–288.

Mabrey-Gaud, S., 1981. Differential scanning calorimetry of liposomes. In: Knight, C.G. (Ed.), Liposomes: From Physical Structure to Therapeutic Applications. Elsevier, Amsterdam, pp. 105-138.

MacDonald, R.C., MacDonald, R.I., Menco, B.M., Takeshita, K., Subbarao, N.K., Hu, L.R., 1991. Small-volume extrusion apparatus for preparation of large unilamellar vesicles. Biochim. Biophys. Acta 1061, 297–303.

Maloney, K.M., Grandbois, M., Grainger, D.W., Salesse, C., Lewis, K.A., Roberts, M.F., 1995. Phospholipase A_2 domain formation in hydrolyzed asymmetric phospholipid monolayers at the air/water interface. Biochim. Biophys. Acta 1235, 395–405.

Mathias, S., Dressler, K.A., Kolesnick, R.N., 1991. Characterization of a ceramide-activated protein kinase: stimulation by tumor necrosis factor α. Proc. Natl. Acad. Sci. USA 88, 10009–10013.

Mathias, S., Younes, A., Kan, C.-C., Orlow, I., Joseph, C., Kolesnick, R.N., 1993. Activation of the sphingomyelin signaling pathway in intact EL4 cells and in a cell-free system by IL-1β. Science 259, 519–522.

Maulik, P.R., Atkinson, D., Shipley, G.G., 1986. X-ray scattering of vesicles of N-acyl sphingomyelins. Determination of bilayer thickness. Biophys. J. 50, 1071–1077.

McIntosh, T.J., Stewart, M.E., Downing, D.T., 1996. X-ray diffraction analysis of isolated skin lipids: reconstitution of intercellular lipid domains. Biochemistry 35, 3649–3653.

McKeone, B.J., Pownall, H.J., Massey, J.B., 1986. Ether phosphatidylcholines: comparison of miscibility with ester phosphatidylcholines and sphingomyelin, vesicle fusion, and association with apolipoprotein A-I. Biochemistry 25, 7711–7716.

McElhaney, R.N., 1982. The use of differential scanning calorimetry and differential thermal analysis in studies of model and biological membranes. Chem. Phys. Lipids 30, 229–259.

McMullen, T.P.W., Lewis, R.N.A.H., McElhaney, R.N., 1993. Differential scanning calorimetric study of the effect of cholesterol on the thermotropic phase behavior of a homologous series of linear saturated phosphatidylcholines. Biochemistry 32, 516–522.

McMullen, T.P.W., McElhaney, R.N., 1995. New aspects of the interaction of cholesterol with dipalmitoylphosphatidylcholine bilayers as revealed by high-sensitivity differential scanning calorimetric. Biochem. Biophys. Acta 1234, 90–98.

Michell, R.H., Wakelam, M.J.O., 1994. Sphingolipid signalling. Curr. Biol. 4, 370373.

Mouritsen, O.G., Bloom, M., 1984. Mattress model of lipid–protein interactions in membranes. Biophys. J. 46, 141–153.

Mustonen, P., Virtanen, J.A., Somerharju, P.J., Kinnunen, P.K.J., 1987. Binding of cytochrome c to liposomes as revealed by the quenching of fluorescence from pyrene-labeled phospholipids. Biochemistry 26, 2991–2997.

Niculescu, F., Rus, H., Shin, S., Lang, T., Shin, M.L., 1993. Generation of diacylglycerol and ceramide during homologous complement activation. J. Immunol. 150, 214–224.

Obeid, L.M., Hannun, Y.A., 1995. Ceramide: a stress signal and mediator of growth suppression and apoptosis. J. Cell. Biochem. 58, 191–198.

Olson, F., Hunt, C.A., Szonka, F.C., Vail, W.J., Papahadjopoulos, D., 1979. Preparation of liposomes of defined size distribution by extrusion through polycarbonate membranes. Biochim. Biophys. Acta 557, 9–23.

Okazaki, T., Bell, R.M., Hannun, Y.A., 1989. Sphingomyelin turnover induced by vitamin D_3 in HL-60 cells. J. Biol. Chem. 264, 19076–19080.

Okazaki, T., Bielawska, A., Domae, N., Bell, R.M., Hannun, Y.A., 1994. Characteristics and partial purification of a novel cytosolic, magnesium-independent, neutral sphingomyelinase activated in the early signal transduction of 1α,25-dihydroxyvitamin D_3-induced HL-60 cell differentiation. J. Biol. Chem. 269, 4070–4077.

Ortiz, A., Villalain, J., Gõmes-Fernãndez, J.C., 1988. Interaction of diacylglycerols with phosphatidylcholine vesicles as studied by differential scanning calorimetry and fluorescence probe depolarization. Biochemistry 27, 9030–9036.

Pascher, I., 1976. Molecular arrangements in sphingolipids. Conformation and hydrogen bonding of ceramide and their implication on membrane stability and permeability. Biochim. Biophys. Acta 455, 433–451.

Prendergast, F.G., Haugland, R.P., Callahan, P.J., 1981. 1-[4-(Trimethylamino)phenyl]-6-phenylhexa-1,3,5-triene: synthesis, fluorescence properties, and use as a fluorescence probe of lipid bilayers. Biochemistry 20, 7333–7338.

Quintans, J., Kilkus, J., McShan, C.L., Gottschalk, A.R., Dawson, G., 1994. Ceramide mediates the apoptotic response of WEHI 231 cells to anti-immunoglobulin, corticosteroids and irradiation. Biochem. Biophys. Res. Commun. 202, 710–714.

Ramachandran, C.K., Murray, D.K., Nelson, D.H., 1990. Dexamethasone increases neutral sphingomyelinase activity and sphingosine levels in 3T3-L1 fibroblasts. Biochem. Biophys. Res. Commun. 167, 607–613.

Ruiz-Argüello, M.B., Basáñez, G., Goñi, F.M., Alonso, A., 1996. Different effects of enzyme-generated ceramides and diacylglycerols in phospholipid membrane fusion and leakage. J. Biol. Chem. 271, 26616–26621.

Saba, J.D., Obeid, L.M., Hannun, Y.A., 1996. Ceramide: an intracellular mediator of apoptosis and growth supression. Phil. Trans. R. Soc. London B. 351, 233–241.

Sackmann, E., 1980. Physical basis of triggerprocess and membrane structures. In: Chapman, D. (Ed.), Biological Membranes, vol. 5. Academic Press, London, pp 105–143.

Sackmann, E., Feder, T., 1995. Budding, fission and domain formation in mixed lipid vesicles induced by lateral phase separation and macromolecular condensation. Mol. Membr. Biol. 12, 21–28.

Schurer, N.Y., Elias, P.M., 1991. The biochemistry and function of stratum corneum lipids. Adv. Lipid Res. 24, 27–56.

Schütze, S., Machleidt, T., Kronke, M., 1994. The role of diacylglycerol and ceramide in tumor necrosis factor and interleukin-1 signal transduction. J. Leukocyte Biol. 56, 533–541.

Shah, J., Atienza, J.M., Rawlings, A.V., Shipley, G.G., 1995. Physical properties of ceramides: effect of fatty acid hydroxylation. J. Lipid Res. 36, 1945–1955.

Silvius, J.R., 1982. Thermotrophic phase transitions of pure lipids in model membranes and their modifications by membrane proteins. In: Jost, P.C., Griffith, O.H. (Eds.), Lipid–Protein Interactions, vol. 2. John Wiley & Sons, Inc., New York, pp. 239–281.

Smaby, J.M., Muderhwa, J.M., Brockman, H.L., 1994. Is lateral phase separation required for fatty acid to stimulate lipases in a phosphatidylcholine interface?. Biochemistry 33, 1915–1922.

Somerharju, P.J., Virtanen, J.A., Eklund, K.K., Vainio, P., Kinnunen, P.K.J., 1985. 1-palmitoyl-2-pyrenedecanoyl glycerophospholipid as membrane probes: evidence for regular distribution in liquid crystalline phosphatidylcholine bilayers. Biochemistry 24, 2773–2781.

Strum, J.C., Small, G.W., Pauig, S.B., Daniel, L.W., 1994. 1-β-D-Arabinofuranosylcytosine stimulates ceramide and diglyseride formation in HL-60 cells. J. Biol. Chem. 269, 15493–15497.

Xiang, T.-X., 1993. A computer simulation of free volume distribution and related structural properties in a model lipid bilayer. Biophys. J. 65, 1108–1120.

ELSEVIER

Chemistry and Physics of Lipids
88 (1997) 15–20

CPL
CHEMISTRY AND
PHYSICS OF LIPIDS

On periodic curvature and standing wave motions in cell membranes

Kåre Larsson

Camurus Lipid Research, Ideon Science Park, S-223 70 Lund, Sweden

Received 9 April 1997; accepted 4 June 1997

Abstract

Cell membranes can form cubic arrangements and there is evidence for the occurrence of periodic curvature in simple membranes. The periodicity of the bilayer implies a standing wave character of vibrational motions. It is proposed that the periodic curvature reflects a dominating mode of standing wave oscillations, with the different cubic bilayer structures representing alternative standing wave conformations of the bilayer. The wave motions in lamellar liquid-crystalline phases, as well as in vesicles and membranes, which lack lateral periodicity, are known to exhibit statistically distributed undulations. The standing wave character of conformational fluctuations of periodically curved membranes, on the other hand, results in an organisation in time and space. Calculated models of standing wave conformations of membranes are demonstrated, and functional aspects of such biomembranes are discussed.

Keywords: Membrane structure; Bilayer conformation; Membrane dynamic; Standing wave motions

1. Introduction

In connection with work on cubic lipid-water phases demonstrating the occurrence of periodically curved infinite lipid bilayers, (Hyde et al., 1984), it was proposed that two-dimensional analogues to this bilayer conformation might occur in cell membranes (Larsson and Andersson, 1986; Larsson, 1988, 1989). Helfrich (1989) has proposed a similar model for 'membrane roughness' involving 'highly localised saddles of very large curvature', which later was confirmed in electron microscopy studies of phospholipid vesicles (Klösgen and Helfrich, 1993).

A modification of the earlier minimal surface description of cubic lipid bilayer was recently proposed, where the bilayer conformation is a result of standing wave oscillations (Jacob et al., 1997). This approach proved to be very useful when describing the structure and properties of colloidal particles of cubic lipid-water phases (Gustavsson et al., 1996). Additional evidence for

PII S0009-3084(97)00041-8

this description of cubic bilayer structures are given below, including the dynamic conformation of cell membranes.

2. A standing wave description of the infinite bilayer in cubic lipid-water phases

The introduction of the infinite periodic minimal surface (IPMS) concept resulted in a significant progress in the understanding of the structure of cubic lipid-water phases. According to the IPMS description, the surface separating each half of the bilayer follows one of three fundamental IPMSs; The so-called primitive surface corresponds to the Q_P-phase with space group Im3m, the diamond surface corresponds to the Q_D-phase with space group Pn3m, and the gyroid surface corresponds to the C_G-phase with space group Ia3d. The relations between the two cubic structures exhibited by glycerolmonooleate, for example, could be explained by this description (Hyde et al., 1984). In the search for mathematical approximations for the complex analytical representation of IPMSs, von Schnering and Nesper (1991) discovered the nodal surface (NS) description. These surfaces are obtained by simple trigonometric functions, which in the case of the P, D and G surfaces are very close to the corresponding IPMS. von Schnering and Nesper (1991) performed Fourier series calculations like those used to calculate the electron density distribution within the unit cell. Only one structure factor with lowest order index was used, and setting this function equal to zero, a surface separating space into two congruent regions of opposite sign was obtained. This surface was found to follow the corresponding IPMS closely. In the case of the P-surface, for example, a structure factor (with an arbitrary absolute value) with index (100) and phase angle equal to zero was used. The space group symmetry then gives the function:

$$\cos x + \cos y + \cos z$$

Setting this function equal to zero, its roots are obtained (or, regarding it as a wave function, its nodes). Similar simple expressions were obtained in the case of the D- and G-surfaces.

As pointed out by von Schnering and Nesper (1991) their calculated NSs have no direct physical meaning, and the lack of explanation of the agreement between IMPSs and NSs was also recently discussed by Hoffman (1996). It is proposed here that the NS-description applied on cubic lipid-water phases has revealed the true dynamic structure of the bilayers.

Wave motions, 'undulations', is a generally accepted structural feature of the lipid bilayer in lamellar liquid-crystalline phase, and wave-lengths and amplitudes have even been evaluated experimentally from dimensions determined by X-ray diffraction. The molecular disorder is almost the same in a cubic bilayer (Lindblom et al., 1979), and a similar degree of wave motions due to thermal excitations as in lamellar phases must be expected. The three-dimensional periodicity of the cubic bilayer means that the mobility must form standing waves. It seems natural to consider standing wave conformations of the bilayer with the same periodicity and symmetry as exhibited by the observed cubic unit cell. (The symmetry as determined by X-ray diffraction corresponds to the time-average of all motions, due to the frequency of the X-ray light compared to any vibrational motion.) This is in fact the conformation provided by the NS-description. It is assumed that this wave conformation represents one dominating oscillation mode, which seems reasonable with regard to the uniform character of undulations in lamellar phases.

If we again consider the P-surface, the centre of the cubic bilayer will follow the wave equation (Jacob et al., 1997):

$$\cos x + \cos y + \cos z - p = 0$$

where p at a particular point (xyz) varies with time, and when $p = 0$ the nodal surface is reached. If we consider one structure unit of the C_P-phase, these wave oscillations represent the breathing mode of the unit (joined by six catenoids to adjacent units in the x-, y-, and z-directions). When a structure unit on one side of the bilayer is expanding, the unit on the other side is compressed. The phase of these standing wave breathing oscillations will vary from one unit cell to the next, as defined by the wave vector.

The standing-wave description takes into account the dynamic behaviour of the bilayer. Different arguments used in favour of the IPMS description of the bilayer are usually based on consequences of the zero value of the average curvature, for example that there is no difference in hydrostatic pressure between the two sides of such a bilayer. In the standing wave description, oscillations of the bilayer results in pressure fluctuations within the lipid monolayer and the water channel networks on each side of the surface at the centre of the bilayer. The main evidence supporting the standing wave model of the cubic bilayer is the possibility to describe physical phenomena exhibited by cubic membrane assemblies (cubosomes) as direct consequences of wave conformation changes. Fusion or bud-off processes of vesicles in relation to cubosomes in calculated bilayer models were thus observed as direct effects of minor variations in wave conformation (Jacob et al., 1997). Cubic cell membrane assemblies occur frequently (Hyde et al., 1997), and these phenomena are therefore of biological interest.

3. Periodically curved bilayer conformation occurring in a cell membrane implies standing wave oscillations

Some consequences of standing wave motions in a two-dimensional bilayer forming a membrane have been considered earlier (Larsson et al., 1996), and an extended discussion is presented here as a basis for the proposal that this dynamic conformation represents a relevant structural state of cell membranes. As mentioned earlier the mere existence of crystallographic periodicity means that the molecular motions are coupled, forming standing waves. This must also be the case in a two-dimensional structure with periodic curvature, such as a cell membrane. A uniform elastic rigidity is a requirement for the periodicity. The elasticity of the bilayer is determined by the desired average molecular shape of the lipid molecules. The transition from a lamellar liquid-crystalline phase into a cubic bilayer phase can be described as a change in average molecular shape; from a cylindrical to a conical shape. Sometimes this transition is a result of increased thermal disorder of the hydrocarbon chains (Lindblom et al., 1979), resulting in an increased inner pressure in the bilayer. In a similar way, the formation of a bilayer with periodic curvature in two dimensions, analogous to a cubic bilayer, is favoured by a conical average molecular shape. Expected two-dimensional structure analogues of the C_D-phase is a bilayer along the (111)-plane, of the C_P-phase a bilayer along the (100)-plane and of the C_G-phase a bilayer along the (111)-plane (Larsson, 1989). Such curved bilayers are expected to have a higher inner pressure and consequently a higher elastic rigidity than the bilayer of lamellar phases.

Membrane lipids usually form a lamellar liquid-crystalline phase with water, with existence range very close to a transition into a reversed phase, either cubic or reversed hexagonal (Lindblom and Rilfors, 1989; de Kruijff, 1997). Furthermore variations in environmental factors, like pressure or temperature, results in changes in the membrane composition so as to keep the conformation of the bilayer close to the transition into a reversed phase. As mentioned earlier the reversed structures, such as a cubic bilayer, are characterised by an average conical molecular shape and a higher inner packing pressure. It might be expected that membrane-embedded enzymes controlling membrane lipid composition are monitored by the inner packing pressure of the bilayer (Larsson, 1988). Seddon (1990) has analysed the mechanical properties of the bilayer, and from the stress profile it is concluded that non-planar spontaneous curvatures should occur frequently. This tendency should be more pronounced in cell membranes, with an asymmetric lipid distribution over the bilayer. Therefore it seems likely that the membrane can exhibit periodic curvature, with mechanisms for control of inner pressure (determining elastic rigidity and wave structure).

Wave conformations of a membrane can be illustrated by applying the NS-description of the C_P-, C_D- or C_G-structures on a surface, assuming that the curvature of the bilayer in two-dimensions is related to that of cubic bilayer phases. Such conformations can be calculated using the exponential structure description approach by Andersson and Jacob (1997). One feature of this

description is a continuous change from inner periodicity to outer shape. An illustration of standing wave oscillations of a membrane of spherical shape is given in Fig. 1. The variations in amplitude of the oscillations is obtained here by applying a weight factor to the NS-function. An almost identical membrane conformation of L-form cells from *Streptomyces hygroscopicus* and from vesicles formed by their lipids has been observed (Meyer et al., 1990).

A similar calculation modelling an oscillating periodic membrane with outer cylindrical shape is shown in Fig. 2. These calculations should only be regarded as indications of possible standing wave conformations. In order to get a uniform wave conformation in this way, the outer shape must follow the $C_P(100)$-, $C_D(111)$ or $C_G(111)$-surface structure (giving square or hexagon repetition units) in all directions. It can also be mentioned that the C_G-surface can provide chirality to the membrane curvature.

As discussed above in connection with cubosomes, it is assumed that there is one dominating mode of wave oscillations, which is directly related to the periodicity of the curvature. The oscillations represents contraction and expansion of the bilayer in relation to the time-averaged conformation. This average conformation is assumed to be of the same order of magnitude as observed in erythrocyte membranes (Zeeman et al., 1990) with a wave-length of about 100 nm. and an amplitude of about 10 nm. The frequency of this kind of bilayer motions is considered to be about 10 Hz (Sackmann, 1996). There are less information available on probable size of the standing wave conformational variations, which is related to the elastic rigidity of the bilayer. They can be expressed as variations in average cross-section area per lipid molecule, and there are some data on this from X-ray studies of bilayer dimensions of cubic phases with different curvatures (Hyde et al., 1984).

Wave-like motions of lipid bilayers in vesicles and membranes have earlier been frequently dis-

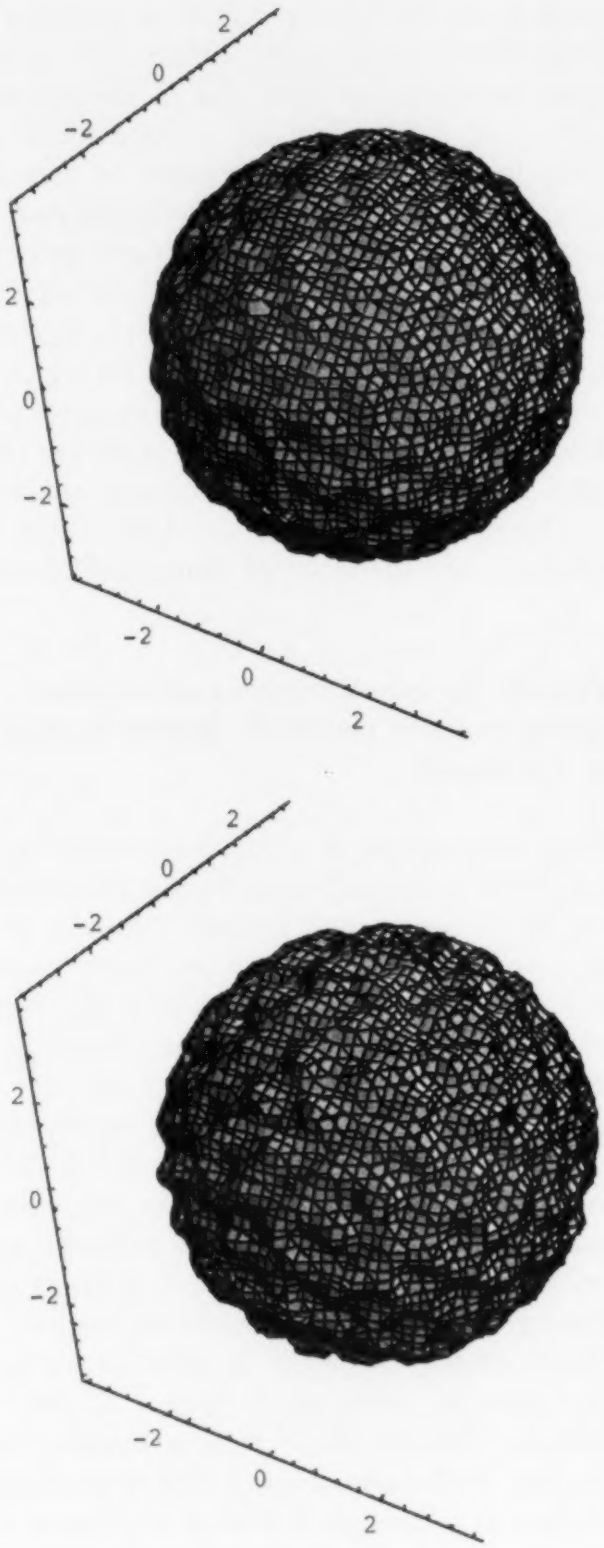

Fig. 1. Illustration of the time-averaged extremes of the conformations of standing wave oscillations of a membrane of spherical shape, calculated using Mathematica version 2.2 for Macintosh. In the case of a spherical shape it is possible to add the NS-function directly to the sphere. The NS-description of the gyroid surface with weight factors $w = 0.4$ and $w = 0.6$, respectively were applied according to:

$$w(\cos 2\pi x \sin 2\pi z + \cos 2\pi y \sin 2px + \cos 2\pi x \sin 2\pi y) + x^2 + y^2 + z^2 = 12$$

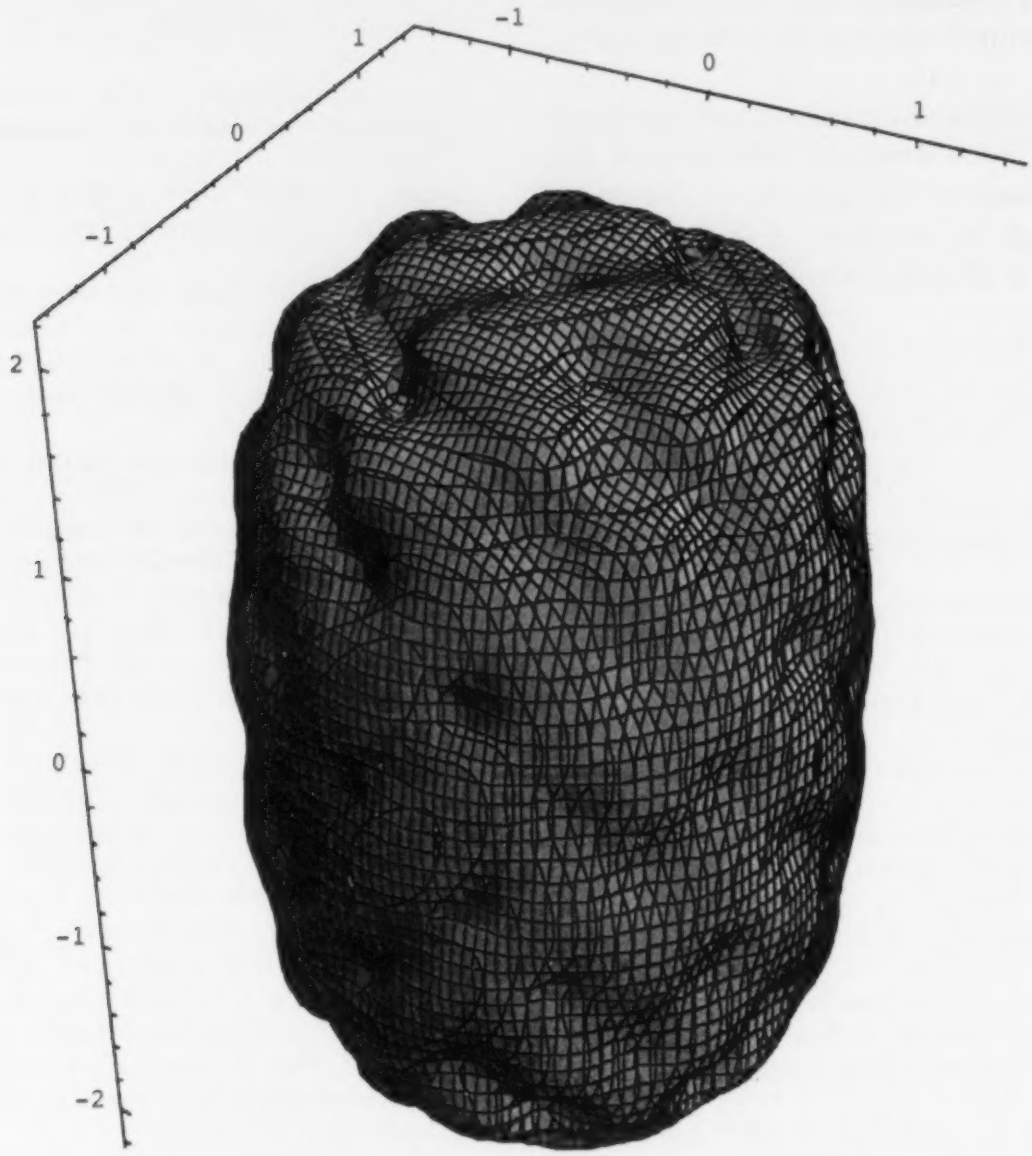

Fig. 2. Illustration of the time-averaged conformation of a cylindrical membrane with standing wave oscillations according to the NS-function of the D-surface, calculated using the exponential structure description by Andersson and Jacob (1997) according to: $0.8(e^{\cos 2\pi x \cos 2\pi y \cos 2\pi z + \sin 2\pi x \sin 2\pi y \sin 2\pi z}) + e^{X^2} + e^{Y^2} + e^{Z} + e^{-Z} = 10$.

cussed, cf. (Lipovsky, 1991; Sackmann, 1996). These undulations/fluctuations have been assumed to occur statistically along the bilayer, and the bilayer units moving in and out have been modelled as a two-dimensional gas. It seems natural to assume this kind of wave movement when the bilayer lacks lateral periodicity. With periodic curvature occurring in the membrane, the bilayer will exhibit standing waves, providing an organisation of the membrane in time and space. The elastic rigidity of the bilayer will determine whether or not standing wave motions will occur. The membrane might in this respect be compared with a violin string. Standing waves can not be obtained unless the string is under tension.

4. Functional aspects of standing wave conformations in membranes

A membrane with periodic curvature, which therefore shows standing wave motions, represents a mechanical equilibrium along the whole membrane surface. A mechanical disturbance, the fusion of a vesicle, or a conformational change inside the bilayer of a membrane protein will be

sensed over the whole membrane within the time of the standing wave frequency (neglecting damping effects).

Another consequence of standing wave motions of a membrane is the dynamic behaviour of the electric field induced by the electric double-layer, involving sensing of motion of neighbouring membranes and a tendency towards synchronisation.

References

Andersson, S., Jacob, M., 1997. The Mathematics of Structures. The Exponential Scale. R. Oldenburg Verlag, Munchen.

Gustavsson, J., Ljusberg-Wahren, H., Almgren, M., Larsson, K., 1996. Cubic lipid-water phases dispersed into submicron particles. Langmuir 12, 4611–4613.

Helfrich, W., 1989. Hats and saddles in lipid membranes. Liq. Cryst. 5, 1647–1685.

Hoffman, D., 1996. A new turn for Archimedes. Nature 384, 28–29.

Hyde, S.T., Andersson, S., Ericsson, B., Larsson, K., 1984. A cubic structure consisting of a lipid bilayer forming an infinite periodic minimal surface of the gyroid type in the glycerolmonooleate-water system. Z. Kristallogr. 168, 213–219.

Hyde, S.T., Andersson, S., Larsson, K., Blum, Z., Lidin, S., Ninham, B., 1997. Language of Shape. The role of curvature in condensed matter, physics chemistry and biology. Elsevier, Amsterdam.

Jacob, M., Larsson, K., Andersson, S., 1997. Lipid bilayer standing wave conformations in aaqueous cubic phases. Z. Kristallogr. 212, 5–8.

Klösgen, B., Helfrich, W., 1993. Special features of phosphatidylcholine vesicles as seen in cryo-transmission electron microscopy. Eur. Biophys. J. 22, 329–340.

de Kruijff, B., 1997. Lipids beyond the bilayer. Nature 386, 129–130.

Larsson, K., Andersson, S., 1986. A phase transition model of cooperative phenomena in membranes. Acta Chem. Scand. B 40, 1–5.

Larsson, K., 1988. Lipid phase transitions in membranes involving intrinsic periodic curvature. Chem. Phys. Lipids 49, 65–67.

Larsson, K., 1989. Cubic lipid-water phases: Structures and biomembrane aspects. J. Phys. Chem. 93, 7304–7314.

Larsson, K., Jacob, M., Andersson, S., 1996. Lipid bilayer standing waves in cell membranes. Z. Kristallogr. 211, 875–878.

Lipovsky, R., 1991. The conformation of membranes. Nature 349, 475–481.

Lindblom, G., Larsson, K., Johansson, L., Fontell, K., Forsen, S., 1979. The cubic phase in mono-glyceride-water systems. Arguments for a structure based upon lamellar bilayer units. J. Am. Chem. Soc. 101, 5465–5470.

Lindblom, G., Rilfors, L., 1989. Non-lamellar phases formed by membrane lipids. Biochim. Biophys. Acta 988, 221–256.

Meyer, H.W., Richter, W., Gumpert, J., 1990. Periodically curved bilayer structures observed in hyphal cells of a Streptomyces strain, and liposomes formed by extracted lipids. Biochim. Biophys. Acta 1026, 171–178.

Sackmann, E., 1996. Supported membranes: Scientific and practical applications. Science 271, 43–48.

von Schnering, H.G., Nesper, R., 1991. Nodal surfaces of Fourier series: Fundamental invariants of structured matter. Z. Phys. B-Condensed Matter 83, 407–412.

Seddon, J., 1990. Structure of the inverted hexagonal phase, and nonlamellar phase transitions in lipids. Biochim. Biophys. Acta 1031, 1–69.

Zeeman, K., Engelhart, H., Sackmann, E., 1990. Bending modulation and elasticity of the erythrocyte membrane: Effect of cell shape and membrane organization. Eur. Biophys. J. 18, 203–219.

ELSEVIER

Chemistry and Physics of Lipids
88 (1997) 21–36

CPL
CHEMISTRY AND PHYSICS OF LIPIDS

Formation of high-axial-ratio-microstructures from natural and synthetic sphingolipids

Alex S. Goldstein [a], Anatoly N. Lukyanov [b], Paul A. Carlson [b], Paul Yager [b,*], Michael H. Gelb [a]

[a] *Departments of Chemistry and Biochemistry, University of Washington, Box 351700, Seattle, WA 98195-1700, USA*
[b] *University of Washington, Molecular Bioengineering Program, Center for Bioengineering, Box 352255, Seattle, WA 98195-2255, USA*

Received 19 March 1997; received in revised form 9 June 1997; accepted 9 June 1997

Abstract

Amphiphiles that form high-axial-ratio-microstructures (HARMs) are being considered as novel materials for controlled release of drugs and other biologically functional molecules. HARMs consisting of tubules, ribbons, solid rods and helices are formed from sphingolipids by addition of water to a solution of amphiphile in DMF. Single molecular species of galactocerebroside (GalCer) containing long unsaturated fatty acid chains or natural GalCer containing mixed-length, non-hydroxy fatty acids (NFA-GalCer) or α-hydroxy fatty acids (HFA-GalCer) form cylindrical structures. In contrast, single molecular species of GalCer containing long saturated fatty acids form ribbons and helices. GalCer HARMs are typically under 100 nm in diameter and have lengths of several microns. The importance of the amide of GalCer for HARM formation was evaluated using psychosine, which forms solid fibers, whereas sphingosine and an analog of GalCer in which the amide is reduced to a secondary amine form amorphous aggregates. Single molecular species of ceramide containing long unsaturated fatty acid chains form cylindrical structures, whereas those with long saturated fatty acids form ribbons and helices. Short chain saturated ceramide also forms cylindrical structures. GalCer analogs with *N*-acetyl-glycine in place of the galactose form fibers whereas those with *N*-acetyl-proline yield amorphous material. The *N*-acetyl-proline-containing amphiphile can de doped into pure GalCer or NFA-GalCer without perturbing tubule formation. © 1997 Elsevier Science Ireland Ltd.

Keywords: Cerebroside; Ceramide; Nanostructure; Tubule; Helix; Drug delivery

1. Introduction

Recently there have been reports demonstrating that two-chain amphiphiles can self-organize into

* Corresponding author.

PII S0009-3084(97)00042-X

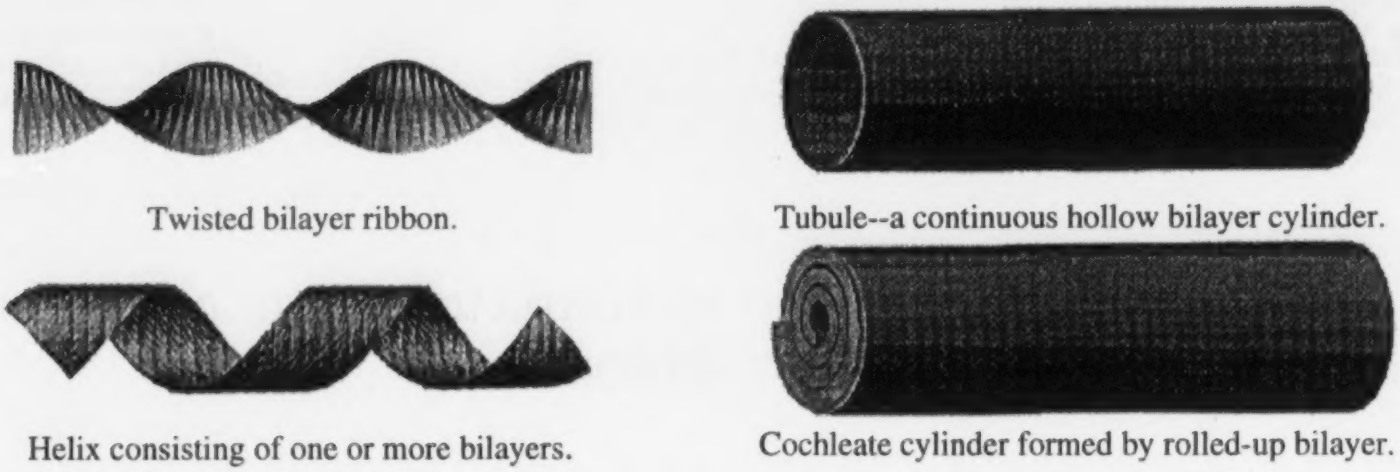

Fig. 1. Schematic images of tubules, cochleate cylinders, ribbons and helices.

stable, crystalline, nonliposomal microstructures when suspended in aqueous media (Yamada et al., 1984; Nakashima et al., 1984; Fuhrhop et al., 1988; Shimizu and Hato, 1993; Yager and Schoen, 1984; Georger et al., 1987). Such high-axial-ratio-microstructures (HARMs) include tubules, twisted ribbons, helices, and cochleate cylinders (Fig. 1). Theories on microstructure formation have been advanced for synthetic lipid systems such as phosphatidylcholine with butadiyne-containing hydrocarbon chains, and such theories have been applied to other HARM systems (Selinger et al., 1996; Nandi and Bagchi, 1996 and references therein). In short, such theories propose that HARM formation is the result of intrinsic bending of rectangular bilayer lipid sheets due to chiral packing of molecules in a membrane. Interest in natural and synthetic HARMs has stemmed primarily from their potential use as templates for mineralization and metallation, for their appearance in biological structures, for their implication in lipid storage diseases and as drug-delivery systems (Schnur et al., 1990; Behroozi et al., 1990; Chappell and Yager, 1992; Schnur et al., 1994; Mann et al., 1993; Rudolph et al., 1988; Archibald and Mann, 1994; Schnur et al., 1987). Such lipid molecular assemblies should have several advantages over current delivery systems: they require neither a macroscopic matrix nor a pump to achieve continuous drug release (by a zero-order kinetic dissolution process), they can limit drug exposure to the desired site of action and such assemblies may provide better shielding of the drug from premature metabolic degradation.

Sphingolipids have been reported to form HARMs (Kulkarni et al., 1995; Archibald and Mann, 1993; Archibald and Yager, 1992; Curatolo and Neuringer, 1986). Cerebrosides are the simplest mammalian glycosphingolipids. These lipids consist of a galactose or glucose headgroup attached to a nonpolar ceramide. Due to order-disorder transition temperatures (T_m) well above body temperature, cerebrosides are thought to impart order to membranes (Curatolo and Neuringer, 1986). In lipid storage diseases such as Gaucher's and Krabbe's disease, cerebroside accumulation disrupts normal membrane function and forms intracellular lipid deposits (Naito et al., 1988). Such deposits give rise to microstructures within the afflicted cells (Yunis and Lee, 1970). Furthermore, galactocerebroside (GalCer) is a major component of myelin and the intestinal brush border and thus contributes to these membrane's physical properties. Ceramide (Cer), the product of hydrolytic removal of the sugar from cerebroside, is thought to serve in cell signal transduction (Bielawska et al., 1996). Further hydrolysis yields, in addition to fatty acids, sphingosine, which also participates in cell signaling (Bielawska et al., 1996).

Earlier investigations into the ability of sphingolipids to form microstructures focused on the development of new formation techniques and, to a limited extent, pure GalCer species. In this paper, we demonstrate that it is possible to form

HARMs from various pure GalCer and Cer species using a new formation technique. Furthermore, synthesized GalCer analogs were converted to microstructures either as single molecular species or as a component of binary mixtures. These studies are a necessary prelude to understanding the basic structural requirements for sphingolipid molecular assemblies.

2. Experimental procedures

2.1. Materials

All materials were of reagent grade purity and used as received. D-erythro-sphingosine was purchased from Avanti Polar Lipids. All other non-synthesized lipids were purchased from Sigma (St. Louis, MO). ^{1}H NMR spectra were obtained in $CDCl_3$ using a Bruker 300 MHz or 500 MHz NMR spectrometer with tetramethylsilane as an internal standard. Silica gel (EM Science Silica Gel 60, 230-400 Mesh) was used for all flash chromatography. Thin layer chromatography was performed using Silica Gel 60 F254 (EM Science).

2.1.1. Microscopy

Phase contrast optical micrographs were taken using a Zeiss ICM 405 microscope (Carl Zeiss, Thornwood, NY) with 40 × (NA 0.75) phase contrast lenses. Transmission electron micrographs (TEM) were obtained using a Philips EM 410 electron microscope operating at an acceleration potential of 80 kV. Samples were applied to Formvar-coated 150 mesh copper TEM sample grids with and without negative stain (2% aqueous ammonium molybdate pH 5.0).

2.1.2. Calorimetery

Differential scanning calorimetery was performed using a Seiko DSC-100 high sensitivity calorimeter. Known concentrations of aqueous lipid suspensions (50 μl) were heated from 1–95°C at 1°C/min in 70 μl silver calorimetery pans. In order to insure proper hydration of the lipids, each sample was pre-heated under the same conditions before the actual run. After calorimetery, the pan's contents were analyzed for decomposition by thin layer chromatography.

2.2. Chemical synthesis

The chemical synthesis of amphiphiles not commercially available is shown in Fig. 2.

2.2.1. N-hydroxysuccinimide ester of nervonic acid

The *N*-hydroxysuccinimide ester of nervonic acid was prepared according to Lapidot et al. (1967): Nervonic acid (0.558 g, 1.52 mmol) and *N*-hydroxysuccinimide (0.175 g, 1.52 mmol) in 60 ml anhydrous EtOAc were stirred overnight with dicyclohexylcarbodiimide (0.314 g, 1.52 mmol). The white precipitate was removed, and the supernatant evaporated in vacuo. The residue was recrystallized from EtOH to provide the *N*-hydroxysuccinimide ester of nervonic acid as fine white needles (0.539 g, 76%): m.p. 58–60°C; R_f ($CHCl_3$) 0.24; ^{1}H NMR (500 MHz) 5.35 (t, 2H, C-15, C-16, J = 5.0 Hz), 2.81 (d, 4H, succinimide, J = 4.5 Hz), 2.60 (t, 2H, C-2, J = 7.6 Hz), 2.01 (m, 4H, C-14, C-17), 1.74 (t, 2H, C-3, J = 5.5 Hz), 0.88 (t, 3H, C-24, J = 7.0 Hz).

2.2.2. N-nervonoyl ceramide (24:1-cer)

N-nervonoyl ceramide was prepared according to Ong and Brady (1972): The *N*-hydroxysuccinimide ester of nervonic acid (0.092 g, 198.4 μmol)

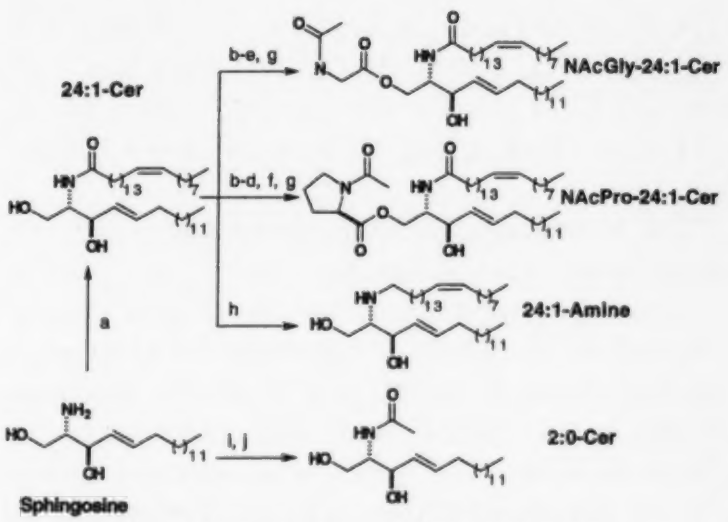

Fig. 2. Chemical synthesis of amphiphiles not commercially purchased.

and sphingosine (0.062 g, 207.0 μmol) were dissolved in 10 ml anhydrous THF and stirred overnight under Ar. Flash chromatography (1:0:0-90:10:1 $CHCl_3$:MeOH:NH_4OH) provided *N*-nervonoyl ceramide as a white solid (0.118 g, 91%): R_f (9:1 $CHCl_3$:MeOH) 0.47; ^1H NMR (500 MHz) 6.22 (d, 1H, NH, J = 7.1 Hz), 5.73 (m, 1H, C-5), 5.53 (dd, 1H, C-4, J = 6.3, 15.4 Hz), 5.34 (t, 2H, C-15′, C-16′, J = 4.6 Hz), 4.30 (t, 1H, C-3, J = 3.8 Hz), 3.96 (dd, 1H, C-1, J = 3.1, 11.0 Hz), 3.91 (m, 1H, C-2), 3.71 (dd, 1H, C-1, J = 3.1, 11.0 Hz), 2.22 (t, 2H, C-2′, J = 7.4 Hz), 2.00 (m, 6H, C-6, C-14′, C-17′), 1.60 (t, 2H, C-3′, J = 7.8 Hz), 0.88 (t, 6H, C-18, C-24′, J = 6.3 Hz).

2.2.3. *N-nervonoyl-1-0-triphenylmethyl ceramide*

N-nervonoyl ceramide (0.018 g, 27.8 mmol), triphenylmethyl chloride (0.015 g, 55.5 mmol) and *N*,*N*-dimethyl-4-aminopyridine (0.007 g, 55.5 mmol) in 20 ml anhydrous toluene were refluxed for 16 h under Ar. The solvent was removed by rotary evaporation and the residue purified by flash chromatography (9:1-1:1 hexane:EtOAc) to provide *N*-nervonoyl-1-0-triphenylmethyl ceramide as a white solid (0.018 g, 72%): R_f (3:1 hexane:EtOAc) 0.21; ^1H NMR (300 MHz) 7.42-7.22 (m, 15H), 6.06 (d, 1H, NH, J = 7.9 Hz), 5.63 (m, 1H, C-5), 5.35 (t, 2H, C-15′, C-16′, J = 5.2 Hz), 5.25 (dd, 1H, C-4, J = 6.2, 15.5 Hz), 4.18 (m, 1H, C-2), 3.69 (dd, 1H, C-3, J = 3.9, 7.8 Hz), 3.32 (m, 2H, C-1), 2.20 (t, 2H, C-2′, J = 8.1 Hz), 2.00 (m, 4H, C-14′, C-17′), 1.91 (m, 2H, C-6), 1.64 (m, 2H, C-3′), 0.88 (t, 6H, C-18, C-24′, J = 6.5 Hz).

2.2.4. *N-nervonoyl-1-0-triphenylmethyl-3-O-[t-butyldiphenylsilyl] ceramide*

The title compound was prepared according to Numata et al. (1988): *N*-nervonoyl-1-*O*-triphenylmethyl ceramide (0.108 g, 0.12 mmol), imidazole (0.066 g, 0.97 mmol), and *t*-butylchlorodiphenylsilane (0.79 ml, 3.03 mmol) were stirred 19.5 h in 25 ml anhydrous DMF under Ar. Twenty five ml of H_2O was added and the mixture extracted with Et_2O (3 × 15 ml). The ether extracts were washed with 10 ml H_2O and 10 ml saturated NaCl (aq). Flash chromatography (15:1-2:1 hexane:EtOAc and 1 ml triethylamine/100 ml of solvent) provided the title compound as a white solid (0.090 g, 66%): R_f (3:1 hexane:EtOAc) 0.66; ^1H NMR (300 MHz) 7.70–7.23 (m, 25H), 5.36–5.25 (m, 5H, NH, C-4, C-5, C-15′, C-16′), 4.39 (t, 1H, C-3, J = 5.4 Hz), 4.18 (m, 1H, C-2), 3.94 (dd, 1H, C-1, J = 5.1, 10.4 Hz), 3.70 (dd, 1H, C-1, J = 5.1, 10.4 Hz), 2.00 (m, 4H, C-14′, C-17′), 1.86 (m, 2H, C-2′), 1.72 (m, 2H, C-6), 1.44 (m, 2H, C-3′), 1.04 (s, 9H, *t*-Bu), 0.88 (t, 6H, C-18, C-24′, J = 7.3 Hz).

2.2.5. *N-nervonoyl-3-O-[t-butyldiphenylsilyl] ceramide*

Compound 2.2.4. was detritylated according to Koike et al. (1986): *N*-nervonoyl-1-0-triphenylmethyl-3-*O*-[*t*-butyldiphenylsilyl] ceramide (0.093 g, 82.4 μmol) was stirred for 4 h with *p*-toluenesulfonic acid monohydrate (0.010 g, 49.4 μmol) in 20 ml 1:1 MeOH:CH_2Cl_2. Et_2O (40 ml) was added, and the solution was washed with 10 ml 5% $NaHCO_3$ (aq) and 10 ml H_2O. Flash chromatography (6:1-0:1 hexane:EtOAc) provided product as a white solid (0.034 g, 47%): R_f (3:1 hexane:EtOAc) 0.15; ^1H NMR (500 MHz) 7.67–7.30 (m, 10H), 5.93 (d, 1H, NH, J = 7.1 Hz), 5.42–5.33 (m, 4H, C-4, C-5, C-15′, C-16′), 4.34 (t, 1H, C-3, J = 4.5 Hz), 3.97-3.82 (m, 2H, C-1, C-2), 3.60 (m, 1H, C-1), 3.14 (m, 1H, OH), 1.98 (m, 6H, C-2′, C-14′, C-17′), 1.86 (m, 2H, C-6), 1.55 (m, 2H, C-3′), 1.07 (s, 9H, *t*-Bu), 0.88 (t, 6H, C-18, C-24′, J = 7.0 Hz).

2.2.6. *N-nervonoyl-1-O-(N-acetyl-glycine)-3-O-[t-butyldiphenylsilyl] ceramide*

Amino acylation was adapted from the procedure of Neises and Steglich (1985): *N*-nervonoyl-3-*O*-[*t*-butyldiphenylsilyl] ceramide (0.021 g, 23.7 μmol), *N*-acetyl-glycine (0.006 g, 47.4 μmol), and *N*,*N*-dimethyl-4-aminopyridine (0.06 g, 47.4 mmol) in 21 ml 2:5 CH_3CN:CH_2Cl_2 (anhydrous) were stirred for 2 h under Ar. Dicyclohexylcarbodiimide (0.010 g, 47.4 mmol) was added and the reaction stirred for 24 h under Ar. The solvents were removed in vacuo. Flash chromatography (5:1-0:1 hexane:EtOAc) of the residue provided product as a white solid (0.016 g, 70%):

R_f (1:1 hexane:EtOAc) 0.23; ^{1}H NMR (300 MHz) 7.67–7.57 (dd, 4H), 7.46–7.33 (m, 6H), 6.09 (bs, 1H, NH), 5.51–5.29 (m, 4H, C-4, C-5, C-15′, C-16′), 4.40 (dd, 1H, C-3, J = 2.9, 10.8 Hz), 4.26 (bs, 2H, C-1), 4.12 (m, 1H, C-2), 3.93 (t, 2H, glycine, J = 11.3 Hz), 2.00 (s, 3H, NAc), 1.05 (s, 9H, *t*-Bu), 0.88 (t, 6H, C-18, C-24′, J = 6.4 Hz).

2.2.7. N-nervonoyl-1-O-(N-acetyl-l-proline)-3-O-[t-butyldiphenylsilyl] ceramide

N-nervonoyl-3-*O*-[*t*-butyldiphenylsilyl] ceramide (0.034 g, 38.4 μmol), *N*-acetyl-L-proline (0.010 g, 63.6 μmol), and *N*,*N*-dimethyl-4-aminopyridine (0.011 g, 90.0 μmol) in 15 ml 1:2 CH_3CN:CH_2Cl_2 (anhydrous) were stirred for 30 min under Ar. Dicyclohexylcarbodiimide (0.012 g, 57.5 μmol) was added and the reaction stirred for 24 h under Ar. The white precipitate was removed by vacuum filtration and the solvents evaporated in vacuo. Flash chromatography (6:1-0:1 hexane:EtOAc) of the residue provided product as a white solid (0.029 g, 74%): R_f (1:1 hexane:EtOAc) 0.29; ^{1}H NMR (300 MHz) 7.68–7.59 (dd, 4H), 7.43–7.26 (m, 6H), 6.14 (d, 1H, NH, J = 8.8 Hz), 5.41–5.29 (m, 3H, C-4, C-15′, C-16′), 5.14 (dt, 1H, C-5, J = 4.0, 8.8 Hz), 4.69 (d, 1H, α, J = 7.7 Hz), 4.39 (dd, 1H, C-3, J = 3.6, 8.1 Hz), 4.27 (d, 2H, C-1, J = 12.4 Hz), 4.02 (t, 1H, C-2, J = 7.3 Hz), 3.44 (t, 2H, δ, J = 6.4 Hz), 2.16 (m, 2H, β), 2.02-1.91 (m, 13H, C-6, C-2′, C-14′, C-17′, γ, NAc), 1.49 (m, 2H, C-3′), 1.03 (s, 9H, *t*-Bu), 0.88 (t, 6H, C-18, C-24′, J = 6.6 Hz).

2.2.8. N-nervonoyl-1-O-(N-acetyl-glycine) ceramide (NAcGly-24:1-Cer)

Desilylation was performed according to Hanessian and Lavallee (1975): *N*-nervonoyl-1-*O*-(*N*-acetyl-glycine)-3-*O*-[*t*-butyldiphenylsilyl] ceramide (0.009 g, 9.1 μmol) in 10 ml anhydrous THF and 0.01 ml 1.0 M *n*-butylammonium fluoride in THF were stirred for 1 h under Ar. The solvent was removed by rotary evaporation and the residue purified by flash chromatography (2:1-0:1 hexane:EtOAc) to provide compound product as a white solid (0.002 g, 29%): R_f (EtOAc) 0.25; ^{1}H NMR (500 MHz) 6.11 (bs, 1H, NH), 6.01 (bs, 1H, NH), 5.76 (dt, 1H, C-5, J = 6.7, 15.5), 5.48 (dd, 1H, C-4, J = 6.2, 15.5 Hz), 5.33 (t, 2H, C-15′, C-16′, J = 5.0 Hz), 4.33 (d, 2H, gly), 4.15 (m, 2H, C-2, C-3), 4.00 (m, 2H, C-1), 2.17 (t, 2H, C-2′, J = 4.4 Hz), 2.03 (s, 3H, NAc), 0.86 (t, 6H, C-18, C-24′, J = 6.6 Hz).

2.2.9. N-nervonoyl-1-O-(N-acetyl-L-proline) ceramide (NAcPro-24:1-Cer)

Desilylation was performed according to Hanessian and Lavallee (1975): *N*-nervonoyl-1-*O*-(*N*-acetyl-L-proline)-3-*O*-[*t*-butyldiphenylsilyl] ceramide (0.021 g, 20.5 μmol) in 12 ml anhydrous THF and 0.01 ml 1.0 M *n*-butylammonium fluoride (in THF) were stirred for 2 h under Ar. The solvent was removed by rotary evaporation and the residue purified by flash chromatography (3:1-0:1 hexane:EtOAc) to provide product as a white solid (0.011 g, 69%): R_f (EtOAc) 0.31; ^{1}H NMR (500 MHz) 6.66 (d, 1H, NH, J = 7.7 Hz), 5.70 (dt, 1H, C-5, J = 6.7, 15.5), 5.47 (dd, 1H, C-4, J = 6.2, 15.5 Hz), 5.32 (t, 2H, C-15′, C-16′, J = 4.6 Hz), 4.47-4.26 (m, 4H, α, C-2, C-3), 4.06 (bs, 2H, C-1), 3.64-3.50 (dm, 2H, δ), 3.30 (bs, 1H, OH), 2.18 (m, 2H, β), 2.07 (s, 3H, NAc), 1.99 (m, 10H, C-6, C-2′, C-14′, C-17′, γ), 1.59 (m, 2H, C-3′), 0.86 (t, 6H, C-18, C-24′, J = 7.0 Hz).

2.2.10. N-tetracos-15(Z)-enyl-sphingosine (24:1-Amine)

Nervonoyl ceramide (0.015 g, 23.1 μmol) was dissolved in 12 ml anhydrous Et_2O. Lithium aluminum hydride (0.021 g, 485.8 μmol) was added, and the mixture was refluxed for 1.5 h and then stirred at room temperature for 48 h. Excess hydride reagent was quenched by addition of 3 ml EtOAc followed by 1 drop of saturated Na_2SO_4 (aq). The resultant white precipitate was filtered and the solution purified by flash chromatography (1:0-20:1 $CHCl_3$:MeOH) to provide 24:1-Amine as a white solid (0.051 g, 33%): R_f (9:1 $CHCl_3$:MeOH) 0.19; ^{1}H NMR (500 MHz) 5.87 (dt, 1H, C-5, J = 6.7, 15.5), 5.45 (dd, 1H, C-4, J = 5.7, 15.5 Hz), 5.35 (t, 2H, C-15′, C-16′, J = 4.9 Hz), 4.69 (bs, C-3), 4.05 (dd, 1H, C-1, J = 4.6, 12.9 Hz), 3.90 (dd, 1H, C-1, J = 4.6, 12.9 Hz), 3.46 (m, 1H, NH), 2.95 (m, 1H, C-2), 2.08-1.99 (m, 6H, C-6, C-14′, C-17′), 0.88 (t, 6H, C-18, C-24′, J = 6.7 Hz).

2.2.11. N-acetyl ceramide (2:0-Cer)

Sphingosine (0.008 g, 26.7 μmol) in 10 ml 1:1 CH_2Cl_2:pyridine and 1 ml acetic anhydride were stirred for 4.5 h and then evaporated in vacuo. The residue was dissolved in 10 ml MeOH, and K_2CO_3 (0.025 g, 180.8 μmol) was added. After stirring overnight, the solvent was removed in vacuo and the residue purified by flash chromatography (1:0-20:1 $CHCl_3$:MeOH) to provide product as a white solid (0.004 g, 44%): R_f (9:1 $CHCl_3$:MeOH) 0.35; ^{1}H NMR (300 MHz) 6.32 (d, 1H, NH), 5.78 (dt, 1H, C-5, J = 6.7, 15.5), 5.50 (dd, 1H, C-4, J = 3.6, 15.5 Hz), 4.35 (bt, 1H, C-3, J = 5.8 Hz), 3.97 (dd, 1H, C-1, J = 3.5, 11.2 Hz), 3.93 (m, 1H, C-2), 3.71 (dd, 1H, C-1, J = 3.5, 11.2 Hz), 2.30 (t, 3H, C-6, J = 9.0 Hz), 2.05 (m, 7H, NAc, C-14′, C-17′), 0.89 (t, 3H, C-18 J = 3.4 Hz).

2.3. Microstructure formation studies

Several methods were employed to determine the tendency of the lipids to form HARMs.

2.3.1. DMF/H_2O

Amphiphile (0.1 mg) was dissolved in anhydrous DMF so that the concentration was 1.0 mM. Water was added in $\approx$10 μl increments until the solution became cloudy. The resulting suspensions were incubated at 20°C for 2–24 h. For larger amounts of amphiphile, water was added with vortex mixing ($\approx$3 s) between additions.

2.3.1.1. DMF/saline. To NFA-GalCer dissolved in DMF (0.8 mg/ml) was added a saturated saline solution of LiBr, LiCl, NaCl or $MgCl_2$ (50% by volume) while hand swirling. The resultant white gel was incubated at 20°C for 16 h.

2.3.2. Pyridine evaporation

Amphiphile (0.1 mg) was dissolved in pyridine so that the concentration was 1.0 mM. Water was added in $\approx$10 μl increments until the solution became cloudy. The samples were incubated at 20°C so that solvent evaporated and a precipitate formed (typically 24–48 h).

2.3.3. Freeze-thaw

This procedure follows the method of Kulkarni et al. (1995): Amphiphile (0.1 mg) was suspended in 1 ml of aqueous buffer (10 mM KH_2PO_4, 100 mM NaCl, 1.5 mM NaN_3, pH = 6.6). The suspension was thrice incubated for 3 min at 90°C, vortexed for 20 s at room temperature and then sonicated (Laboratory Supplies and Company, Hicksville, NY, output 80 KC) for 20 s at room temperature. Next, the suspension was placed in *i*-PrOH/dry ice for 2 min, thawed rapidly ($\approx$20 s) and then vortexed 20 s. The freeze-thaw procedure was repeated three times except that after the last freeze the sample was allowed to warm to room temperature over 1.5 h.

2.3.4. Thermal cycling

This procedure follows the method of Archibald and Yager (1992): amphiphile was placed in ethylene glycol:water (either 19:1) to a final concentration of 1 mg/ml. The suspension was thrice incubated for 10 min at 99°C and sonicated at 50°C (12 × 30 s pulses with 30 s pauses). After the final sonication, the suspension was allowed to cool from 99°C to room temperature over 2.5 h.

2.4. Mixed lipid studies

2.4.1. NAcPro-24:1-Cer: 24:1-GalCer

Particles from the mixtures of NAcPro-24:1-Cer and 24:1-GalCer (1:1, 1:3, 1:5, 1:7 mol:mol) were prepared as in Section 2.3.1 and incubated for 24 h at 20°C. In order to determine the ratio of the lipids incorporated in the HARMs, samples were pelleted (2500 g for 30 min) and a known percentage of the supernatants removed. Supernatants and pellets were dried in vacuo and the residues weighed (mass corrections were made for the portion of supernatant that remained with the pellet).

2.4.1.1. Qualitative assessment of incorporation. Supernatant and pellet material (from Section 2.4.1) was heavily spotted on silica TLC plates (4 cm length) and developed in EtOAc. The plates were stained with phosphomolybdic acid reagent (Aldrich, Milwaukee, WI) and then heated (NAcPro-24:1-Cer R_f = 0.31 and 24:1-GalCer R_f = 0.0).

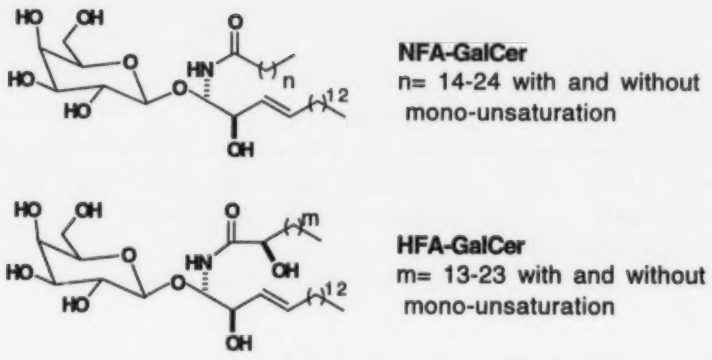

Fig. 3. The subfractions of Galactocerebroside.

2.4.1.2. A quantitative assessment of incorporation. The dried and weighed 1:3 doped supernatant and pellet (Section 2.4.1) were dissolved in CD_3OD and the amphiphile ratio was determined by comparison of the integrands of the NAcPro-24:1-Cer αH (δ 4.5) and vinyl NMR signals.

2.4.2. NAcPro-24:1-Cer : 24:1-Cer

The procedure was identical to the NAcPro-24:1-Cer: nervonoyl-GalCer mixed lipid study (Section 2.4.1). Compositional NMR analysis of the amphiphile ratio was effected by comparison of the integrands of NAcPro-24:1-Cer αH (δ 4.5) and C-4 vinyl (δ 5.4) in CD_3OD.

2.4.3. NAcPro-24:1-Cer : NFA-GalCer

Performed as per NAcPro-24:1-Cer: nervonoyl-GalCer mixing studies (Section 2.4.1).

3. Results and discussion

3.1. HFA-GalCer and NFA-GalCer

GalCer can be divided into two major subfractions, that containing non-hydroxy fatty acids (NFA-GalCer) and that containing more polar α-hydroxy fatty acids (HFA-GalCer) (Fig. 3). The ability of GalCer to self-organize has been previously investigated using pyridine evaporation, thermal and freeze-thaw cycling techniques to form microstructures. Archibald and Yager found that submission of HFA-GalCer to pyridine evaporation or thermal cycling resulted in the formation of cochleate cylinders of dimensions 5–30 × 100–300 nm, whereas NFA-GalCer formed tubules and helical ribbons using pyridine evaporation or thermal cycling (Archibald and Yager, 1992). Brown and coworkers, using a freeze-thaw method, found that NFA-GalCer formed tubules and multilamellar liposomes (Kulkarni et al., 1995). All of these observations were confirmed in the present study.

In the present study, we developed a DMF/H_2O precipitation method for the exploration of HARM formation. Application of this technique to NFA-GalCer yields cylindrical structures (Fig. 4a). Submission of HFA-GalCer to aggregate formation using DMF/H_2O provides cylindrical structures with some helical ribbon content (Fig. 4b). This is in stark contrast to the cochleate cylinders produced by thermal cycling of the same amphiphile (Fig. 4c). Depending on the formation methodology the HFA-GalCer HARMs have different dimensions (Table 1). This implies that the formation methodology/solvent can affect HARM morphology.

The differences in tubule diameter and length may be influenced by solvent, electrolytes, lipid concentration and variations in composition of NFA-GalCer and HFA-GalCer. The freeze-thaw method uses 100 mM NaCl whereas the DMF/H_2O method is carried out in the absence of salt. An early tubule formation theory argues that a tilted phase of chiral molecules must be electrostatically polarized which, in turn, can cause a membrane strip to collapse upon itself and form a cylinder (de Gennes, 1987). In this theory salts should increase the tubule radius because electrostatic interactions would be shielded. Along this line, Archibald noted that the dimensions of HFA-GalCer cochleate cylinders formed by thermal cycling were larger when formed in the presence of salt (Archibald and Yager, 1992). Furthermore, in the better studied HARMs composed of phosphatidylcholine with butadiyne containing hydrocarbon chains, the tubule outer diameter increased as the salt concentration was increased in the formation medium, but this is possibly the result of more bilayers in the tubule

Table 1
Effect of formation methodology/solvent on HARM morphology

Amphiphile	T_m (°C)[a]	Method[b]	Structure	Size (nm)[c]	Reference
NFA-GalCer	69.5	Pyridine	Tube/ribbon	$85 \times \geq 10\,000$	Archibald and Yager (1992)
		Thermal	Tube/ribbon	$85 \times \geq 10\,000$	Archibald and Yager (1992)
		Freeze	Tube/liposome	$40–100 \times 500–5000$	Kulkarni et al. (1995)
		Freeze	Cochleate	$100–150 \times \geq 1000$	Kulkarni and Brown (1996)
	70.5	DMF(35)	Tube	25–50	
HFA-GalCer		Pyridine	Cochleate	$5–30 \times 10\,000–30\,000$	Archibald and Yager (1992)
		Thermal	Cochleate	$5–30 \times 10\,000–30\,000$	Archibald and Yager (1992)
	66.1	DMF(35)	Tube/ribbon	$40–100 \times 2000–7000$	
24:1-GalCer	59.3	Freeze	Tube	$25–30 \times 250–400$	Kulkarni et al. (1995)
		DMF(12)	Tube	20×600	
22:1-GalCer		Freeze	Tube	25–35	Kulkarni and Brown (1996)
20:1-GalCer		Freeze	Ribbon	40–50	Kulkarni and Brown (1996)
18:1-GalCer		Freeze	Liposome/sheet/ multilamellar tubes		Kulkarni and Brown (1996)
	45.4	DMF(35)	Tube	30–60	
24:0-GalCer	84.1	Freeze	Ribbon	$100–250 \times 2000–10\,000$	Kulkarni et al. (1995)
18:0-GalCer	81.1	DMF(35)	Ribbon	$8–16 \times 1250$	
16:0-GalCer		H_2O	Tube	100	Curatolo and Neuringer (1986)
		DMF(35)	Ribbon	24	
Psychosine		Thermal	Amorphous		Archibald and Yager (1992)
	40.1	DMF(105)	Fiber	$50 \times 13\,000$	
Sphingosine		MeOH(12)	Cochleate	50	Archibald and Mann (1993)
	42.3	DMF(150)	Amorphous		
Ceramide		Thermal	Amorphous		Archibald and Yager (1992)
24:1-Cer		Thermal	Amorphous		
		Pyridine	Amorphous		
	71.8	DMF(3)	Tube	$55–140 \times 40\,000$	
18:1-Cer	48.3	DMF(70)	Tube	19–24	
18:0-Cer		DMF(35)	Ribbon	8–11	
16:0-Cer		DMF(35)	Ribbon	11–25	
6:0-Cer	51.2	DMF(70)	Tube	50–75	
2:0-Cer	49.3	DMF(30)	Amorphous		
24:1-Amine	36.5	DMF(20)	Amorphous		
NAcPro-24:1-Cer	42.0	Pyridine	Amorphous		
		Thermal	Amorphous		
		Freeze	Amorphous		
		DMF(16)	Amorphous		
NAcGly-24:1-Cer		DMF(30)	Tube	110–200	

[a] T_m measurements refer to the major transition.
[b] Pyridine refers to pyridine evaporation method. Thermal and freeze refer to thermal and freeze-thaw cycling methodologies, respectively. DMF refers to DMF/H_2O precipitation. MeOH refers to MeOH/H_2O precipitation. H_2O refers to suspension of lyophilized powder in water. The number in parenthesis refers to the volume percentage of water added.
[c] If no second measurement is provided then the length was indeterminate.

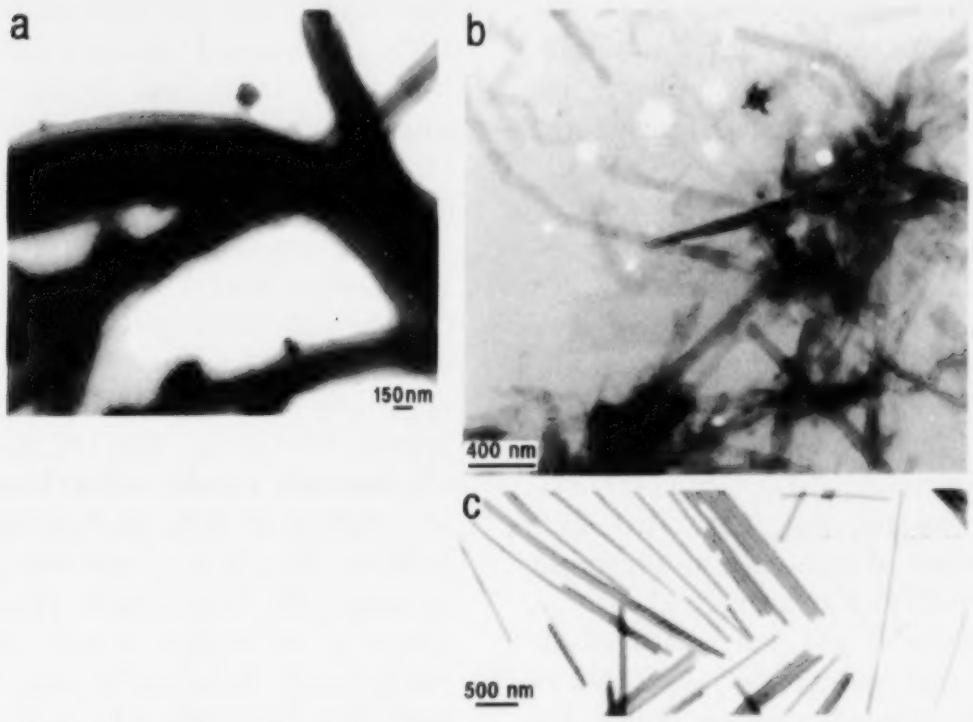

Fig. 4. Negatively stained TEM images of: (a) NFA-GalCer HARMs formed by DMF/H_2O precipitation; (b) HFA-GalCer HARMs formed by DMF/H_2O precipitation shows some helical ribbon content in addition to cylindrical structures; (c) HFA-GalCer formed by thermal cycling.

(Chappell and Yager, 1991). In the present study, it was found that precipitation of NFA-GalCer from DMF by addition of saturated saline solutions (LiBr, LiCl, NaCl, $MgCl_2$) rather than pure water still forms cylindrical structures; however, the tubules are irregularly shaped but, on average, the dimensions remain unchanged (not shown).

The lipid concentration should not perturb tubule formation as long as the lipid concentration is above the critical micelle concentration (CMC). In all cases, cerebroside concentration was above 12.3 μM. Although not measured, cerebroside CMC values should be vanishingly low (less than nanomolar) due to high, long-chain fatty acid content, thus transfer of lipid to crystalline HARMs from other fluid lipid structures, at room temperature, should be prohibitively slow. On the other hand, lipid concentration may affect tubule wall thickness (Spector et al., 1996). As shown in studies involving solvent precipitation of phosphatidylcholine containing butadiyne hydrocarbon chains, more concentrated lipid solutions formed wider tubules due to multiple bilayer wrappings. Contrary to this, 24:1-GalCer tubules prepared by DMF/H_2O precipitation are narrower than Brown's freeze-thaw tubules (described later) despite being formed from a more concentrated solution (Kulkarni et al., 1995). Lastly, natural variations in HFA- and NFA-GalCer fatty acid composition and unsaturation may affect HARM formation and dimensions.

3.2. Pure galactocerebrosides

To better understand the structural requirements of cerebrosides to form HARMs, single molecular specifies of GalCer-based amphiphiles were studied. Using DMF/H_2O precipitation, pure 24:1-GalCer forms cylindrical nanostructures of dimensions 20×600 nm as evidenced by negative stained TEM (Fig. 5a, Table 1). Using freeze-thaw cycling, Brown found that 24:1-GalCer formed tubules, but these are shorter and wider than those formed by the DMF/H_2O method (Table 1) (Kulkarni et al., 1995).

Replacement of the mono-unsaturated, 24-carbon fatty acid chain with the shorter mono-unsaturated oleoyl chain (18:1-GalCer) results in an amphiphile that also forms cylindrical structures using DMF/H_2O precipitation (Fig. 5b, Table 1). In contrast, Brown found that 18:1-GalCer formed multilamellar cylindrical bilayers, sheets, and liposomes when prepared by freeze-thaw cycling (Kulkarni and Brown, 1996). Brown also studied 22:1-GalCer which formed cylindrical microstructures whereas 20:1-GalCer formed helical ribbons (Kulkarni and Brown, 1996).

The cerebroside lignoceroyl-GalCer (24:0-GalCer), which possesses the long saturated 24:0 chain formed a mixture of ribbons and liposomes using freeze-thaw cycling (Kulkarni et al., 1995). In the present study we found that stearoyl-GalCer (18:0-GalCer) and palmitoyl-GalCer (16:0-GalCer) also form twisted ribbons using the DMF/H_2O method (Fig. 5c–d, Table 1). In contrast, Curatolo reported that lyophilized 16:0-GalCer formed 100 nm diameter multilamellar tubules when suspended in water (Curatolo and Neuringer, 1986). In general, the widths of DMF/H_2O precipitated ribbons are narrower than Brown's freeze-thawed 24:0-GalCer ribbons. The lengths were also many microns but intertwining of the fibers made this difficult to accurately determine.

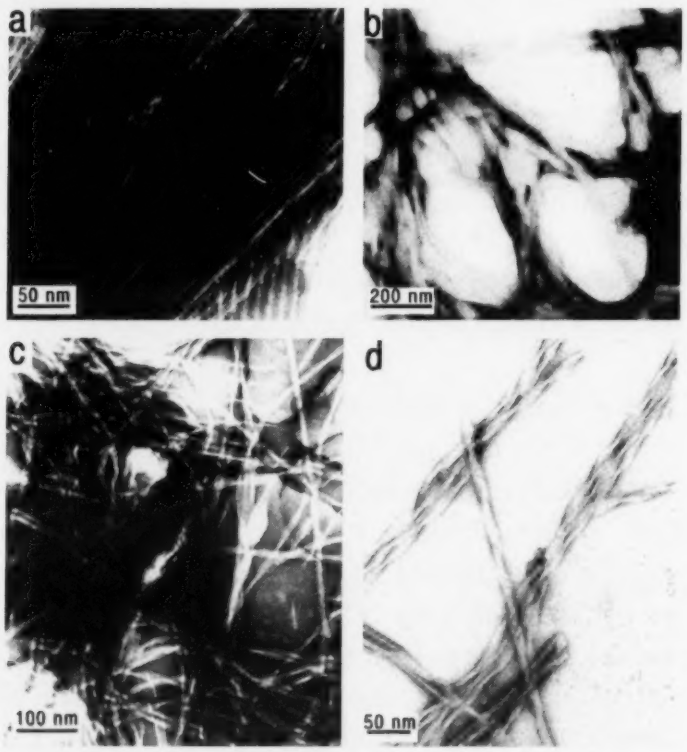

Fig. 5. Negatively stained, DMF/H_2O precipitated TEM images of: (a) 24:1-GalCer: (b) 18:1-GalCer: (c) 18:0-GalCer: (d) 16:0-GalCer. The unsaturated sphingolipids form cylindrical structures whereas the saturated lipids form ribbons.

The unsaturated fatty acyl containing GalCer, 24:1-GalCer and 18:1-GalCer, as well as NFA-GalCer and HFA-GalCer HARMs are suspected to be hollow based on negative stained TEM. A negatively stained TEM of a lipid HARM should appear uniformly dark if the object is solid whereas two parallel white lines would be prevalent against a dark background if the object is hollow. Brown's freeze-fracture electron microscopy on freeze-thaw prepared 24:1-GalCer which is of similar size to that of DMF/H_2O precipitated 24:1-GalCer was unable to unambiguously determine if the tubules were hollow or filled. The observation that some HFA-GalCer tubules terminate in a helical ribbon (upper left of Fig. 4b) supports the idea that these structures may be hollow.

Collectively, these results suggest that a mono-unsaturated fatty acyl chain GalCer is required for cylindrical tubule formation. Furthermore, the unsaturation requirement is not alleviated by shortening the acyl chain. Perhaps the *cis* double bond kink in 24:1-GalCer and 18:1-GalCer fatty acids relaxes the rigidity of the system allowing tubule formation as opposed to ribbons (reduces curvature frustration).

3.3. Pure ceramides

Despite earlier reports that ceramide containing a mixture of fatty acid chains was unable to form HARMs by thermal cycling, (Archibald and Yager, 1992) we are able to show that pure single molecular species of ceramide form HARMs using DMF/H_2O precipitation. Nervonoyl-Cer (24:1-Cer) forms cylindrical HARMs when viewed by TEM (Fig. 6a, Table 1). The density appears uniform across the diameter of the fibers suggesting that solid or cochleate cylinders are being formed. This is in contrast to the cylindrical nanostructures formed from 24:1-GalCer prepared under identical conditions (compare Fig. 5a

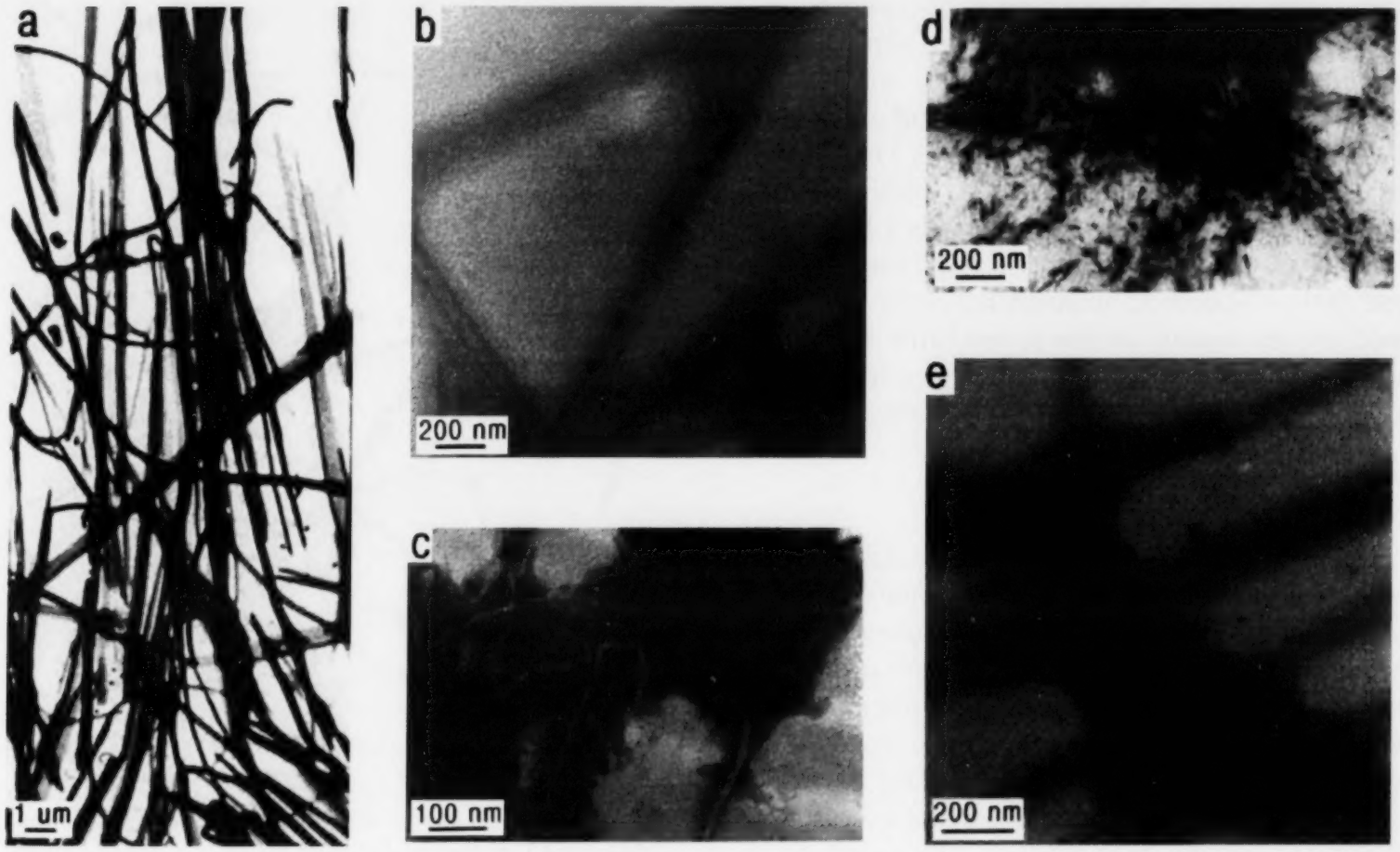

Fig. 6. TEM images of DMF/H_2O precipitated: (a) unstained 24:1-Cer; (b) negatively stained 18:1-Cer; (c) negatively stained 18:0-Cer; (d) negatively stained 16:0-Cer; (e) unstained 6:0-Cer.

and Fig. 6a). Similar dense HARMs are formed from pure oleoyl-Cer (18:1-Cer, Fig. 6b, Table 1). On the other hand, long saturated fatty acid chain-containing ceramides, stearoyl-Cer (18:0-Cer) and palmitoyl-Cer (16:0-Cer) form twisted ribbons (Fig. 6(c and d), Table 1). The short chain hexanoyl-Cer (6:0-Cer) forms cylindrical structures (Fig. 6e, Table 1), and acetyl-Cer (2:0-Cer) did not form any discernible HARMs (not shown).

These results imply that the hydrophilic galactose headgroup is not required for HARM formation, although the presence of the carbohydrate influences HARM morphology. Furthermore, the ceramide study supports the notion that the presence of saturated fatty acid chains favors twisted ribbons whereas the presence of mono-unsaturated chains favors cylindrical HARMs (except for 6:0-Cer). In the case of 6:0-Cer, the fatty acid side chain is much shorter than the sphingosine hydrocarbon chain. This high degree of chain mismatch may cause the headgroup to have a larger tilt relative to the hydrophobic alkyl region which may cause a significant packing perturbation.

3.4. Amide importance

The importance of an amide versus a secondary amine in the ceramide structure for HARM formation was studied by preparing the secondary amine formed by hydride reduction of the amide in 24:1-Cer (24:1-Amine). DMF/H_2O precipitation of 24:1-amine produced amorphous structures with no discernible HARMs (not shown). Amphiphiles that lack the fatty acid chain were also studied. Archibald and Mann reported that sphingosine formed cochleate cylinders by precipitation from water by addition of methanol (Archibald and Mann, 1993). In the present

study, DMF/H_2O precipitation of sphingosine fails to form any HARMs. On the other hand, psychosine (GalCer lacking the fatty acid chain) forms long thin HARMs when submitted to DMF/H_2O treatment (Fig. 7, Table 1). In contrast, thermal cycling of aqueous dispersions of psychosine did not lead to HARMs (Archibald and Yager, 1992). Collectively, these results suggest that two-chain sphingolipids require the presence of an amide carbonyl to form HARMs; however, a single-chain sphingolipid does not require the carbonyl for HARM formation.

3.5. Amino acid headgroups

One of the long term goals of these studies is to fabricate HARMs composed of lipidated drugs, such as lipidated peptides, for novel drug delivery strategies. In this context, we examined cerebroside-based amphiphiles that contain amino acids in place of the polar galactose headgroup. Modeling studies using proline in place of galactose suggested that microstructure formation would not be perturbed. Proline, like galactose, is cyclic, has hydrogen bond donors/acceptors and is of comparable size. Surprisingly, NAcPro-24:1-Cer did not form any discrete HARMs using

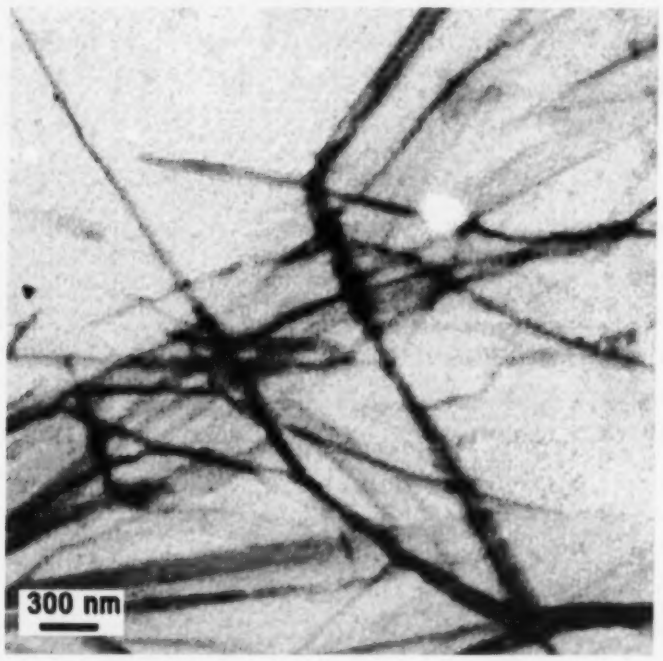

Fig. 7. TEM image of unstained, DMF/H_2O precipitated psychosine.

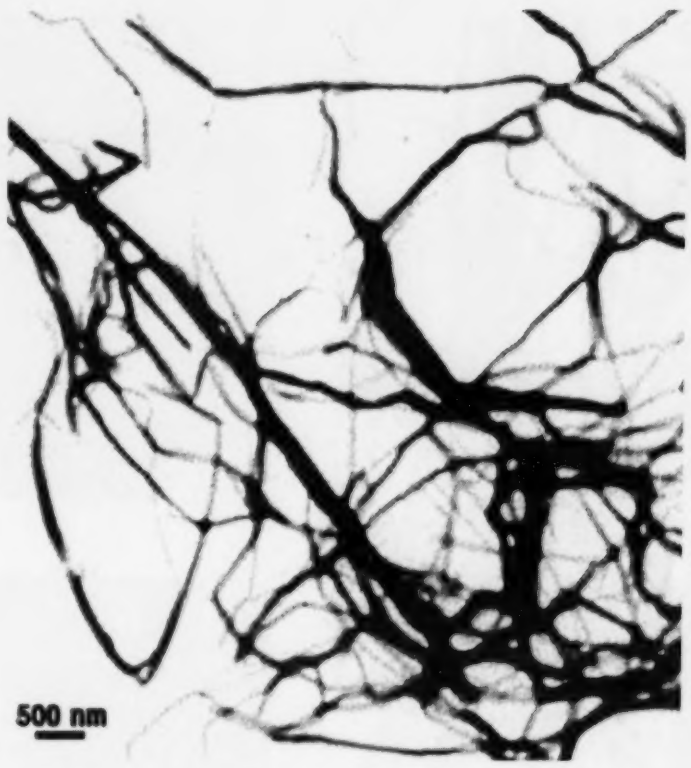

Fig. 8. TEM image of negatively stained, DMF/H_2O precipitated NAcGly-24:1-Cer.

DMF/H_2O precipitation, thermal or freeze-thaw cycling, or pyridine evaporation (not shown). NAcGly-24:1-Cer, containing a smaller head group, forms long thin fibers (Fig. 8). Clearly the structure of the head group greatly influences HARM morphology.

3.6. Mixed lipid systems

Despite the inability of NAcPro-24:1-Cer to independently form discrete structures, we tried doping NAcPro-24:1-Cer into HARMs formed from 24:1-Cer, 24:1-GalCer, or NFA-GalCer (matrix). An intimate mixture of NAcPro-24:1-Cer with the HARM-forming amphiphile was first made using DMF. Water was then added to cause precipitation (Section 2). TEM images of the structures are similar to those obtained from DMF/H_2O precipitation of the pure matrix amphiphiles. The HARMs were isolated and submitted to compositional analysis by NMR (Section 2). NAcPro-24:1-Cer could be doped into either 24:1-GalCer or NFA-GalCer HARMs up to 25 mole% without affecting tubule formation. On average, the tubules were very long (micrometers)

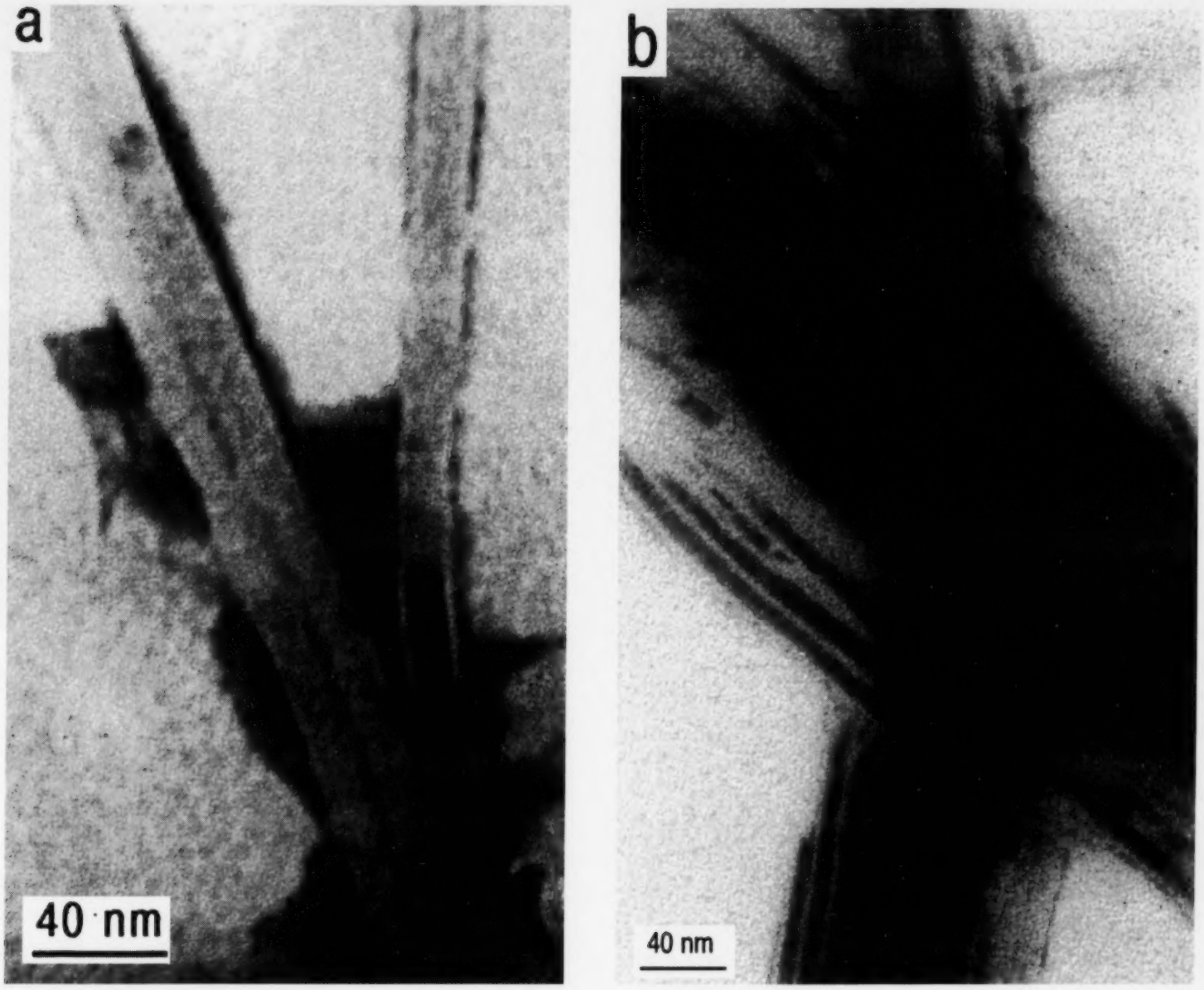

Fig. 9. TEM images of negatively stained, DMF/H_2O precipitated: (a) 1:3 NAcPro-24:1-Cer : 24:1-GalCer mixed lipid system: (b) 1:3 NAcPro-24:1-Cer : NFA-GalCer mixed lipid system.

with diameters of 13-20 nm (Fig. 9, Table 1). Increasing the NAcPro-24:1-Cer component beyond 25% resulted in the formation of vesicles in addition to tubules (not shown).

NMR analysis of the tubules formed from the 1:3 NAcPro-24:1-Cer : 24:1-GalCer or 1:3 NAcPro-24:1-Cer : NFA-GalCer mixed lipid systems retain the original solution composition. In the former case, differential scanning calorimetery was employed to determine if the lipids were ideally mixed (Fig. 10). Intimately mixed binary systems should show a single exothermic peak between the T_m of either pure component alone. As evident, the doped systems exhibit two transitions near the T_m of pure lipids implying non-ideal mixing. The presence of small transitions before and after the main NFA-GalCer transition (52 and 75°C) may be due to the presence of previously reported metastable states (Maggio et al., 1985a,b; Haas and Shipley, 1995; Curatolo, 1982). In pure NFA-GalCer, these metastable states are related to the hydration state of the sphingolipid. Furthermore, the magnitude and onset temperature of these transitions are dependent on heating and cooling rates.

Since differential scanning calorimetry indicated non-ideal mixing, a second set of experiments with NAcPro-24:1-Cer and NFA-GalCer was carried out to help determine the spatial relationship of the two lipids. Three mixing possibilities are: (1) both lipids coexist in the HARM as an intimate mixture; (2) both lipids coexist in the HARM but one lipid coats the other lipid's microstructure as it precipitates from solution; or (3) both lipids independently precipitate from solution. NFA-GalCer and NAcPro-24:1-Cer microstructures were independently formed by DMF/H_2O precipitation (Fig. 11). The cerebroside, when visualized by optical microscopy, appear as thread-like structures with occasional 'crystalline' patches whereas NAcPro-24 : 1-Cer forms only spherical aggregates. The independently precipitated species were then combined so that their concentration was identical to that of the 1:3 NAcPro-24:1-Cer : NFA-GalCer mixed lipid system. Optical micrographs of the preformed then mixed lipids show a mixture of threads with spherical aggregates, whereas intimately mixed, then precipitated lipids, show only threads. Thus possibility (3) is eliminated.

Solubility arguments may be able to distinguish between coating and coprecipitation. A more hydrophobic lipid should precipitate first upon water addition to an organic solution of mixed lipids. Although not measured, NAcPro-24:1-Cer

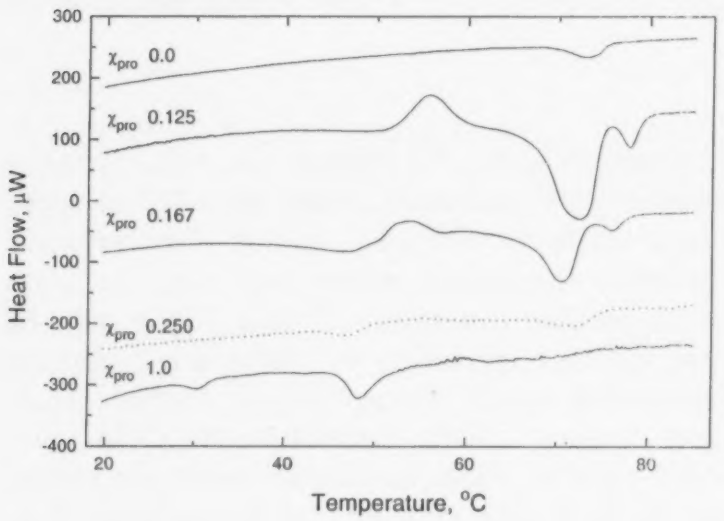

Fig. 10. Differential scanning calorimetery heating curves of NAcPro-24:1-Cer : NFA-GalCer mixed lipid systems showing that the lipids are not ideally mixed.

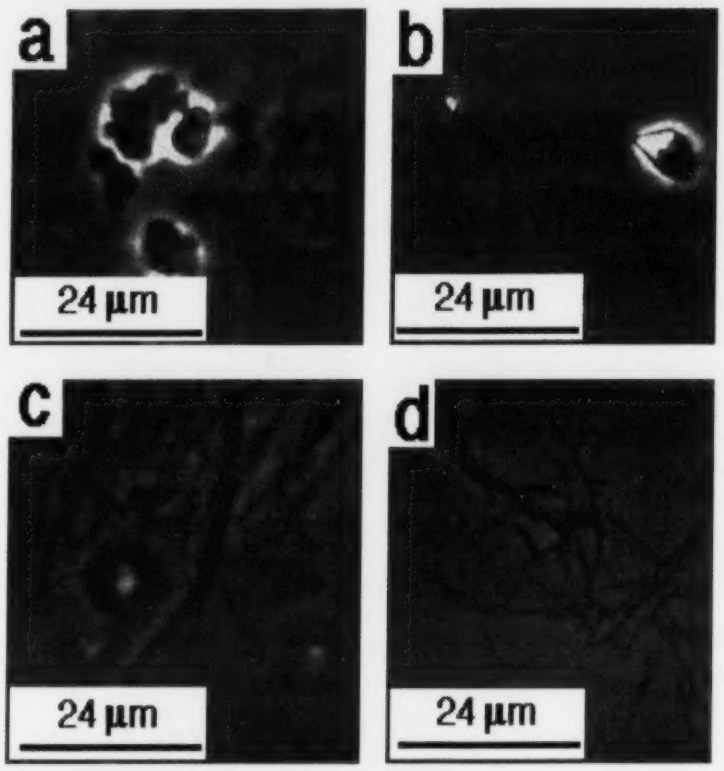

Fig. 11. Optical micrographs of DMF/H_2O precipitated: (a) NAcPro-24:1-Cer; (b) NFA-GalCer; (c) NAcPro-24:1-Cer: NFA-GalCer aggregates independently formed then mixed; (d) NAcPro-24:1-Cer : NFA-GalCer mixed and then precipitated.

should be more hydrophobic than NFA-GalCer; therefore, the amino acylated lipid should fall out of solution and form circular aggregates which would then be coated by NFA-GalCer. However, this is clearly not the case since only thread-like HARMs were seen in the mixed lipid precipitation.

In contrast, HARMs formed from NAcPro-24:1-Cer mixed into 24:1-Cer exclude the amino acid-containing amphiphile as revealed by NMR analysis and thin layer chromatography. Furthermore, optical microscopy showed that mixtures containing NAcPro-24:1-Cer in excess of 17 mole% also contained liposomes in addition to HARMs (not shown). Although it is known that sphingolipids can partition into fluid membranes to some degree, the precipitated HARMs are crystalline (Merrill et al., 1991; Maggio et al., 1985a,b). Furthermore, exclusion from the nanostructures during precipitation may be caused by significant differences in the amphiphile's aqueous solubility.

4. Conclusion

The demonstrated fact that ceramides with amino acid headgroups can independently or as a component of a binary mixture form HARMs is encouraging from the drug delivery point of view. It may be possible to attach peptides of therapeutic interest to the ceramide and still form HARMs. Due to tight crystal packing, such aggregates may be protected from proteolysis and provide a means for constant drug release via dissolution only from the ends of the HARMs. In addition, such microstructures are unlikely to be rapidly cleared from the body due to their lipophilicity, and thus may be immobilized at the desired site of action. This potentially long in vivo lifetime may make such a delivery system an ideal way to induce a strong immune response, and this may be useful for vaccine development. In mixed lipid systems, the inexpensive mixed NFA-GalCer may be used in place of the more costly single molecular galactocerebroside species. A final advantage of using such a natural tubule-forming lipid is that the human body already has enzymes that can metabolize the drug-stripped lipid core.

Acknowledgements

The authors wish to express their thanks to Ms. K. Lee for helpful discussions. This work was supported by a grant from the Whitaker Foundation.

References

Archibald, D.D., Mann, S., 1993. Structural studies of lipid fibers formed by sphingosine. Biochim. Biophys. Acta 1166, 154–162.

Archibald, D.D., Mann, S., 1994. Self-assembled microstructures from 1,2-ethanediol suspensions of pure and binary mixtures of neutral and acidic biological galactosylceramides. Chem. Phys. Lipids 69, 51–64.

Archibald, D.D., Yager, P., 1992. Microstructural polymorphism in bovine brain galactocerebroside and its two major subfractions. Biochemistry 31, 9045–9055.

Behroozi, F., Orman, M., Reese, R., Stockton, W., Calvert, J., Rachford, F., Schoen, P., 1990. Interaction of metallized tubules with electromagnetic radiation. J. Appl. Phys. 68 (7), 3688–3693.

Bielawska, A., Greenberg, M., Perry, D., Jayadev, S., Shayman, J., McKay, C., Hannun, Y., 1996. (1S,2R)-D-erythro-2-(*N*-myristoylamino)-1-phenyl-1-propanol as an inhibitor of ceramidase. J. Biol. Chem. 271, 12646–12654.

Chappell, J., Yager, P., 1991. Electrolyte effects on bilayer tubule formation by a diacetylenic phospholipid. Biophys. J. 60, 952–956.

Chappell, J.S., Yager, P., 1992. Formation of mineral microstructures with a high aspect ratio from phospholipid bilayer tubules. J. Mat. Sci. Lett. 11, 633–636.

Curatolo, W., 1982. Thermal behavior of fractionated and unfractionated bovine brain cerebrosides. Biochemistry 21, 1761–1764.

Curatolo, W., Neuringer, L., 1986. The effects of cerebrosides on model membrane shape. J. Biol. Chem. 261, 17177–17182.

de Gennes, P.-G., 1987. Electrostatic buckling of chiral lipid bilayers. C.R. Acad. Sci. Paris 304, 259.

Fuhrhop, J., Schnieder, P., Boekema, E., Helfrich, W., 1988. Lipid bilayer fibers from diastereomeric and enantiomeric *N*-octylaldonamides. J. Am. Chem. Soc. 107, 510–512.

Georger, J., Price, R., Singh, A., Schnur, J.M., Schoen, P.E., Yager, P., 1987. Helical and tubular microstructures formed by polymerizable phosphatidylcholines. J. Am. Chem. Soc. 109, 6169–6175.

Haas, N., Shipley, G., 1995. Structure and properties of *N*-palmitoleoylgalactosylsphingosine (cerebroside). Biochim. Biophys. Acta 1240, 133–141.

Hanessian, S., Lavallee, P., 1975. The Preparation and Synthetic Utility of *tert*-Butyldiphenylsilyl Ethers. Can. J. Chem. 53, 2975–2977.

Koike, K., Numata, M., Sugimoto, M., Nakahara, Y., Ogawa, T., 1986. A Highly Stereoselective Synthesis of 2(S), 3(R), 4E-and 2(S), 3(R), 4Z-*N*-Tetracosanoylsphingenine from D-Glucose. Carbohydr. Res. 158, 113–123.

Kulkarni, V.S., Anderson, W.H., Brown, R.E., 1995. Bilayer nanotubes and helical ribbons formed by hydrated galactosylceramides: Acyl chain and headgroup effects. Biophys. J. 69, 1976–1986.

Kulkarni, V.S., Brown, R.E., 1996. Modulation of tubular microstructural self-assembly in galactosylceramides: Influence of *N*-linked fatty acyl chains. Proc. Microsc. Microanal., 936–937.

Lapidot, Y., Rappoport, S., Wolman, Y., 1967. Use of esters of *N*-hydroxysuccinimide in the synthesis of *N*-acylamino acids. J. Lipid Res. 8, 142–145.

Maggio, B., Ariga, T., Sturtevant, J., Yu, K., 1985a. Thermotropic behavior of glycosphingolipids in aqueous dispersions. Biochemistry 24, 1084–1092.

Maggio, B., Ariga, T., Sturtevant, J., Yu, K., 1985b. Thermotropic behavior of binary mixtures of dipalmitoylphosphatidyl choline and glycosphingolipids in aqueous dispersions. Biochim. Biophys. Acta 818, 1–12.

Mann, S., Archibald, D.D., Didymus, J.M., Douglas, T., Heywood, B.R., Meldrum, F.C., Reeves, N.J., 1993. Crystallization at inorganic-organic interfaces: Biominerals and biomimetic synthesis. Science 261, 1286–1292.

Merrill, A., Wang, E., Reddy, R., Menaldino, D., Geisler, V., Liotta, D., 1991. Federation of American Societies for Experimental Biology, 75th Annual Meeting, Atlanta, Georgia (April 21–25, 1991) Part II, Abs. 4032.

Naito, M., Takahashi, K., Hojo, H., 1988. An ultrastructural and experimental study on the development of tubular structures in the lysosomes of gaucher cells. Lab. Invest. 58, 590–598.

Nakashima, N., Asakuma, S., Kim, J., Kunitake, T., 1984. Helical superstructures are formed from chiral ammonium bilayers. Chem. Lett., 1709–1712.

Nandi, N., Bagchi, B., 1996. Molecular origin of the intrinsic bending force for helical morphology observed in chiral amphiphilic assemblies: Concentration and size dependence. J. Am. Chem. Soc. 118, 11208–11216.

Neises, B., Steglich, W., 1985. Esterification of carboxylic acids with Dicyclohexylcarbodiimide/4-Dimethylaminopyridine: *tert*-Butyl Ethyl Fumarate. In: Saucy, G. (ed.), Organic Syntheses, vol. 63. Wiley, New York, pp. 183-187.

Numata, M., Sugimoto, M., Shibayama, S., Ogawa, T., 1988. A total synthesis of Hematoside, α-NeuGc-(2→3)-β-Gal-(1→4)-β-Glc-(1→1)-Cer. Carbohydr. Res. 174, 73–85.

Ong, D., Brady, R., 1972. Synthesis of ceramides using *N*-hydroxysuccinimide esters. J. Lipid Res. 13, 819–822.

Rudolph, A.S., Calvert, J.M., Schoen, P.E., Schnur, J.M., 1988. In: Gaber, B.P., Schnur, J.M., Chapman, D. (eds.), Biotechnological Applications of Lipid Microstructures, Plenum, New York, pp. 305–320.

Schnur, J.M., Price, R., Rudolph, A.S., 1994. Biologically engineered microstructures: controlled release applications. J. Control. Release 28, 3–13.

Schnur, J.M., Price, R., Schoen, P., Yager, P., Calvert, M., Georger, J., Singh, A., 1987. Lipid-based tubule microstructures. Thin Solid Films 152, 181–206.

Schnur, J.M., Schoen, P.E., Yager, P., Calvert, J.M., Georger, J.H., Price, R., 1990. US Patent 4911981.

Selinger, J., MacKintosh, F., Schnur, J., 1996. Theory of cylindrical tubules and helical ribbons of chiral lipid membranes. Phys. Rev. E 53, 3804–3818.

Shimizu, T., Hato, M., 1993. Self-assembling properties of synthetic peptidic lipids. Biochim. Biophys. Acta 1147, 50–58.

Spector, M., Easwaran, K., Jyothi, G., Selinger, J., Singh, A., Schnur, J., 1996. Chiral molecular self-assembly of phospholipid tubules: A circular dichroism study. Proc. Natl. Acad. Sci. USA 93, 12943–12946.

Yager, P., Schoen, P.E., 1984. Formation of tubules by a polymerizable surfactant. Mol. Cryst. Liq. Cryst. 106, 371–381.

Yamada, K., Ihara, H., Ide, T., Fukumoto, T., Hirayama, C., 1984. Formation of helical super structure from single-walled bilayers by amphiphiles with oligo-L-glutamic acid-head group. Chem. Lett. 10, 1713–1716.

Yunis, E.J., Lee, R.E., 1970. Tubules of globoid leukodystrophy: a right handed helix. Science 169, 64–66.

ELSEVIER

Chemistry and Physics of Lipids
88 (1997) 37–43

CPL
CHEMISTRY AND PHYSICS OF LIPIDS

Slow fusion of liposomes composed of membrane-spanning lipids

Marieke G.L. Elferink [a], Jan van Breemen [b], Wil N. Konings [a], Arnold J.M. Driessen [a,*], Jan Wilschut [c]

[a] *Department of Microbiology and the Groningen Biomolecular Sciences and Biotechnology Institute, University of Groningen, Kerklaan 30, 9751 NN Haren, The Netherlands*
[b] *Department of Structural Electronmicroscopy and the Groningen Biomolecular Sciences and Biotechnology Institute, University of Groningen, Nijenborgh 4, 9747 AG Groningen, The Netherlands*
[c] *Department of Physiological Chemistry and the Groningen-Utrecht Institute for Drug Exploration, University of Groningen, Antonie Deusinglaan 1, 9713 AV Groningen, The Netherlands*

Received 10 April 1997; received in revised form 10 June 1997; accepted 11 June 1997

Abstract

The fusion characteristics of large unilamellar liposomes composed of bipolar tetraether lipids extracted from the thermophilic archaeon *Sulfolobus acidocaldarius*, was investigated. These lipids span the entire membrane and form single monolayer liposomes in aqueous media [Elferink, M.G.L., de Wit, J.G., Demel, R., Driessen, A.J.M. and Konings, W.N., (1992) J. Biol. Chem. 267, 1375–1381]. In the presence of calcium-phosphate, slow mixing of the aqueous liposome contents and membrane lipids occurred, demonstrating that these liposomes are fusion-competent. The fusion process was essentially nonleaky. The rate of fusion increased with the pH and the concentration of calcium and phosphate. Fusion resulted in an increase of the size of the liposomes. These data demonstrate that a monolayer organization of lipids in a membrane does not per se interfere with membrane fusion competence. © 1997 Elsevier Science Ireland Ltd.

Keywords: Slow fusion; Liposomes; Membrane-spanning lipids

1. Introduction

Membrane fusion is a critical event in a variety of cell-biological processes. Since the primary function of membranes is to maintain the integrity of cells within their environment and the organi-

* Corresponding author. Tel.: +31 5 3632164; Fax: +31 5 3632154; e-mail: A.J.M.DRIESSEN@BIOL.RUG.NL

PII S0009-3084(97)00044-3

zation of subcellular compartments inside the cell, membrane fusion must be strictly controlled in space and time. Recent investigations of intracellular membrane trafficking and virus–cell interactions have revealed many aspects of the molecular mechanisms involved in the control of biological membrane fusion reactions (White, 1992). Yet, little is known about the physical reorganization of lipids occurring during the process of membrane merging per se.

Early work by Palade (Palade, 1975) revealed pentalaminar structures and trilaminar diaphragms at the contact sites of interacting membranes, suggestive of the involvement of a hemifusion intermediate in the process of membrane merging. In later morphological studies of fusing membranes, relying on modern rapid-freezing techniques, such hemifusion structures were not seen, the earlier observations on trilaminar diaphragms being attributed to fixation artefacts (Chandler and Heuser, 1980). Yet, recent investigation of influenza virus has provided convincing evidence to indicate that membrane fusion of this virus may well proceed via a hemifusion intermediate (Kemble et al., 1994; Melikyan et al., 1995), although, rather than expanding into a extensive area of contact, the hemifusion intermediate would rapidly develop into a localized fusion pore (Palade, 1975; Tse et al., 1993). The notion of a fusion mechanism involving a distinct hemifusion stage with formation of a subsequent pore ('stalk-pore' mechanism) is further supported by recent theoretical and experimental work of Chernomordik and coworkers (Chernomordik et al., 1995).

Formation of a hemifusion intermediate requires a temporal separation of the leaflets of the interacting membranes. In this perspective, we considered it of interest to investigate the fusion competence of lipid vesicles composed of membrane-spanning lipids. Membranes of the thermoacidophile *Sulfolobus acidocaldarius* contain 99.9% tetraether lipids, which are comprised of a mixture of diglyceroltetraethers and nonitolglyceroltetraethers (Langworthy and Pond, 1986). In such systems, where the vesicular membranes, in fact, consist of a monolayer of bipolar lipids, separation of two bilayer leaflets is not possible. Here, we demonstrate that, nevertheless, such vesicles are capable of undergoing nonleaky fusion, be it that this fusion reaction can only be induced under extreme conditions and proceeds at a relatively slow rate.

2. Materials and methods

2.1. Materials

Pyridine-2,6-dicarboxylic acid (DPA) was obtained from Sigma (St. Louis, MO), and $TbCl_3$ was from Aldrich (Bornem, Belgium). *N*-(7-nitro-2,1,3-benzoxadiazol-4-yl)-dipalmitoyl-L-α-phosphatidylethanolamine (*N*-NBD-PE) was obtained from Molecular Probes (Eugene, OR), and *N*-(lissamine rhodamine B sulfonyl) diacyl-phosphatidylethanolamine (*N*-Rh-PE) was from Avanti Polar Lipids (Alabaster, AL). Tetraether lipids were isolated from freeze-dried cells of *S. acidocaldarius* (DSM 639) as described (Elferink et al., 1993), and stored in chloroform/methanol/water (65:25:4, v/v/v) at 4°C.

2.2. Liposomes

Lipids were dried by rotary evaporation and suspended at a concentration of 10 mg/ml in an appropriate buffer system. Lipids were dispersed by sonication using a probe-type sonicator (intervals of 15 s sonication and 45 s rest) at 0°C, and stored in liquid nitrogen. Before use, samples were slowly thawed at room temperature and extruded through Unipore polycarbonate filters (Avestin, Ottawa, Canada), with a pore size of 200 nm, using a small-volume extrusion apparatus (Liposofast™ Basic, Avestin) (MacDonald et al., 1991).

2.3. Fusion assays

Lipid mixing was measured with the resonance energy transfer (RET) fusion assay as described (Struck et al., 1981). Liposomes were formed with and without 0.6 mole% each of *N*-NBD-PE and *N*-Rh-PE, and suspended at 10 mg/ml in buffer A

(100 mM NaCl, 1 mM EDTA, 10 mM Na-Hepes, pH 7.4).The lipid concentration of the liposome preparations was determined by phosphate analysis using Malachite Green (Driessen et al., 1991), after destruction of the liposomes with 70% $HClO_4$. Labelled and nonlabelled liposomes were mixed at a one-to-one ratio, and diluted to a final lipid concentration of 50 μM (lipid phosphorous) in buffer A. Fluorescence measurements were performed at 25°C using a Perkin Elmer LS-50B spectrophotofluorimeter using an excitation and emission wavelength of 465 and 535 nm, respectively. A 520 nm cutoff filter was used in the emission path to eliminate light scattering. Ca^{2+} was added to sample and, after 2 min, fusion was initiated by the addition of phosphate to the indicated concentrations. The maximal extent of fusion was determined by subjecting an undiluted one-to-one mixture of labelled and unlabelled liposomes to two cycles of freezing and thawing. This treatment proved to be sufficient for obtaining complete lipid mixing, and further cycles had little effect on the fluorescence level. Fused liposomes were diluted to 50 μM, and the fluorescence level of this suspension was set to 100%.

Mixing of aqueous contents of the liposomes was determined with the Tb/DPA fusion assay (Wilschut and Papahadjopoulos, 1979; Wilschut et al., 1980). Liposomes were prepared, as described above, at a concentration of 10 mg lipid/ml in buffer B (5 mM $TbCl_3$, 50 mM Na-citrate, 10 mM Na-Hepes, pH 7.4), buffer C (50 mM DPA, 20 mM NaCl, 10 mM Na-Hepes pH 7.4), or buffer D (2.5 mM $TbCl_3$, 25 mM Na-citrate, 25 mM DPA, 10 mM NaCl, 10 mM Na-Hepes, pH 7.4), and are referred to as 'Tb-loaded', 'DPA-loaded' and 'Tb/DPA-loaded' liposomes, respectively. After extrusion, the nonencapsulated material was removed by gel filtration of the liposomes on Sephadex G-25M columns PD-10 (Pharmacia, Uppsala, Sweden) in buffer A. Tb- and DPA-loaded liposomes were mixed at a one-to-one ratio in buffer A at a final lipid concentration of 50 μM. The formation of the Tb/DPA complex was measured with an SLM-4000 spectrophotofluorimeter using excitation and emission wavelengths of 276 and 545 nm, respectively. A 530 nm cutoff filter was placed in the emission path to eliminate possible contributions of light scattering to the signal. Our instrument has a 'T' format design which allows the simultaneous registration of fluorescence and 90° light scattering. Light scattering was measured in the second emission channel at 430 nm wavelength. The temperature of the sample holder was maintained at 25°C, and the solution in the cuvette was continuously stirred. Fusion was induced as described for the RET assay. Tb/DPA-loaded liposomes were used to calibrate the signal to 100% fusion, and to determine liposome leakage under the conditions of the fusion experiment.

2.4. Electron microscopy

Cryo transmission electron microscopy was performed using a Philips CM 10 electron microscope with a liquid nitrogen-cooled gatan cryo device. Sample preparation involved liquid propane fast cooling.

3. Results and discussion

Mixing of membrane lipids was measured with the resonance energy transfer (RET) assay. To ensure that the RET probes mix appropiately with the tetraether lipids a calibration curve was constructed in which the percentage of *N*-NBD-PE fluorescence was plotted as a function of the mol% *N*-NBD-PE and *N*-Rh-PE. *N*-NBD-PE fluorescence in the absence of *N*-Rh-PE was set at 100%. The straight line observed at the lower probe concentrations indicated that distribution of the probes was random. For the fusion experiments liposomes were prepared of tetraether lipids and 0.6 mol % of *N*-NBD-PE and *N*-Rh-PE. Labelled liposomes were mixed with an equal quantity of non-labelled liposomes. Upon fusion, the fluorophores dilute into the plane of the non-labelled liposomes resulting in a decrease in energy transfer efficiency. This can either be measured as an increase in the fluorescence of the energy donor NBD, or a decrease of the fluorescence of the acceptor rhodamine. We monitored the change in the NBD fluorescence intensity. In the presence of calcium and phosphate, a slow

increase in the NBD fluorescence was evident (Fig. 1). This suggests that calcium/phosphate induces fusion and intermixing of membrane lipids among the liposomes composed of tetraether lipids. This process is, however, slow as compared to calcium/phosphate-induced fusion of liposomes composed of acidic phospholipids. Under the conditions employed, it appeared that the fusion reaction was not completed after 110 min.

To ensure that mixing of lipids, as detected with the RET assay, was the result of a bona fide membrane fusion process and not due to just probe transfer, fusion was also measured with the Tb/DPA assay. This method monitors the mixing of aqueous liposomal contents. For this purpose, one population of liposomes was loaded with terbium and the other population was loaded with DPA. Fusion of the liposomes results in the formation of the fluorescent Tb/DPA complex, while a low concentration of the chelator EDTA in the external medium, even in the presence of an excess of calcium, prevents the formation of the complex outside the liposomes. In the presence of calcium and phosphate, a slow increase in the Tb fluorescence occurred, indicative for fusion of the liposomes (Fig. 2A, trace *a*). Fusion proceeded during 110 min up to 38%, with kinetics very similar to the kinetics observed in the lipid mixing experiment (Fig. 1). No signal was observed when liposomes were used that were not loaded with Tb or DPA (trace *b*).

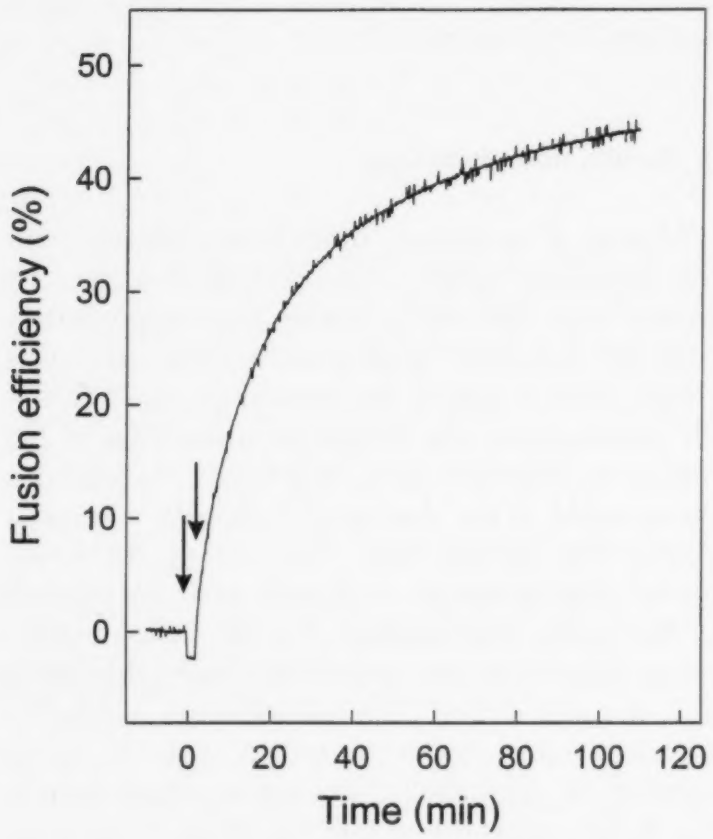

Fig. 1. Mixing of membrane lipids during the calcium-phosphate induced fusion of liposomes composed of tetraether lipids. Liposomes labelled and nonlabelled with 0.6 mol % of *N*-NBD-PE and *N*-Rh-PE were mixed at a one-to-one ratio at a lipid concentration of 50 μM in buffer A. Fusion was initiated, 2 min after the addition of $CaCl_2$ to a final concentration of 4.5 mM (first arrow), by the addition of potassium phosphate to a concentration of 10 mM (second arrow).

Importantly, the calcium/phosphate-induced fusion process was found to be completely non-leaky. Leakage of the liposomal contents was measured with liposomes pre-loaded with the Tb/DPA complex. Fig. 2B shows that there was essentially no leakage of the Tb/DPA complex to the external medium during the first 80 min of the fusion process. At approximately 110 min, the fluorescence level suddenly dropped to lower values. This phenomenon was accompanied with a large increase in the light scattering properties of the sample (Fig. 2C), and has also been observed in studies of calcium/phosphate-induced fusion of acidic phospholipid vesicles (Fraley et al., 1980). It is associated with the conversion of amorphous calcium/phosphate (ACP) into octacalciumphosphate (OCP) and subsequently into hydroapatite (HAP). During this conversion, a thick precipitate appeared in the cuvette that floated on top of the surface and sticked to the glass walls. The drop in fluorescence level was only to a limited extend caused by release of the Tb/DPA complex to the medium. It was primarily due to clearance of the aggregated liposomes from the light beam, since rigorous shaking of the cuvette largely recovered the fluorescence signal (Fig. A and B, broken line). A similar effect was observed when an excess of EDTA (20 mM) was added to the suspension to dissolve the calcium/phosphate precipitates (not shown). This indicates that during the conversion of ACP via OCP to HAP the contents of the fused liposomes is largely retained.

The calcium/phosphate-induced fusion of the tetraether liposomes, as followed by the Tb/DPA assay, was further characterized by varying the

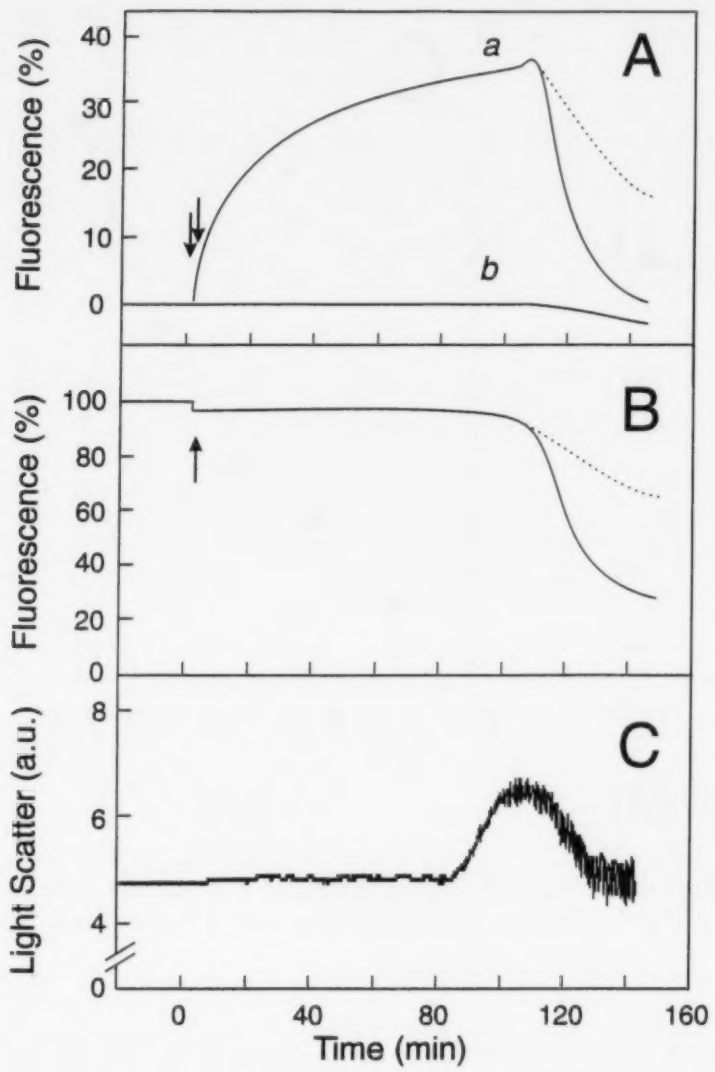

Fig. 2. Mixing of aqueous contents (A), leakage (B) and light scatter (C) during the calcium-phosphate induced fusion of liposomes composed of tetraether lipids. A. Tb-loaded liposomes were mixed at a one-to-one ratio with DPA-loaded liposomes at a lipid concentration of 50 μM in buffer A (trace *a*). Fusion was initiated, 2 min after the addition of $CaCl_2$ to a final concentration of 4.5 mM (arrow 1), by the addition of potassium phosphate to a concentration of 10 mM (arrow 2). Fusion was followed fluorometrically by monitoring the formation of the Tb/DPA complex (solid line). The potential contribution of light-scattering to the fluorescence signal was checked by following the fusion of liposomes that were not loaded with Tb and DPA (trace *b*). B. Leakage of aqueous contents was measured by the use of liposomes loaded with the Tb/DPA complex. The loss of the fluorescent signal after 110 min is largely due to precipitation of the fused liposomes. Manual shaking of the cuvette recovered most of the signal (broken lines). C. Light-scattering was measured at 430 nm at 90° incidence of the excitation beam.

concentration of Ca^{2+} and phosphate, and by changing the pH of the suspension (Fig. 3). The rate at which calcium/phosphate converts from ACP to HAP determines in part the kinetics of vesicle fusion and leakage in a calcium/phosphate-containing medium, and the kinetics of the calcium/phosphate conversions, in turn, are strongly dependent of the relative concentrations of calcium and phosphate and on the pH. Fusion was strictly Ca^{2+} dependent (Fig. 3A). In the absence of phosphate, very slow fusion of the liposomes occurred in the presence of high Ca^{2+} concentrations, i.e. ≥ 20 mM (data not shown). High phosphate concentrations, i.e. >15 mM, favour the formation of the hydroxyapatite complex, and caused the rapid formation of aggregates and leakage. A similar phenomenon was observed when the pH was increased to values above pH 7.4. An increase in the temperature resulted in apparent lower fusion rates. For instance, at 50°C, already 3 min after the addition of phosphate the formation of a thick precipitate was evident. This made the liposomes almost completely leaky.

The liposomes fused upon calcium/phosphate addition were examined with cryo transmission electronmicroscopy. For this purpose, it was necessary to use a lipid concentration that was at least four-fold higher than that used in the fluorescence fusion assays. Under these conditions, also a high concentration of Ca^{2+} is required to induce fusion. By following the light scatter properties of the liposomal suspension it was established that the time course of fusion was almost identical to the one shown in Fig. 2, when 7.5 mM of Ca^{2+} was used instead of 4.5 mM. The electron micrographs show that the liposomes increased in size when exposed to calcium/phosphate for increasing periods of time (Fig. 4A,B). At the later stage of the fusion, extensive aggregation of the liposomes was evident (Fig. 4C).

This study demonstrates that liposomes composed of bipolar membrane-spanning lipids have the ability to undergo membrane fusion, as evidenced by the occurrence of mixing of the lipids of the interacting vesicles and nonleaky coalescence of their aqueous volumes. Fusion could only be induced by calcium/phosphate and it proceeded at a comparatively slow rate. Calcium/phosphate-induced fusion has also been observed for anionic phospholipid vesicles, composed of

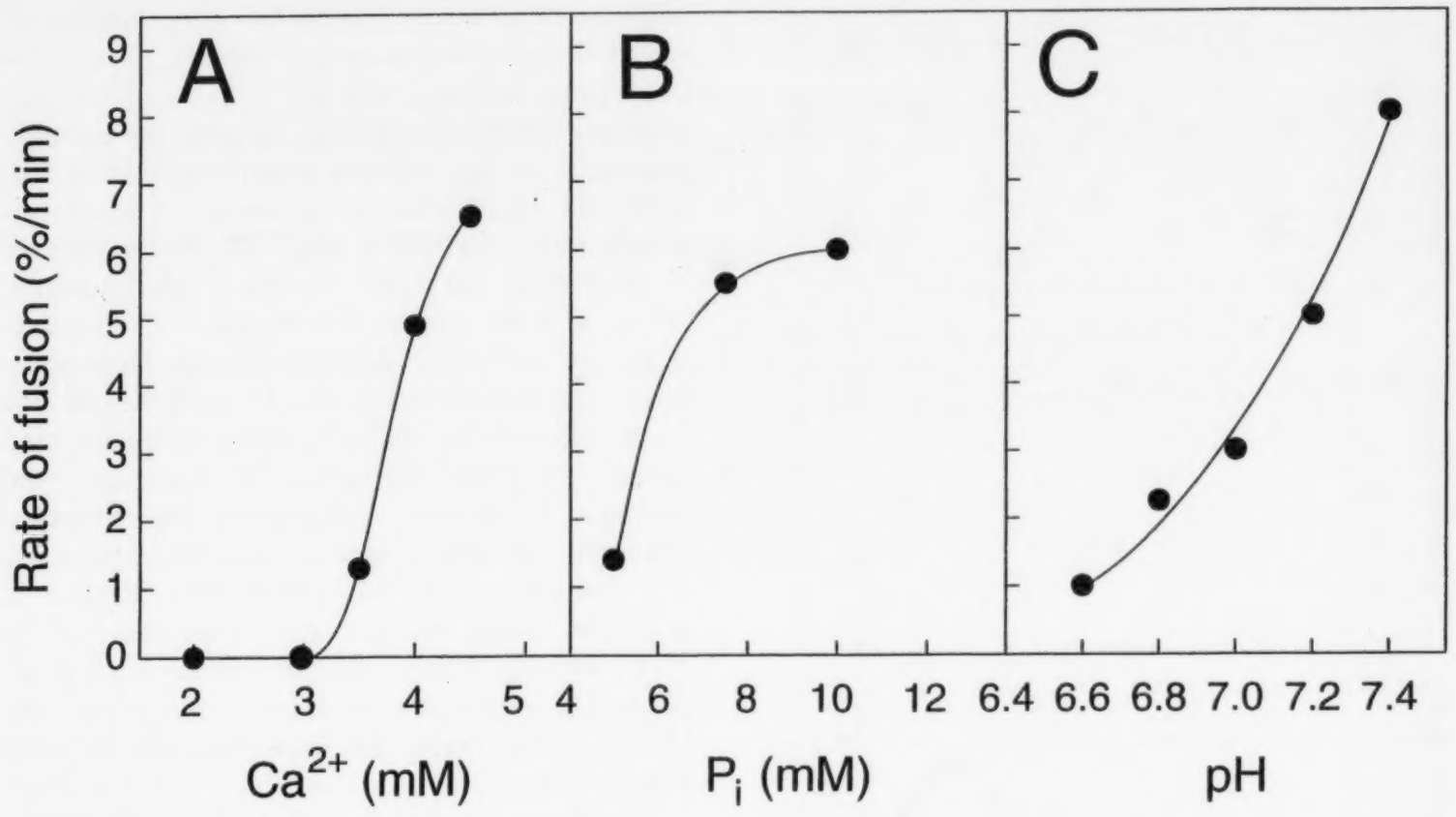

Fig. 3. Ca^{2+} (A), phosphate (B), and pH (C) dependency of fusion of liposomes composed of tetraether lipids. Fusion was measured with the Tb/DPA assay, as described in Section 2 and in the legend to Fig. 2. The assay conditions used were: 4.5 mM $CaCl_2$, 10 mM potassium phosphate, pH of 7.4, unless indicated otherwise.

phosphatidylserine and cholesterol (Fraley et al., 1980), and for erythrocyte ghosts (Hoekstra et al., 1983). In these earlier investigations, like in the present study, the rates of fusion and vesicle leakage were strongly dependent on the relative concentrations of calcium and phosphate, the pH, and the temperature, each affecting the rate of conversion of the calcium/phosphate complex from ACP to HAP. It is not clear how calcium/phosphate mediates membrane fusion. The initial complex, formed upon addition of phosphate to calcium, presumably establishes close contact between the interacting membranes, the subsequent conversions in the complex inducing membrane merging and ultimate lysis when HAP is formed. Irrespective of the precise mechanism, it is interesting that membranes consisting of bipolar lipids fuse at all under these conditions. Freeze-fracturing experiments show that there is no fracture plane to break the membranes into two leaflets, rather cross-fracturing of the whole membrane was observed (Elferink et al., 1992). This is consistent with a monolayer organization of the membrane. Accordingly, it is very unlikely that the fusion process in this system involves temporal separation of membrane leaflets. This implies that membranes can fuse through a mechanism that does not involve a distinct hemifusion intermediate. Whether or not this is of physiological relevance remains to be seen. Perhaps the slow rate of fusion seen in our present study, as compared to the faster fusion of anionic phospholipid vesicles (Fraley et al., 1980) or erythrocyte ghosts (Hoekstra et al., 1983) in the presence of calcium/phosphate reflects the large energy barrier involved in fusion of membranes composed of bipolar lipids. This would argue in favour of fusion of 'normal' bilayer membranes composed of monopolar lipids through a process that does involve transient separation of the two bilayer leaflets and the formation of a hemifusion intermediate structure. Yet we feel it is intriguing, that in principle, membranes may have access to alternative mechanisms of fusion.

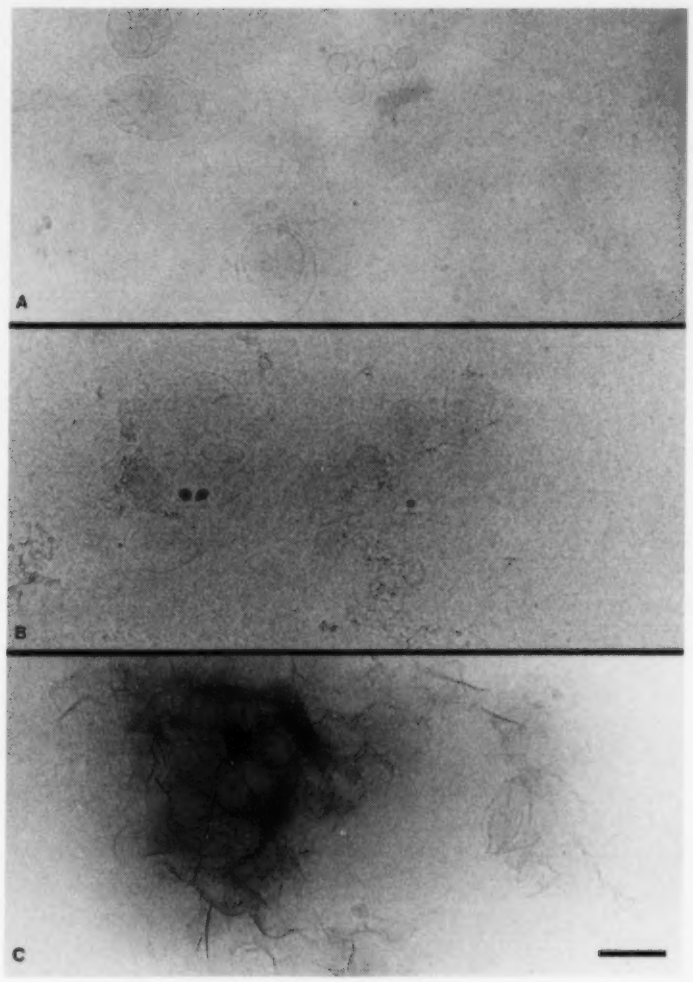

Fig. 4. Cryo transmission electron microscopical images of different stages of the calcium-phosphate induced fusion of liposomes composed of tetraether lipids. Liposomes were suspended in buffer A at a lipid concentration of 200 μM. Fusion was induced by the addition of $CaCl_2$ and potassium phosphate (pH 7.4) to final concentrations of 7.5 mM and 10 mM, respectively. The images represent 0 (A), 60 (B), and 120 (C) min time points. Bar represents 0.2 μm.

References

Chandler, D.E., Heuser, J.E., 1980. Arrest of membrane fusion events in mast cells by Quick-freezing. J. Cell Biol. 86, 666–674.

Chernomordik, L., Kozlov, M., Zimmerberg, J., 1995. Lipids in biological membrane fusion. J. Membrane Biol. 146, 1–19.

Driessen, A.J.M., Brundage, L., Hendrick, J.P., Schiebel, E., Wickner, W., 1991. Preprotein translocase of *Escherichia coli*: Solubilization, purification and reconstitution of the integral membrane subunits SecY/E. Methods Cell Biol. 34, 147–165.

Elferink, M.G.L., de Wit, J.G., Demel, R., Driessen, A.J.M., Konings, W.N., 1992. Functional reconstitution of membrane proteins in monolayer liposomes from bipolar lipids of *Sulfolobus acidocaldarius*. J. Biol. Chem. 276, 1375–1381.

Elferink, M.G.L., de Wit, J.G., Driessen, A.J.M., Konings, W.N., 1993. Energy transducing properties of primary proton pumps reconstituted into archaeal bipolar lipid vesicles. Eur. J. Biochem. 214, 917–925.

Fraley, R., Wilschut, J., Düzgünes, N., Smith, C., Papahadjopuolos, D., 1980. Studies on the mechanism of membrane fusion: Role of phosphate in promoting calcium ion induced fusion of phospholipid vesicles. Biochemistry 19, 6021–6029.

Hoekstra, D., Wilschut, J., Scherphof, G., 1983. Kinetics of calcium phosphate-induced fusion of human ghosts monitored by mixing of aqueous contents. Biochim. Biophys. Acta 732, 327–331.

Kemble, G.W., Danieli, T., White, J.M., 1994. Lipid-anchored influenza hemagglutin promotes hemifusion, not complete fusion. Cell 76, 383–391.

Langworthy, T.A., Pond, J.L., 1986. Archaebacterial ether lipids and chemotaxonomy. Syst. Appl. Microbiol. 7, 235–257.

MacDonald, R.C., MacDonald, R.I., Menco, B.Ph.M., Takeshita, K., Subbarao, N.K., Hu, L., 1991. Small-volume extrusion apparatus for preparation of large, unilamellar vesicles. Biochim. Biophys. Acta 1061, 297–303.

Melikyan, G.B., White, J.M., Cohen, F.S., 1995. GPI-anchored influenza hemagglutinin induces hemifusion to both red blood cells and planar bilayer membranes. J. Cell Biol. 131, 679–691.

Palade, G.E., 1975. Intracellular aspects of the process of protein synthesis. Science 189, 347–358.

Struck, D.K., Hoekstra, D., Pagano, R.E., 1981. Use of resonance energy transfer to monitor membrane fusion. Biochemistry 20, 4093–4099.

Tse, F.W., Iwata, A., Almers, W., 1993. Membrane flux through the pore formed by a fusogenic viral envelope protein during cell fusion. J. Cell Biol. 121, 543–552.

White, J.M., 1992. Membrane fusion. Science 258, 917–924.

Wilschut, J., Papahadjopoulos, D., 1979. Ca^{2+}-induced fusion of phosphilipid vesicles monitored by mixing of aqueous contents. Nature 281, 690–692.

Wilschut, J., Düzgünes, N., Fraley, R., Papahadjopoulos, D., 1980. Studies on the mechanism of membrane fusion: Kinetics of calcium ion induced fusion of phosphatidylserine vesicles followed by a new assay for mixing of aqueous vesicle content. Biochemistry 19, 6011–6021.

ELSEVIER

Chemistry and Physics of Lipids
88 (1997) 45–61

CPL
CHEMISTRY AND
PHYSICS OF LIPIDS

Mixing behavior of saturated short-chain phosphatidylcholines and fatty acids
Eutectic points, liquid and solid phase immiscibility, non-lamellar phases

Rumiana Koynova [a,*], Boris Tenchov [a], Gert Rapp [b]

[a] *Institute of Biophysics, Bulgarian Academy of Sciences, 1113 Sofia, Bulgaria*
[b] *European Molecular Biology Laboratory-Outstation Hamburg, D-22603 Hamburg, Germany*

Received 14 April 1997; received in revised form 9 June 1997; accepted 11 June 1997

Abstract

Phase diagrams of the hydrated pseudo-binary mixtures dilauroylphosphatidylcholine (DLPC)/lauric acid (LA) and dimyristoylphosphatidylcholine (DMPC)/myristic acid (MA) have been constructed using high-sensitivity DSC and time-resolved X-ray diffraction. They are of a different type compared to those of the longer chain phosphatidylcholine (PC)/fatty acid (FA) mixtures, the latter being of maximum azeotropic point type. Eutectic points were distinguished in the phase diagrams, at 75 mol% MA and 49°C for the DMPC/MA mixture, and at ca. 67 mol% LA and 29°C for the DLPC/LA mixture. Regions of liquid–liquid and solid–solid phase separation have been located according to the shape of the phase diagrams and observed by X-ray diffraction. Limited regions (2–4°C) of liquid–liquid phase immiscibility exist at compositions with slightly prevailing fatty acid molar content. For instance, at 67 mol% MA, a phase separation between L_α phase enriched in DMPC and H_{II} phase enriched in MA takes place in the temperature range 51–55°C. Solid phase immiscibility is detected between 60 and 90 mol% fatty acid. The studied PC/FA mixtures form compound subgel polymorphic phases (one in the DMPC/MA mixture, with DMPC/MA 1:2 molar stoichiometry, and two in the DLPC/LA mixture, with about 40 and 60 mol% LA, respectively) upon low-temperature equilibration. In the liquid crystalline phase region, non-lamellar phases dominate the phase diagrams, especially in their fatty acid-rich part. With increasing FA content, the nonlamellar phases arrange in the sequence: bicontinuous cubic phases (Ia3d, Pn3m, Im3m) → hexagonal phase (H_{II}) → micellar cubic

Abbreviations: PC, phosphatidylcholine; DLPC, 1,2-dilauroyl-*sn*-glycero-3-phosphocholine; DMPC, 1,2-dimyristoyl-*sn*-glycero-3-phosphocholine; DPPC, 1,2-dipalmitoyl-*sn*-glycero-3-phospho-choline; DSPC, 1,2-distearoyl-*sn*-glycero-3-phosphocholine; LA, lauric acid; MA, myristic acid; PA, palmitic acid; SA, stearic acid; FA, fatty acid; DSC, differential scanning calorimetry; TRXRD, time-resolved X-ray diffraction.

* Corresponding author. Tel.: +359 2 7133685; fax: +359 2 9712493; e-mail: rkoynova@obzor.bio21.acad.bg and rkoynova@bgearn.acad.bg

PII S0009-3084(97)00043-1

phase (Fd3m) → isotropic phase (I). With the eutectic composition (75 mol% MA), only H_{II} phase is detected above the melting transition in the DMPC/MA mixture. At higher FA content (85 mol%), micellar cubic phase of space group Fd3m form in the two PC/FA mixtures. At lower FA content (< 75 mol%), at least three cubic phases (Ia3d, Pn3m, Im3m) form. The order of their appearance with increasing temperature varies with the PC/FA ratio. They exist either as single phases or concurrently to the H_{II} phase. © 1997 Elsevier Science Ireland Ltd.

Keywords: Cubic phase; Lipid membrane; Mesophase; Phase diagram; Phase transition; Polymorphism; (DSC, TRXRD)

1. Introduction

The mesomorphic properties of lipids and lipid mixtures in the liquid crystalline phase have long been subject of distinct interest in view of their relation to the functional phase state of the biological membranes. The scientific interest has further increased after emerging the view that non-lamellar lipid phases are biologically relevant (see. e.g. Seddon, 1990). One such example of lipid mixtures displaying non-lamellar morphologies are the phosphatidylcholine (PC)/fatty acid (FA) mixtures. For this reason, the hydrated PC/FA pseudo-binary mixtures have attracted attention in the last decades (Mabrey and Sturtevant, 1977; Kantor and Prestegard, 1978; Schullery et al., 1981; Marsh and Seddon, 1982; Koynova et al., 1987, 1988; Rama Krishna and Marsh, 1990; Heimburg et al., 1990; Seddon et al., 1990; Erbes et al., 1996), especially the 1:2 (mol/mol) preparations (Marsh and Seddon, 1982; Rama Krishna and Marsh, 1990; Heimburg et al., 1990; Seddon et al., 1990; Erbes et al., 1996).

In the present work, we characterise in greater detail the intriguing phase behavior of PC/FA mixtures (Koynova et al., 1987, 1988). For the hydrated DPPC/PA and DSPC/SA mixtures it was previously reported that the PC/FA 1:2 (mol/mol) stoichiometries melt at temperatures higher than the transition temperatures of both pure components, due to the existence of maximum azeotropic points in their phase diagrams at these compositions. In the present study, phase diagrams of fully hydrated pseudo-binary mixtures DLPC/LA and DMPC/MA have been constructed using high sensitivity DSC. They were found to differ from those of the longer chain PC/FA mixtures, since at all compositions the melting points were in between the transition temperatures of both pure hydrated components. Eutectic points were distinguished in both phase diagrams of DLPC/LA and DMPC/MA mixtures. The phase identification has been carried out by means of time-resolved X-ray diffraction. An assortment of phases has been observed upon changing two variables, the temperature and the lipid molar ratio: lamellar (liquid crystalline, gel, plus several crystalline polymorphs), and non-lamellar (inverted hexagonal, isotropic, as well as several phases of cubic topology). Regions of phase separation in the gel phase exist for the two binaries. Also, limited regions of liquid–liquid immiscibility have been detected. At high temperatures, variety of non-lamellar phases dominate the phase diagrams, especially in their fatty acid-rich part.

2. Materials and methods

2.1. Sample preparation

1,2-Dilauroyl-*sn*-glycero-3-phosphocholine (DLPC), 1,2-Dimyristoyl-*sn*-glycero-3-phosphocholine (DMPC) (Avanti Polar Lipids, Birmingham, AL), Lauric acid (LA) and Myristic acid (MA) (Fluka AG, Basel, > 99% pure) were used without further purification. For the PC/FA mixture samples, appropriate amounts of lipids were mixed as chloroform solutions, the chloroform was removed by rotary evaporation under nitrogen and the lipid mixtures were dried under vacuum for at least 24 h. Double distilled deionized water was added. With the DMPC/MA mixtures,

samples dispersed in 1 M Na_2SO_4 were also prepared. The dispersions were hydrated overnight at 20°C and cycled eight to ten times between about 10°C above the chain melting transition and an ice bath. The samples were vortex-mixed at these temperatures for 1–2 min at each cycle. For the samples of pure phosphatidylcholines and fatty acids, the chloroform step was omitted and the appropriate amount of water was added to the weighed lipid. The lipid concentrations were 0.5–1 mg/ml for calorimetry and 10 and 25 wt% for TRXRD. Unless otherwise indicated, the 10 and 25 wt% lipid samples give identical X-ray diffraction results. The lipid dispersions for DSC showed the same pH values as that of pure water (pH 5.0). Titration of fatty acid in PC bilayers has demonstrated a pK-value of about 10, therefore we expect that the fatty acid in our samples is in fully protonated state (Schullery et al., 1981). For TRXRD measurements, samples were filled into glass capillaries ($d = 1.0$ mm) (Hilgenberg, Malsfeld, Germany) and flame sealed. The samples were stored at 0–4°C for 3–12 days.

2.2. Differential scanning calorimetry

Microcalorimetric measurements were performed using high-sensitivity differential adiabatic scanning microcalorimeters DASM-1M or DASM-4 (Biopribor, Pushchino, Russia) with sensitivity better than 4×10^{-6} cal/K and a noise level less than 5×10^{-7} W (Privalov et al., 1975). Heating and cooling runs were performed at a scan rate of 0.5°C/min. Following equilibration at 0–4°C for 7–12 days prior to the first heating, the samples were scanned two to four times in succession following immediately the first heating scan. The thermograms were corrected for the instrumental baseline and for the instrumental time constant. The onset and the completion temperatures of the phase transition necessary for the construction of the solidus and liquidus line of the phase diagram were determined using a procedure described previously (Koynova et al., 1987).

2.3. Time-resolved synchrotron X-ray diffraction

For time-resolved X-ray diffraction experiments a brass sample holder for glass capillaries was used. The holder was connected to a Peltier temperature control system as described recently (Rappolt and Rapp, 1996). This setup allows linear heating and cooling temperature scans at rates in the range 0.1–10°C/min. Diffraction patterns were recorded on beam line X13 of the EMBL outstation at DESY in Hamburg. The camera comprises a double focusing monochromator-mirror arrangement (Hendrix et al., 1979). X-ray reflections in the small- and wide-angle regimes were recorded simultaneously using a data-acquisition system previously described (Rapp et al., 1995). With this system millisecond time-resolved experiments were feasible at high spatial resolution (Rapp et al., 1993). It consists of two linear detectors with delay line readout (Gabriel, 1977) connected electronically in series. In this configuration, both detectors appear as one single detector to the data-acquisition system (Boulin et al., 1988). One detector covers the small-angle region, the second detector covers the wide-angle region. To minimise the X-ray dose on the sample, a fast solenoid-driven shutter controlled by the data acquisition system was used to prevent irradiation of the sample in those periods when no diffraction data were taken. The signals of an ionisation chamber to measure the incoming X-ray flux and the readings of a thermocouple placed in the sample holder next to the sample were stored together with the detector data. Raw data were normalised for the incident beam intensity. No further corrections were applied. No radiation damage of the lipids was evident from their X-ray patterns. Some samples with longer exposure time were checked by thin layer chromatography after the experiments. However, no products of lipid degradation were detected in these samples. Linear heating-cooling scans were performed at rates from 0.5–2°C/min. The reciprocal spacing $s = 1/d = 2 \sin(\theta)/\lambda$, with wavelength $\lambda = 0.15$ nm and scattering angle 2θ were obtained from dry rat tail collagen (long spacing of 65 nm) and Ag-behenate (5.838 nm) in the

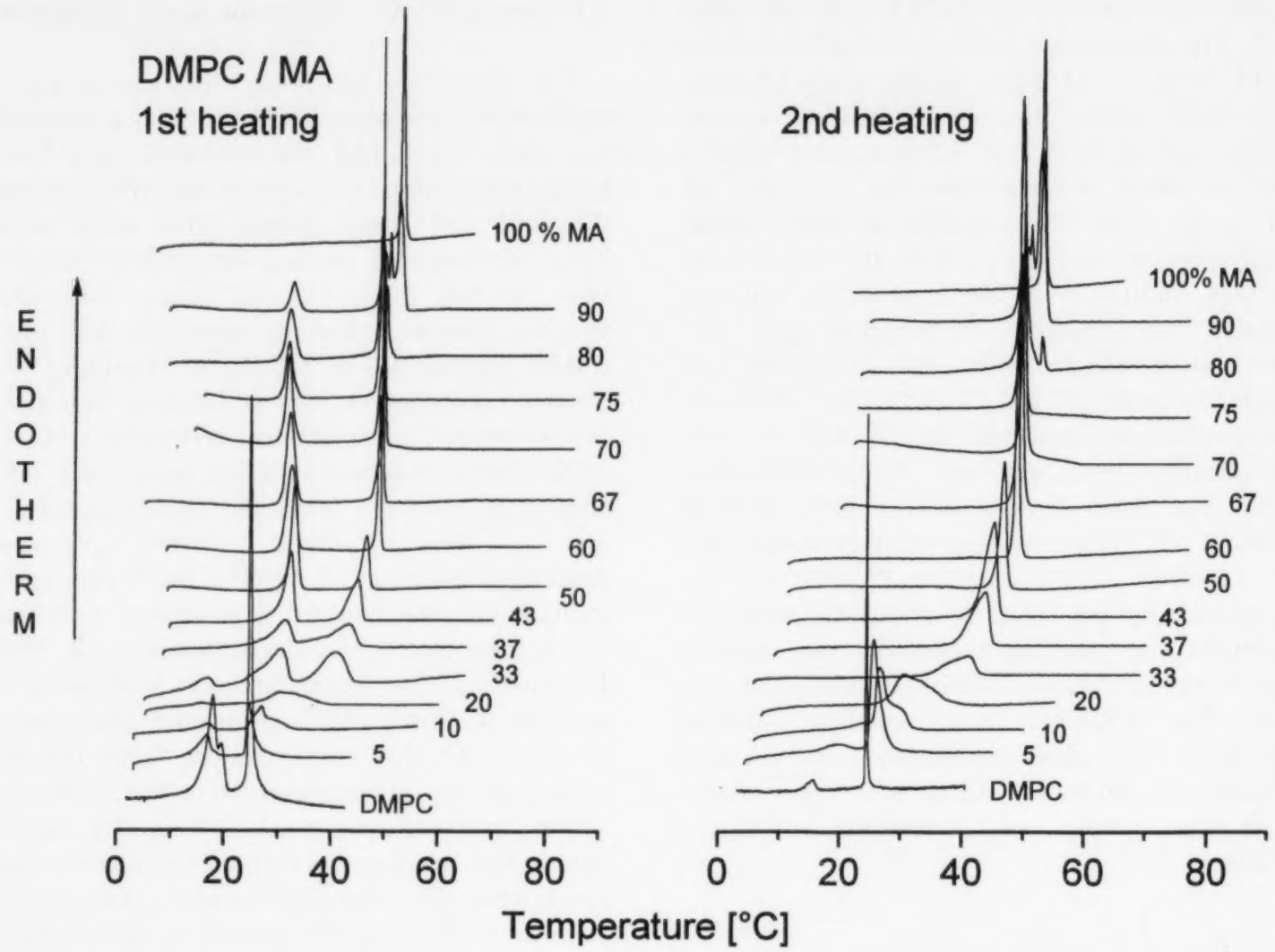

Fig. 1. Heating DSC thermograms of DMPC/MA mixtures of different MA mol% recorded at 0.5°C/min scan rate. Left panel: First scans recorded after 7–12 days storage at 0–4°C; Right panel: Second scans performed immediately after the first ones.

SAXS region and from the spacings of tripalmitin and *p*-bromo benzoic acid in the WAXS region. The data were analyzed using the interactive data evaluating program OTOKO (Boulin et al., 1986).

3. Results and discussion

3.1. DMPC/MA

3.1.1. Differential scanning calorimetry

A selection of thermograms recorded with DMPC/MA dispersions at different MA content upon first and subsequent heating are presented in Fig. 1. For pure hydrated DMPC, subtransition (17.6°C), pretransition (15.4°C) and main transition ($T_m = 23.8$°C, $\Delta H = 6.0$ kcal/mol) were observed with thermodynamic parameters in good agreement with the literature data (NIST Standard Reference Database 34, 1994). For pure MA, the melting transition upon heating was at 53.0°C, $\Delta H = 5.8$ kcal/mol. The reverse transition was recorded at 48.2°C on cooling at 0.5°C/min, with about twice reduced enthalpy (3.1 kcal/mol) and markedly reduced cooperativity (cf. $\Delta T_{1/2} =$ 0.32°C on heating and 3.27°C on cooling).

Upon addition of MA to pure DMPC, the temperature of the pretransition increases and it merges with the main transition at 10 mol% MA (Fig. 1). The subtransition is observed during the first heating after low-temperature storage in samples with up to ca. 30 mol% MA. At higher MA

content, another transition observable only upon first heating after low-temperature incubation appears at 31–33°C. It is a likely result of a co-crystallisation of DMPC and MA at low temperature and formation of a compound crystalline phase, L_c^{com}, similarly to those observed in DPPC/PA and DSPC/SA mixtures (Koynova et al., 1987, 1988). This transition persists in the first heating thermograms up to about 90 mol% MA. Its enthalpy is maximum at 67 mol% MA ($\Delta H = 4.9$ kcal/mol). This is an indication that the amount of lipid involved into the compound formation is maximum at that composition, i.e. the latter composition corresponds to the compound stoichiometry. At other molar ratios, one of the two components of the mixture is in excess and does not participate in the compound formation, thus reducing the transition enthalpy. We therefore conclude that the stoichiometry of the compound crystalline phase L_c^{com} is DMPC/MA 1:2, mol/mol.

The main transition broadens and progressively shifts to higher temperatures upon addition of MA to DMPC (Fig. 1). Mixtures containing up to 40 mol% MA exhibit a broad endotherm while at higher content of MA the transition sharpens and at 60–75 mol% MA it proceeds in a rather cooperative way. The onset temperature of the transition remains fixed at 47.7°C upon addition of MA in a wide range of compositions, from 60 to 90 mol% MA. The temperature where the transition is complete increases up to 50.7°C at 67 mol% MA, then drops down by 1°C in the preparation with 75 mol% MA. The transition has the lowest for this composition range half-width of 0.20°C in the mixture containing 75 mol% MA (transition peak at 49.4°C). At higher MA concentrations (80 and 90 mol%), the peak at ca. 50°C persists, and an additional peak appears at higher temperature, close to the transition temperature of the pure MA.

Small heat capacity anomalies were observed in the thermograms of the samples with 60 and 67 mol% MA at temperatures above the melting transition, not with a reliable reproducibility.

The phase diagram of the DMPC/MA binary mixture constructed based on the calorimetric data is presented in Fig. 2A, the non-lamellar phases were assigned from the X-ray experiments (see below). The eutectic point region of this diagram, corrected for the finite width of the transitions of the pure components, is presented in Fig. 2B. Over the compositional range 0–60 mol% MA, the progressive increase of the transition onset and completion temperatures is indicative for a continuous mixing of the two components. At 60–90 mol% MA, the horizontal portion of the solidus line is characteristic of a gel phase immiscibility. Thus, in this composition range at low temperatures solid phases enriched in DMPC (ca. 60 mol% MA, point B on Fig. 2B) and in MA (≥ 90 mol% MA, point D on Fig. 2B) are assumed to coexist.

The pattern of the liquidus line for 55–75 mol% MA implies the existence of a second region of phase separation in the phase diagram, a liquid–liquid immiscibility region. At these compositions, two liquid crystalline phases are supposed to coexist in a narrow temperature range, one with initially 55 mol% MA (point A on Fig. 2B) and a second with initially 75 mol% MA (point E in Fig. 2B). At 67 mol% MA this temperature range is of maximum width, between 48° and 51°C. Thus, 51°C is a critical solution temperature (point C in Fig. 2B) above which the mixture consists of a single liquid crystalline phase.

Point E in the phase diagram (Fig. 2B) represents an eutectic point. With this molar ratio (DMPC/MA, 1:3 (mol/mol); 75 mol% MA), the sample melts at 49°C into a liquid crystalline phase with composition identical to that of the system. At this composition the transition enthalpy is at a maximum of 6.3 kcal/mol.

3.1.2. X-ray diffraction

Small- and wide-angle diffraction patterns of DMPC/MA samples at different MA content were recorded during heating-cooling cycles using TRXRD. This method was particularly advantageous in the present study by providing means to record data with sufficiently high time resolution during temperature scans. It was thus possible to detect and resolve phase structures existing in rather narrow temperature intervals. The phase identification according to these measurements is incorporated in Fig. 2A.

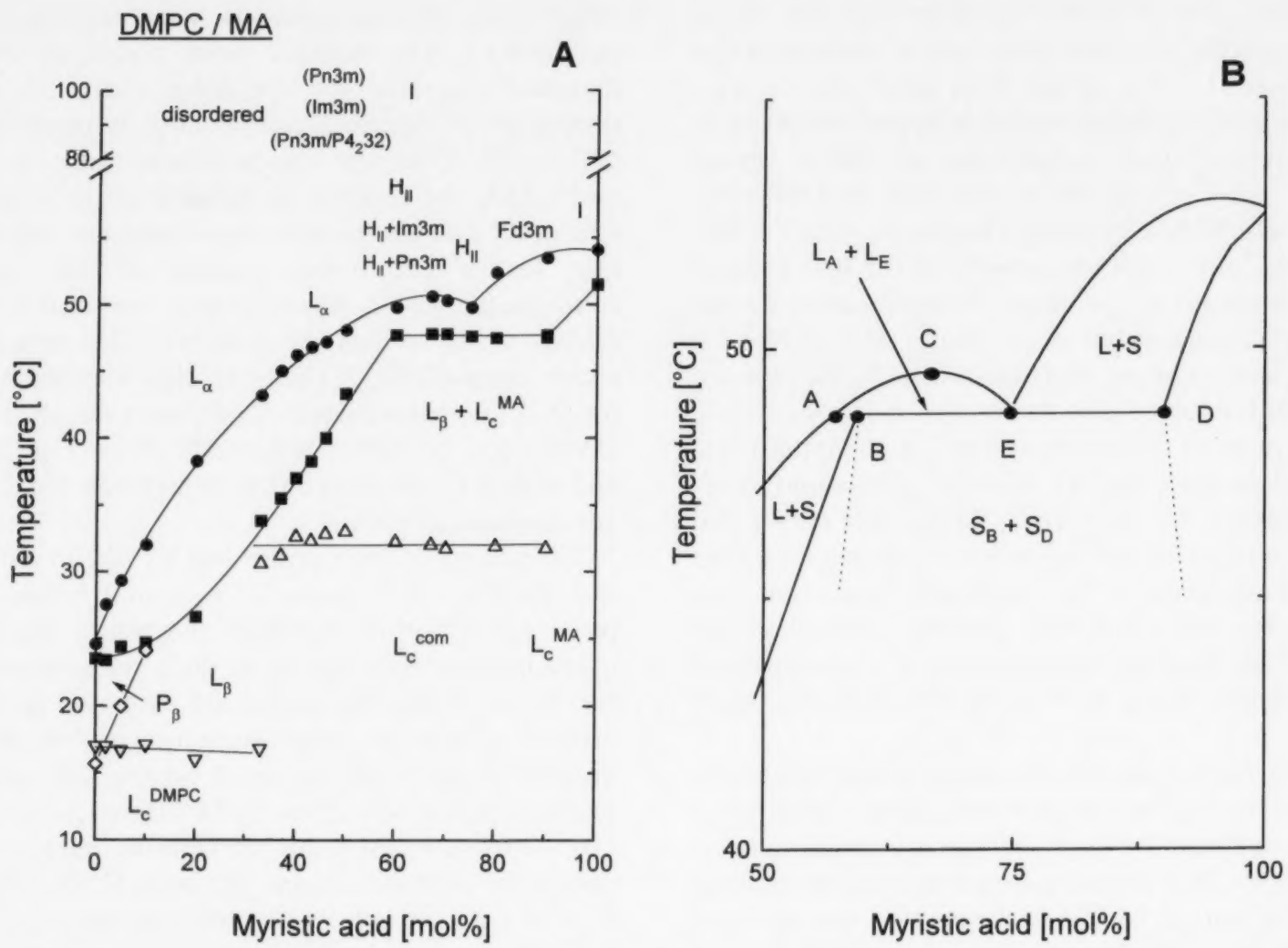

Fig. 2. (A) Phase diagram of the DMPC/MA mixture constructed on the base of the calorimetric data. Phase identification is according to the X-ray data. The phase notations shown in brackets in the high-temperature range, at 50 mol% MA, have been observed with sample dispersed in 1 M Na_2SO_4; (B) Expanded view of the eutectic point region of the same phase diagram corrected for the finite width of the transitions of the pure components (L-liquid phase, S-solid phase; $S_B + S_D$ — coexisting solid phases of compositions corresponding to points B and D indicated on the figure; $L_A + L_E$ — coexisting liquid phases of compositions corresponding to points A and E indicated in the figure).

3.1.2.1. 20 and 33 mol% MA. These samples undergo a broad transition from a lamellar gel (L_β) phase ($d = 6.6$–6.7 nm) into a lamellar liquid crystalline (L_α) phase ($d = 6.4$ nm). At high temperatures (~ 80°C) the low-angle Bragg peak broadens, in parallel with a strong decrease of the scattering intensity in samples with both 10 and 25 wt% lipid. With 33 mol% MA, a shift of the diffraction peak to higher spacings also takes place (Fig. 3). This process is reversible upon cooling where the observed during heating correlated L_α and L_β phases reappear sequentially.

3.1.2.2. 50 mol% MA. A subgel phase ($d = 5.8$ nm) is formed below 35°C after low-temperature equilibration (Fig. 3). The $L_\beta - L_\alpha$ transition takes place with a drop of the d-spacing in the transition region. At temperatures above 70°C the samples with 10 and 25 wt% lipid have different behavior (data not shown). In the sample of 10 wt% lipid, a shift of the d-spacing to higher values takes place, concurrently with a strong decrease of the scattering intensity. With the 25 wt% lipid sample, it is seen that the L_α phase transforms to another liquid crystalline phase with reflections which cannot be indexed on

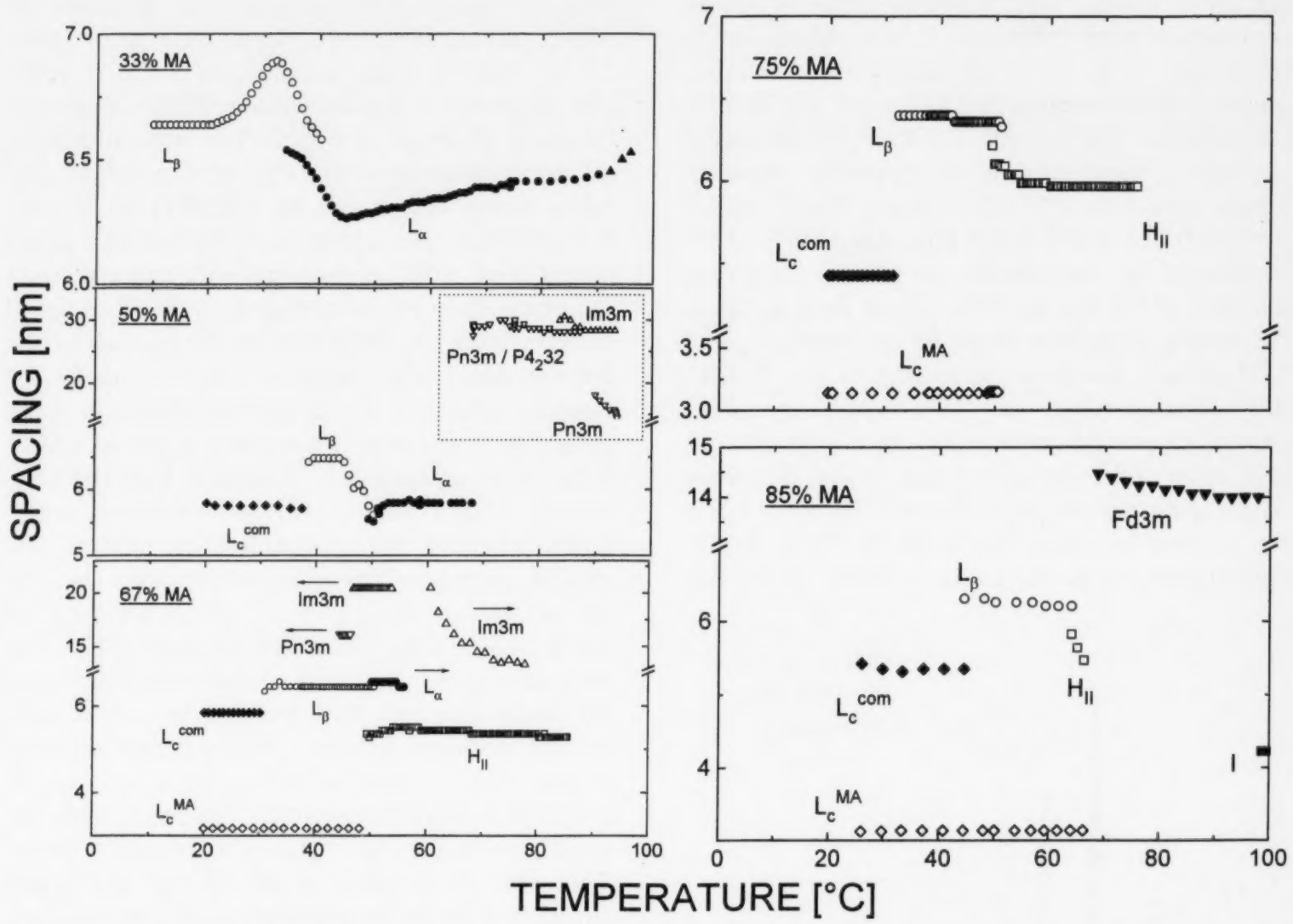

Fig. 3. Dependence of the lattice constants on temperature for different DMPC/MA ratios (○-L_β; ●-L_α; ◆-$L_c^{com.}$; ◇-L_c^{MA}; □-H_{II}; ▼-Fd3m; ▽-Pn3m; △-Im3m; ■-isotropic; ▲-disordered). Lattice constants of the cubic phases are calculated according to their tentative identification, as indicated on the figure. For the H_{II} phase, the lattice constant $a = 2d_{10}/\sqrt{3}$ is plotted for the 75 mol% and 85 mol% MA; in the case of 67 mol%, the *d*-spacing of the (100) reflection is plotted instead of the lattice constant to improve the readability for the figure. The insert (dashed rectangle) at 50 mol% MA refers to dispersion in 1 M Na_2SO_4. The arrows denote phases observed in heating or cooling direction.

a lamellar or on a hexagonal lattice. Due to the low scattering intensity, a proper identification of this phase was not possible. The scattering pattern in this temperature range was much better resolved in the 50 mol% MA sample dispersed in 1 M Na_2SO_4. In this case, a sequence of three phases of presumably cubic structure was observed upon heating. In the first one the SAXS reflections have reciprocal spacings in the ratio $\sqrt{2}$:$\sqrt{3}$:$\sqrt{4}$:($\sqrt{5}$?):$\sqrt{6}$ ($\sqrt{2}$ reflection at 20.7 nm), the second phase with SAXS reflections in the ratio $\sqrt{2}$:$\sqrt{4}$:$\sqrt{6}$:$\sqrt{8}$:$\sqrt{10}$, the $\sqrt{2}$ reflection at 12.2 nm, and the third one with reflections in the ratio $\sqrt{2}$:$\sqrt{3}$:$\sqrt{4}$:$\sqrt{6}$:$\sqrt{8}$, with the $\sqrt{2}$ reflection at 9.8 nm. The first phase does not reappear in cooling direction (Fig. 4). It may belong to cubic phases of cubic aspects #2 ($P4_2$...) or #4 (Pn...), since the existence of the $\sqrt{5}$ reflection is questionable (Table 1). The second set of reflections is consistent with cubic aspect #8 (space group of highest symmetry Im3m), and also with cubic aspect #6 (space group Pn3n) (Kasper and Lonsdale, 1985). The third set of SAXS reflections fits to cubic phases of aspect #4, space groups Pn3m/Pn3.

3.1.2.3. 67 mol% MA. Various kinds of phase coexistence were observed in the whole range below 80°C (Fig. 3). At low temperatures, a compound crystalline phase L_c^{com} ($d = 5.8$ nm; WAXS reflections at 0.429, 0.405, 0.378, 0.374 nm) coexists with a small amount of crystalline phase of almost pure MA, L_c^{MA} ($d = 3.2$ nm; WAXS reflections at 0.412, 0.370, 0.359 nm). At ca. 30°C, L_c^{com} is replaced by the lamellar gel phase with repeat distance of 6.4 nm at 45°C. Upon heating up to the melting transition onset, the coexisting L_β and L_c^{MA} phases disappear according to the WAXS diffraction pattern, and two liquid crystalline phases appear simultaneously, an H_{II} phase with first order reflection at 5.3 nm and an L_α phase with repeat distance of 6.5 nm (Fig. 5A). These two phases coexist in the range 51–55°C. In this temperature range the lattice constant of the H_{II} phase increases with temperature, opposite to what is observed with the H_{II} phase of pure lipids.

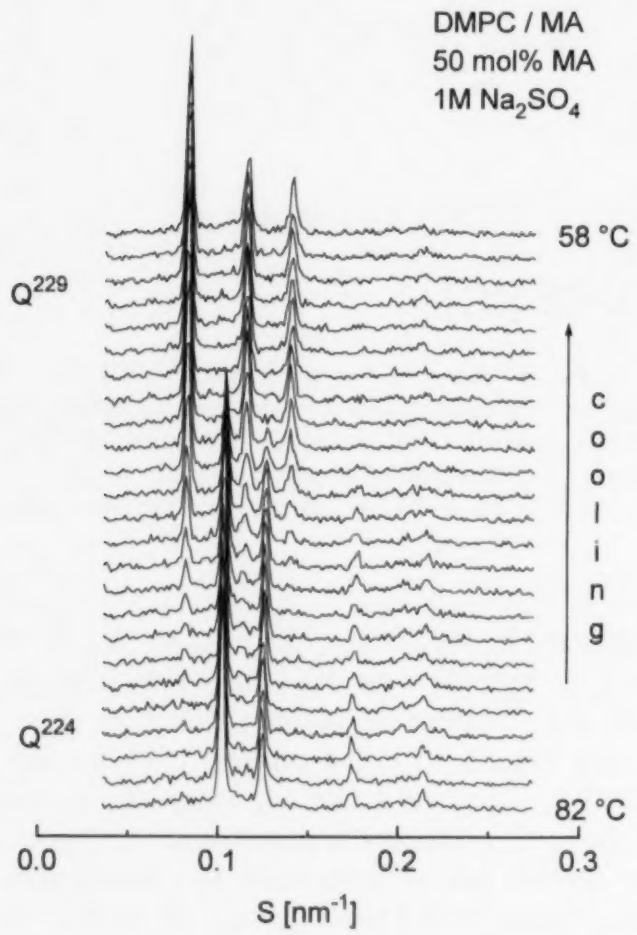

Fig. 4. SAXS patterns illustrating the transformation between two different phases of cubic topology (tentative assignment Pn3m and Im3m) in DMPC/MA (50 mol% MA) mixture dispersed in 1 M Na_2SO_4 upon cooling at 1°C/min. Diffraction data were recorded for 15 s at every 30 s.

The recorded structural changes in the 67 mol% MA preparation well correlate with the calorimetric phase diagram in Fig. 2. The transition temperatures determined by DSC were systematically below those determined by TRXRD by 3–5°C. We consider the transition temperatures determined from DSC as more reliable and construct the phase diagram according to them. The noted above systematic difference might be due to the thermocouple positioning in the air outside the sample capillary in the sample holder of the X-ray setup. At low temperatures, the observed solid–solid phase separation is consistent with the horizontal solidus line in this composition range. Upon reaching the solidus line on heating, the sample undergoes phase separation into two liquid crystalline phases — L_α phase with ca. 55 mol% MA and H_{II} phase with 75 mol% MA — in accordance with the shape of the liquidus line of the phase diagram. With increase in temperature, the compositions of these phases merge until the critical solution temperature (point C in Fig. 2B) is reached where the sample becomes homogeneous, retaining the structure of the H_{II} phase. Thus, the recorded increase of the H_{II} lattice constant with the temperature results from growing amount of DMPC in this phase. Above the critical solution temperature, this dependence reverts to the typically observed decrease of the lattice constant with the temperature (Fig. 3).

At higher temperatures, three additional SAXS reflections (at 14.4, 10.2, and 8.3 nm, ratio $\sqrt{2}:\sqrt{4}:\sqrt{6}$, at 60°C) appear concurrently with the H_{II} phase. They persist up to ca. 77°C and above this temperature, only the H_{II} phase remains. The additional reflection set fits neither to a lamellar nor to a hexagonal structure. Considering the general phase sequences observed in lipid-like amphiphiles, they presumably belong to a phase of cubic topology. This assumption is based also on reported observations of cubic phase in DMPC/MA (1:2, mol/mol) mixture (Rama Krishna and Marsh, 1990; Heimburg et al., 1990; Seddon et al., 1990; Erbes et al., 1996). During the first heating-cooling course, the cubic traces are weak but become better resolved after some

Table 1
Summary of the observed SAXS reflections for the cubic phases discussed in the present work

Cubic aspect	Symbol	Space group #	Permitted reflections	Observed reflections	PC/fatty acid sample
2 ($P4_2$...)	$P4_232$	208	$\sqrt{2}$, $\sqrt{3}$, $\sqrt{4}$, $\sqrt{5}$, $\sqrt{6}$, $\sqrt{8}$, $\sqrt{9}$, $\sqrt{10}$, $\sqrt{11}$, $\sqrt{12}$, $\sqrt{13}$, $\sqrt{14}$, $\sqrt{16}$, $\sqrt{17}$, $\sqrt{18}$, $\sqrt{19}$, $\sqrt{20}$, $\sqrt{21}$, $\sqrt{22}$, $\sqrt{24}$...	$\sqrt{2}$, $\sqrt{3}$, $\sqrt{4}$, ($\sqrt{5}$?), $\sqrt{6}$	50% MA (1 M Na_2SO_4)[a]
4 (Pn...)	Pn3m	224	$\sqrt{2}$, $\sqrt{3}$, $\sqrt{4}$, $\sqrt{6}$, $\sqrt{8}$, $\sqrt{9}$, $\sqrt{10}$, $\sqrt{11}$, $\sqrt{12}$, $\sqrt{14}$, $\sqrt{16}$, $\sqrt{17}$, $\sqrt{18}$, $\sqrt{19}$, $\sqrt{20}$, $\sqrt{21}$, $\sqrt{22}$, $\sqrt{24}$...	$\sqrt{2}$, $\sqrt{3}$, $\sqrt{4}$, ($\sqrt{5}$?), $\sqrt{6}$ $\sqrt{2}$, $\sqrt{3}$, $\sqrt{4}$, $\sqrt{6}$, $\sqrt{8}$ $\sqrt{2}$, $\sqrt{3}$ $\sqrt{2}$, $\sqrt{3}$, $\sqrt{4}$, $\sqrt{6}$	50% MA (1M Na_2SO_4)[a] 50% MA (1M Na_2SO_4) 67% MA 67% LA
8(I...)	Im3m	229	$\sqrt{2}$, $\sqrt{4}$, $\sqrt{6}$, $\sqrt{8}$, $\sqrt{10}$, $\sqrt{12}$, $\sqrt{14}$, $\sqrt{16}$, $\sqrt{18}$, $\sqrt{20}$, $\sqrt{22}$, $\sqrt{24}$...	$\sqrt{2}$, $\sqrt{4}$, $\sqrt{6}$, $\sqrt{8}$, $\sqrt{10}$ $\sqrt{2}$, $\sqrt{4}$, $\sqrt{6}$ $\sqrt{2}$, $\sqrt{4}$, $\sqrt{6}$ $\sqrt{2}$, $\sqrt{4}$, $\sqrt{6}$, $\sqrt{8}$, $\sqrt{10}$ $\sqrt{2}$, $\sqrt{4}$, $\sqrt{6}$	50% MA (1M Na_2SO_4) 67% MA 50% LA 67% LA 75% LA
12 (Ia.d)	Ia3d	230	$\sqrt{6}$, $\sqrt{8}$, $\sqrt{14}$, $\sqrt{16}$, $\sqrt{20}$, $\sqrt{22}$, $\sqrt{24}$...	$\sqrt{6}$, $\sqrt{8}$, $\sqrt{14}$, $\sqrt{16}$, $\sqrt{20}$ $\sqrt{6}$, $\sqrt{8}$, $\sqrt{14}$, $\sqrt{16}$	50% LA 67% LA
15 (Fd...)	Fd3m	227	$\sqrt{3}$, $\sqrt{8}$, $\sqrt{11}$, $\sqrt{12}$, $\sqrt{16}$, $\sqrt{19}$, $\sqrt{24}$, $\sqrt{27}$, $\sqrt{32}$, $\sqrt{35}$ ...	$\sqrt{3}$, $\sqrt{8}$, $\sqrt{11}$, $\sqrt{12}$, $\sqrt{16}$, $\sqrt{19}$, $\sqrt{24}$, $\sqrt{27}$, $\sqrt{32}$ $\sqrt{3}$, $\sqrt{8}$, $\sqrt{11}$, $\sqrt{12}$, $\sqrt{16}$, $\sqrt{19}$, $\sqrt{24}$, $\sqrt{27}$, $\sqrt{32}$, $\sqrt{35}$	85% MA 85% LA

The cubic phase sequences and the temperature intervals of their existence are given in the text and Fig. 2A, Fig. 3, Fig. 4, Fig. 5B, Fig. 9, Fig. 10, Fig. 11, Fig. 12. Notations and permitted SAXS reflections correspond to the International Tables for X-Ray Crystallography (Kasper and Lonsdale, 1985). Only the space group of highest symmetry for each cubic aspect is given in the table.

[a] In this case, distinction between cubic aspects 2 and 4 is not possible from the present data.

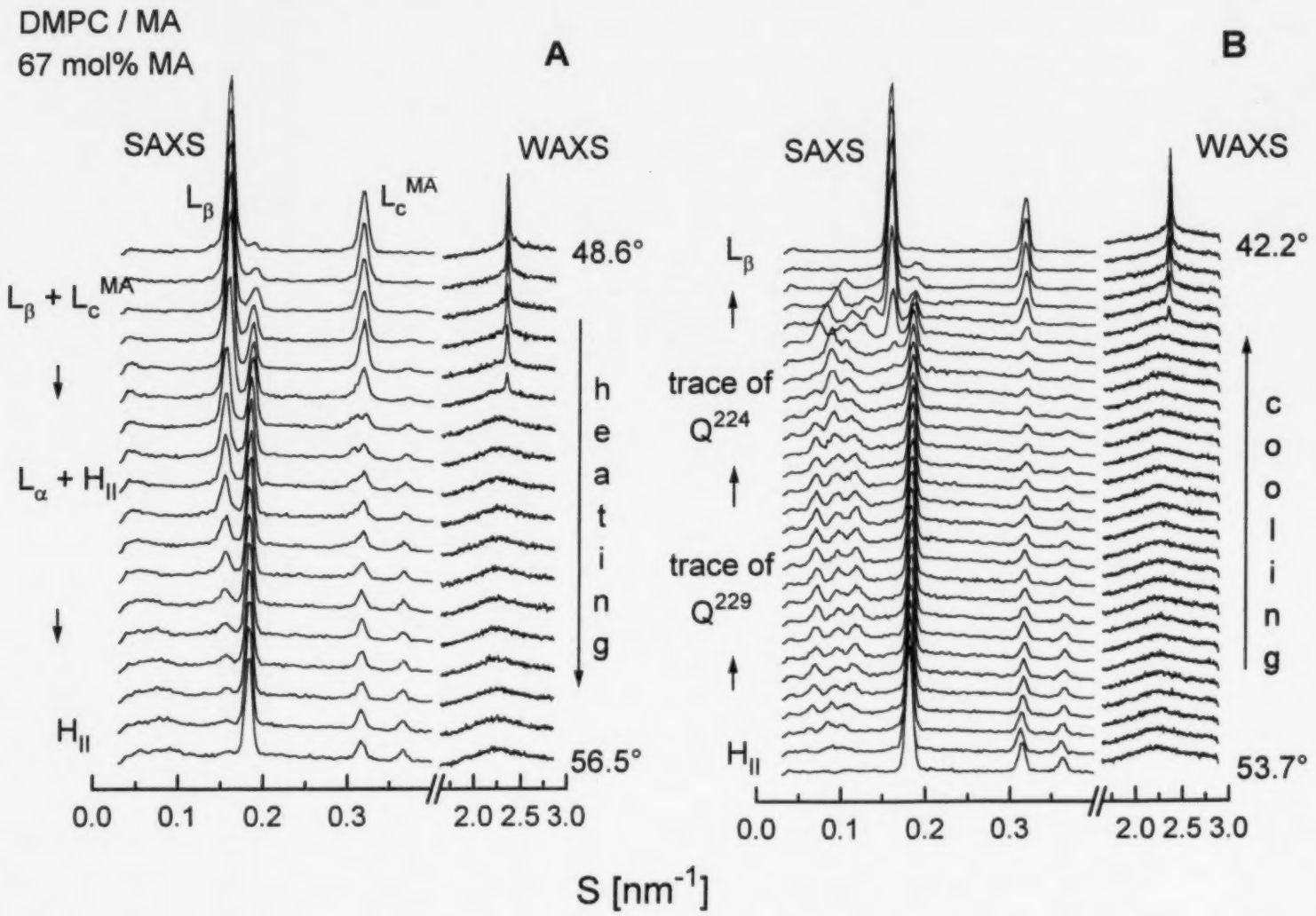

Fig. 5. (A) X-ray diffraction patterns illustrating solid–solid and liquid–liquid phase immiscibility in hydrated DMPC/MA (67 mol% MA) mixture. Heating rate 1°C/min. A similar picture was observed also at 0.5°C/min (not shown). Diffraction data were recorded for 5 s every 30 s. SAXS and WAXS regions are indicated. (B) X-ray diffraction patterns illustrating traces of two different phases of cubic topology in hydrated DMPC/MA (67 mol% MA) mixture upon cooling at 1°C/min after three 57–82°C heating-cooling cycles at 10°C/min. Diffraction data were recorded for 5 s every 30 s. SAXS and WAXS regions are indicated.

temperature cycling. Thus, after three cycles 57–82°C, it is seen that even a transformation between two different, presumably cubic structures takes place at ca. 47°C upon cooling (the higher-temperature one with reflections at 14.4, 10.2, and 8.3 nm, to a lower-temperature one with reflections at 11.4 and 9.3 nm) (Fig. 5B). Unambiguous identification of these phases from the X-ray pattern is not possible. The phase observed on heating and at higher temperatures on cooling may belong to cubic aspects #8 (space group of highest symmetry Im3m) (Table 1), or #6 (space group Pn3n), and the phase appearing at lower temperatures on cooling may belong to cubic aspects #4 (space group Pn3m/Pn3) or #3 (space group $P4_332$) (Kasper and Lonsdale, 1985). The emerging of the first traces of the L_β phase on cooling causes restructuring of the cubic phase prior to its disappearance (Fig. 5B).

3.1.2.4. 75 mol% MA. At low temperatures, the mixture with 75 mol% MA behaves similarly to that with 67 mol% MA — a crystalline phase of almost pure MA coexists initially with L_c^{com}, and above ca. 30°C — with the L_β phase (Fig. 3). During melting, the coexisting solid phases transform in a rather cooperative way in a single H_{II} phase, with (100) reflection at (5.34 nm)$^{-1}$ (Fig. 6). This transition is reversible on cooling.

3.1.2.5. 85 mol% MA. The low temperature behavior of this sample does not differ significantly from the previous two samples, except that the proportion of the coexisting solid phases changes in favor of the L_c^{MA} phase. At the melting onset, the L_β phase transforms into H_{II} phase. The latter phase coexists with the L_c^{MA} phase in a range of 4–5°C (Fig. 3). Such solid–liquid phase coexistence correlates with the shape of the DSC phase diagram in this composition range (Fig. 2). Upon completion of melting, concurrently with the disappearance of the L_c^{MA} traces, a new liquid crystalline mesophase with non-lamellar structure appears, with SAXS reflections in the ratio $\sqrt{3}$:$\sqrt{8}$:$\sqrt{11}$:$\sqrt{12}$:$\sqrt{16}$:$\sqrt{19}$:$\sqrt{24}$:$\sqrt{27}$:$\sqrt{32}$ (Fig. 7; Table 1). This ratio is characteristic for the space groups of cubic aspect # 15, namely Fd3m / Fd3. It is noteworthy that the possibility for indexing as $F4_132$ (cubic aspect # 14) is excluded

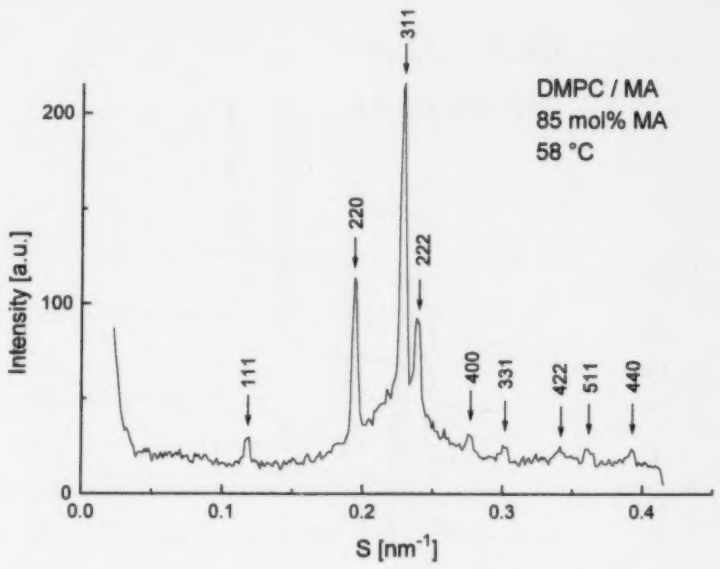

Fig. 7. SAXS pattern from hydrated DMPC/MA (85 mol% MA) mixture obtained by averaging of three successive X-ray frames recorded during a heating scan at 1°C/min. Diffraction data were recorded for 5 s every 30 s.

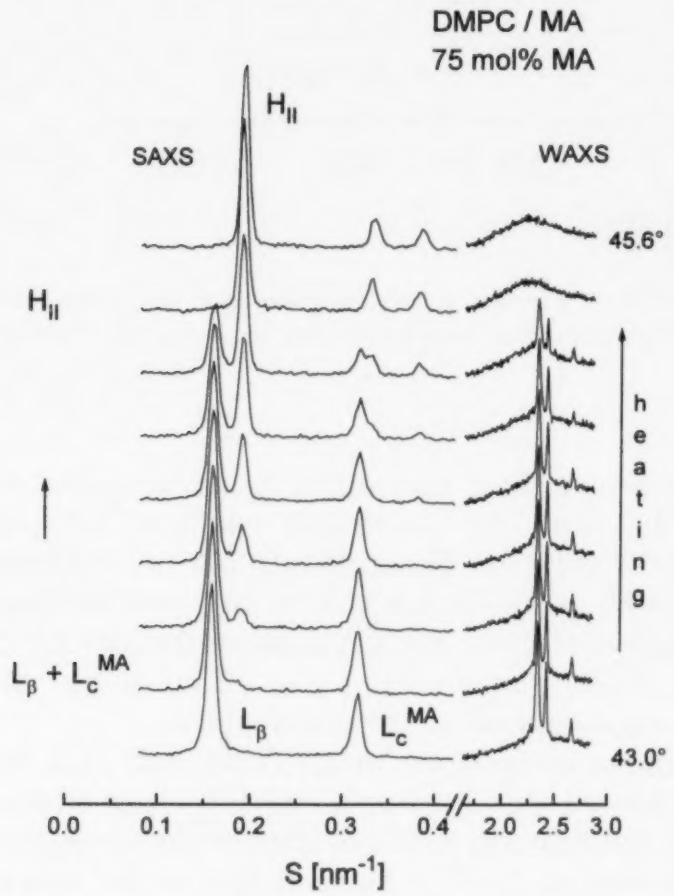

Fig. 6. X-ray diffraction patterns illustrating a direct solid–H_{II} phase transition in hydrated DMPC/MA (75 mol% MA) mixture upon heating at 1°C/min. Diffraction data were recorded for 5 s at every 20 s. SAXS and WAXS regions are indicated.

solely from the absence of a $\sqrt{20}$ reflection (Kasper and Lonsdale, 1985). The lattice parameter of the observed phase (14.5 nm at 70°C) decreases slightly with the temperature (Fig. 3). Phases of the same symmetry but with larger lattice parameters have been recently reported to form in PC/fatty alcohol mixtures at high alcohol concentrations (Huang et al., 1996). At high temperatures (95–100°C) the cubic phase is replaced by an isotropic phase.

3.1.2.6. 100% MA. The pure MA undergoes a cooperative melting transition from lamellar crystalline phase with lamellar repeat distance of 3.16 nm and WAXS reflections at 0.464 (weak), 0.479 (weak), 0.445, 0.439, 0.414 (strong), 0.390, 0.375 (strong), and 0.362 nm (strong), into an isotropic phase (I), possibly micellar. The short lamellar repeat period of the fatty acid crystals has been ascribed to strong tilting of the hydrocarbon chains with respect to the lamellar normal (von Sydow, 1956).

3.2. DLPC/LA

3.2.1. Differential scanning calorimetry

Thermograms of DLPC/LA samples at different molar ratios are shown in Fig. 8. For hydrated pure DLPC it is known that the chain

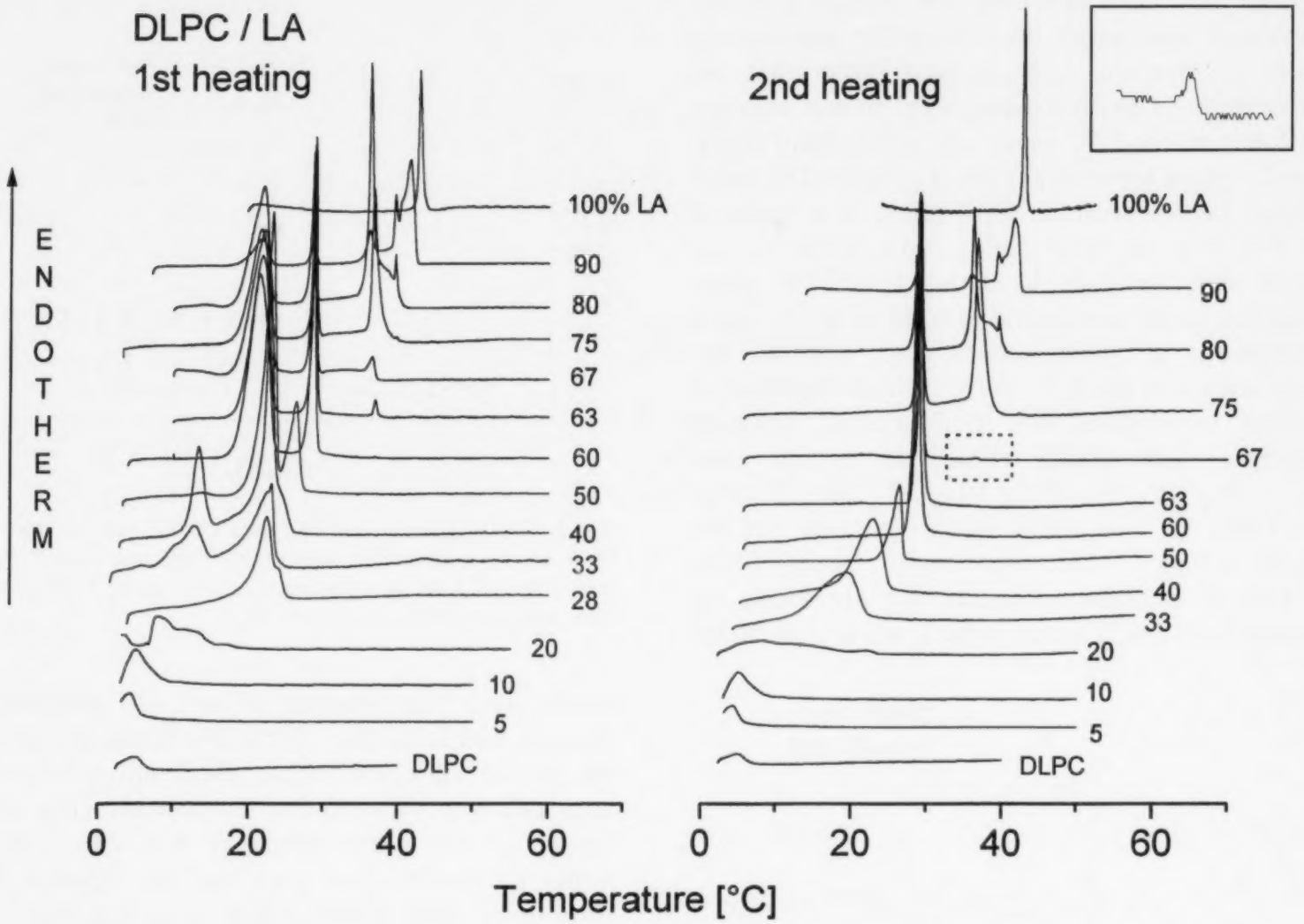

Fig. 8. Heating DSC thermograms of DLPC/LA mixtures of different LA mol% recorded at 0.5°C/min scan rate: Left panel: First scans recorded after 7–12 days storage at 0–4°C; Right panel: Second scans performed immediately after the first ones. The inset is in a 10 × expanded vertical scale.

melting transition proceeds in two steps, at −2° and 5°C, respectively as a $P_{\beta'} - L_x - L_\alpha$ sequence, where L_x is an intermediate liquid crystalline phase, more ordered than the L_α phase (Finegold et al., 1990; Hatta et al., 1994). We recorded only the broad peak at 5°C corresponding to the $L_x - L_\alpha$ portion of the transition. Pure LA exhibits a melting transition at 42.7°C on heating. The transition proceeds with a hysteresis of ca. 5°C on cooling.

Upon addition of LA to DLPC, up to ca. 60 mol% LA, the transition progressively shifts to higher temperature, similar to what was observed with the DMPC/MA mixtures. Preparations containing up to 40 mol% LA exhibit a broad endotherm. At a higher content of LA the transition sharpens and at 67 mol% LA it takes place at 29.3°C with the lowest half width of $\Delta T_{1/2} =$ 0.22°C (Fig. 8). The melting onset for mixtures with 60–95 mol% LA is at nearly constant temperature of 28°C. For LA contents from 67 up to 95 mol%, additional higher temperature endotherms appear in the thermograms.

In the composition range 33–43 mol% LA, an additional endotherm at 12–13°C is observed during first heatings after low-temperature incubation (10 days at 2–4°C). The enthalpy of this transition is maximum at 40 mol% LA (3.6 kcal/mol). Similarly, at 45–95 mol% LA, an endotherm at 22–23°C is observed only during first heating after low-temperature incubation. Its enthalpy is maximum at 60 mol% LA (10.7 kcal/mol). Such

thermal behavior most probably reflects co-crystallisations of DLPC and LA at low temperature and formation of compound crystalline phases of different stoichiometries, L_{c1}^{com} and L_{c2}^{com}. The recorded endotherms are supposed to correspond to the transformation of these compounds subgel phases to the gel L_β phase. The stoichiometries of these compound phases are presumably close to 40 mol% LA for L_{c1}^{com} and 60 mol% LA for L_{c2}^{com}, as judged from the maximum enthalpies of the recorded subgel–gel transition. Similarly to the DMPC/MA mixture, small heat capacity anomalies (without reliable reproducibility) are observed in the thermograms of the samples with 63 and 67 mol% LA at temperatures above the melting transition (Fig. 8, inset).

The phase diagram of the DLPC/LA mixture constructed from the calorimetric data is presented in Fig. 9. The position of the solidus line for LA contents below 30 mol% was determined from the calorimetric data reported in (Finegold et al., 1990). This phase diagram is similar to that of the DMPC/MA mixture. It reflects continuous mixing of the components in both solid and liquid phases up to ca. 60 mol% LA. The horizontal solidus line in the composition range 60–95 mol% LA is a manifestation of a gel phase immiscibility, while the shape of the liquidus line indicates the existence of an eutectic point at 67 mol% LA and 29°C, and a rather narrow region of liquid–liquid immiscibility between 29 and 30°C for 60–67 mol% LA. Thus, the 65 mol% LA and 30°C point is likely a critical solution point.

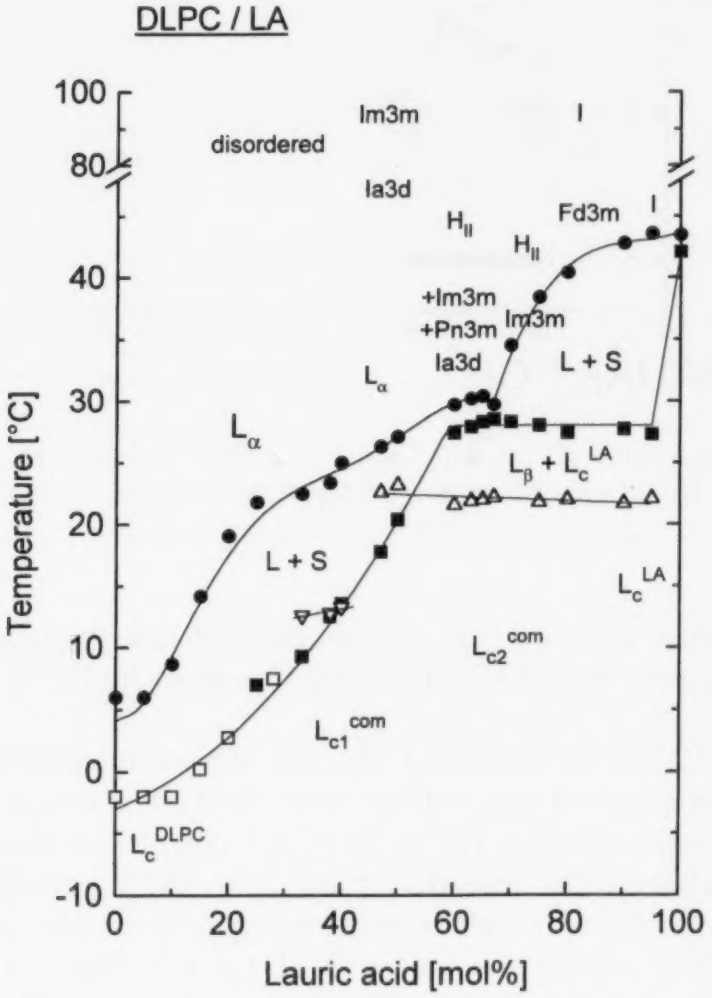

Fig. 9. Phase diagram of the DLPC/LA mixture constructed on the base of the calorimetric results. The position of the solidus line at LA content < 30 mol% (□) is taken from the calorimetric data in (Finegold et al., 1990). The phase identification is according to the X-ray data.

3.2.2. X–ray diffraction

The phase identification according to the TRXRD measurements is incorporated in Fig. 9. The structural parameters for some of the studied DLPC/LA samples are presented in Fig. 10.

3.2.2.1. 33 and 50 mol% LA. The melting transitions are between lamellar gel and lamellar liquid crystalline phases. Similar to what was observed with the DMPC/MA mixtures, the SAXS diffraction peak broadens and strongly decreases in intensity above ca. 80°C. For 10 wt% lipid sample at 50 mol% LA this broadening is accompanied by shift to higher spacings. Increasing the lipid content to 25 wt% in the 50 mol% LA mixture results in an observable transformation of the L_α phase to a non-lamellar structure with SAXS reflections in the ratio $\sqrt{6}:\sqrt{8}:\sqrt{4}:\sqrt{16}:\sqrt{20}$ (Table 1), indexing as a cubic phase of space group Ia3d (Q^{230}), with lattice constant of 14.5 nm. This transformation takes place at about 50°C upon heating. At even higher temperatures (~ 80°C) the Ia3d phase transforms to another non-lamellar phase with reflections in the ratio $\sqrt{2}:\sqrt{4}:\sqrt{6}$, tentatively Im3m.

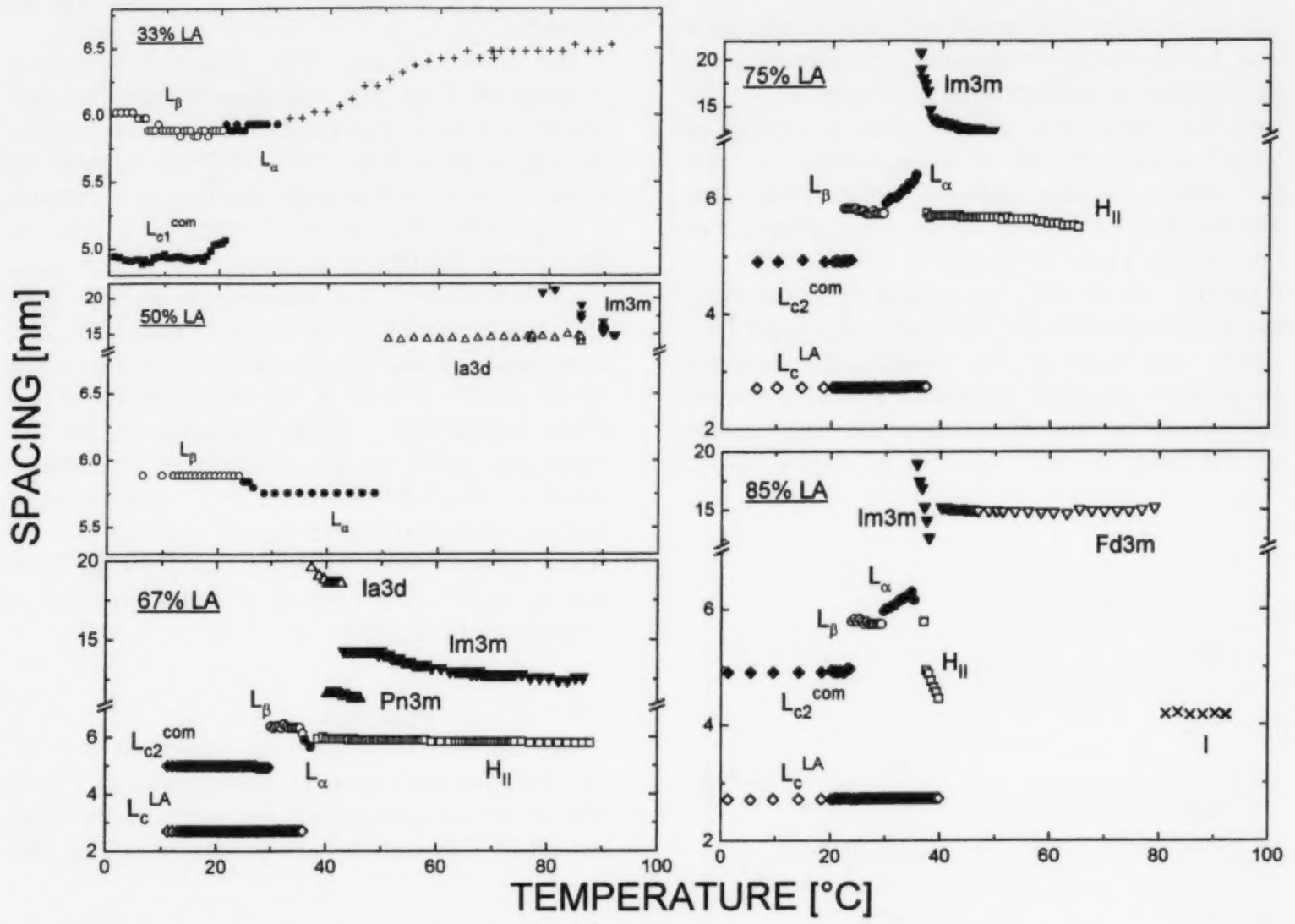

Fig. 10. Dependence of lattice on temperature for different DLPC/LA ratios (○-L_β; ●-L_α; ■-L_{c1}^{com}; ◆-L_{c2}^{com}; ◇-L_c^{LA}; □-H_{II}; △-Ia3d; ▽-Fd3m; ▲-Pn3m; ▼-Im3m; x-isotropic; +-disordered). Lattice constants of the cubic phases, the lattice constant $a = 2d_{10}/\sqrt{3}$ is plotted.

3.2.2.2. 67 mol% LA. The heating of this mixture results in a plenteous phase sequence:

$$L_{c2}^{com} + L_c^{LA} \rightarrow L_\beta + L_c^{LA} \rightarrow L_\alpha \rightarrow Q^{230} \rightarrow Q^{230} + H_{II} \rightarrow Q^{224} + H_{II} \rightarrow Q^{229} + H_{II} \rightarrow H_{II}$$

Thus, at low temperature the system exhibits solid phase coexistence, as it should be expected from its DSC phase diagram. Upon heating, a cooperative melting into L_α phase takes place. Further, interconversions between five different liquid crystalline mesophases have been observed (Fig. 10): L_α , H_{II} and three other non-lamellar phases typified by sets of four to five reflections (Table 1). A tentative identification of the latter three phases is that they are cubic phases of space groups Ia3d (Q^{230}), Pn3m (Q^{224}) and Im3m (Q^{229}).

3.2.2.3. 75 mol% LA. At low temperatures this preparation also exhibits solid–solid phase coexistence of $L_{c2}^{com} + L_c^{LA}$ or $L_\beta + L_c^{LA}$ type, below and above 23°C, respectively. At 28°C, the L_β phase ($d = 5.9$ nm) melts into L_α phase ($d = 6.0$ nm at 29°C) which now coexists with the L_c^{LA} (Fig. 11), as expected from the DSC phase diagram. The lamellar period of the L_α phase increases on heating up to 6.2 nm at 35.5°C. Above this temperature the L_α phase is replaced by a broad diffuse halo at small angles, and later by a non-lamellar

mesophase, presumably Im3m (Table 1). The last traces of the L_c^{LA} phase disappear at 38°C. At this temperature an H_{II} phase forms and coexists with the cubic phase in a broad temperature range up to 60°C. Above the latter temperature a single hexagonal phase is observed. The cubic phase lattice constant decreases with the temperature. Noteworthy, the slope of this dependence is different below and above 38°C, being much higher in the former case (Fig. 10). The described phase sequence is readily reversible on cooling, except that the L_c^{com} phase does not form immediately and requires a several day low-temperature incubation for its recovery.

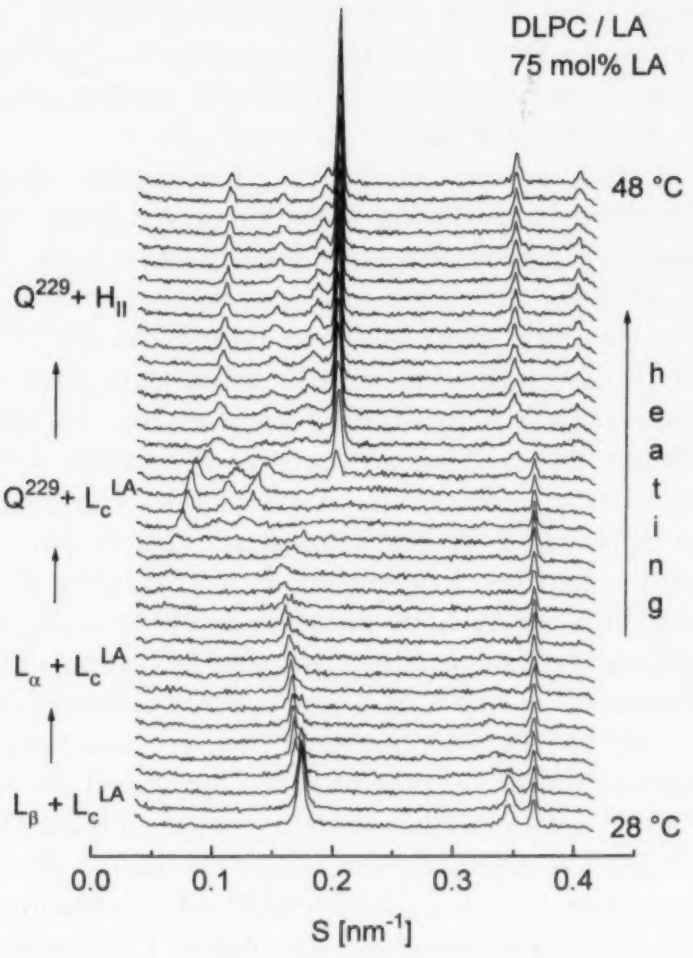

Fig. 11. SAXS patterns illustrating the phase sequence $L_\beta + L_c^{LA} \rightarrow L_\alpha + L_c^{LA} \rightarrow Im3m + L_c^{LA} \rightarrow Im3m + H_{II} \rightarrow H_{II}$ in hydrated DLPC/LA (75 mol% LA) mixture upon heating at 1°C/min. Diffraction data were recorded for 15 s every 30 s.

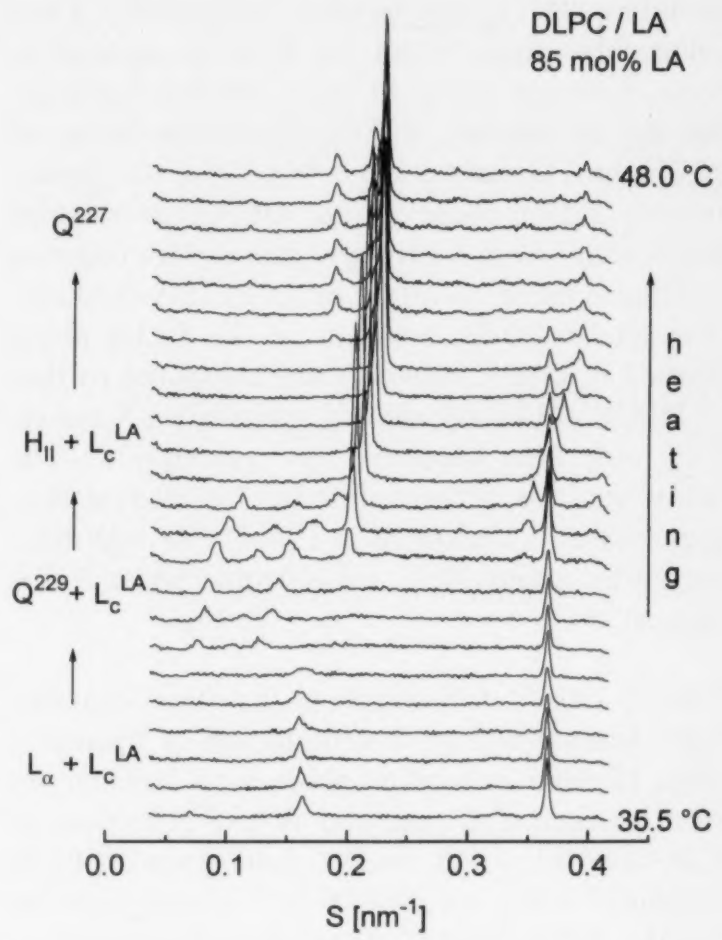

Fig. 12. SAXS patterns illustrating the phase sequence $L_\alpha + L_c^{LA} \rightarrow Q^{229} + L_c^{LA} \rightarrow Q^{227} + L_c^{LA} \rightarrow Q^{227}$ in hydrated DLPC/LA (85 mol% LA) mixture upon heating at 1°C/min. Diffraction data were recorded for 15 s every 30 s.

3.2.2.4. 85 mol% LA. The phase sequence recorded is as follows:

$$L_{c2}^{com} + L_c^{LA} \rightarrow L_\beta + L_c^{LA} \rightarrow L_\alpha + L_c^{LA} \rightarrow Q^{229} + L_c^{LA} \rightarrow H_{II} + L_c^{LA} \rightarrow Q^{227} \rightarrow I$$

Thus, five different kinds of solid–solid and solid–liquid phase separation characterize this mixture during heating up to the liquidus at 45°C. At this temperature the sample becomes homogeneous and forms a non-lamellar phase with SAXS reflections in the ratio $\sqrt{3}$: $\sqrt{8}$: $\sqrt{11}$: $\sqrt{12}$: $\sqrt{16}$: $\sqrt{19}$: $\sqrt{24}$: $\sqrt{27}$: $\sqrt{32}$: $\sqrt{35}$ (Table 1). This is the full set of the first ten reflections indexing as a cubic phase of aspect # 15, space group Fd3m/Fd3. Its lattice constant is practically independent of temperature. Its value of 15.0 nm is only slightly higher than that of 14.5 nm for the corre-

sponding DMPC/MA mixture. Noteworthy, a micellar cubic phase Fd3m was recently reported to form in longer chain PC/fatty alcohol mixtures, but not in mixtures with hydrocarbon chains of 12 C-atoms (Huang et al., 1996). Thus, the formation of Fd3m phase in the DLPC/LA mixture might result from a stronger tendency for negative interfacial mean curvature in the PC/FA mixtures. The smaller lattice constant of the Fd3m phase formed in DMPC/MA mixture compared to that in DMPC/C14 fatty alcohol mixture (14.5 nm vs. 17.5 nm) also supports this assumption. The transformation between different liquid crystalline mesophases is illustrated in Fig. 12. At high temperatures, about 80°C, an isotropic phase forms (not shown).

3.2.2.5. 100% LA. Similarly to the other saturated fatty acids, the pure LA undergoes a transition from lamellar crystalline phase with lamellar repeat distance of 2.7 nm and WAXS reflections at 0.483 (weak), 0.473 (weak), 0.466 (weak), 0.439 (strong), 0.426 (weak), 0.413 (strong), 0.389 (weak), 0.374 (strong), to an isotropic phase.

4. Summary

1. The phase diagrams of hydrated short chain PC/FA mixtures (DLPC/LA and DMPC/MA) have been constructed from DSC and X-ray diffraction data. They contain eutectic points, at 75 mol% MA (DMPC/MA 1:3, mol/mol) and 49°C, and at about 67 mol% LA (DLPC/LA 1:2, mol/mol) and 29°C. The eutectic point is better expressed in the DMPC/MA mixture.

2. Regions of liquid–liquid and solid–solid phase separation have been identified in these phase diagrams. Limited regions (2–4°C) of liquid–liquid phase immiscibility exist at compositions with slightly prevailing FA. For example, at 67 mol% MA, a phase separation between L_α phase enriched in DMPC and H_{II} phase enriched in MA takes place in the temperature range 51–55°C. In the DLPC/LA mixture the region of liquid–liquid phase immiscibility is very narrow (1–2°C, at 60–67 mol% LA) and not so well expressed. Solid phase immiscibility is detected in both binaries, between 60 and 90 mol% FA.

3. The PC/FA mixtures form compound subgel polymorphic phases. In the case of DMPC/MA mixture, one such phase is observed, with a likely stoichiometry DMPC/MA 1:2, mol/mol. In certain sense, this compound behaves as third component in the mixture. From the shape of the phase diagram it appears that the 1:2 compound is well miscible with DMPC but displays gel phase immiscibility with MA. Indeed, the right-hand side of the phase diagram (67–100 mol% MA) represents itself a simple eutectic phase diagram of the mixture with one component being the DMCP/MA (1:2) compound and the other component being pure MA. The eutectic composition of this mixture is (DMPC/MA (1:2))/MA = 1:1 (mol/mol).

The mixing behavior of DLPC/LA mixture is more complicated. Two compound subgel phases appear to form upon low-temperature equilibration. Their stoichiometries are presumably close to 40 mol% LA and to 60 mol% LA.

4. In the liquid crystalline phase region, nonlamellar phases dominate the phase diagrams, especially in their fatty acid-rich part. At 50–70 mol% FA, cubic phases of presumably bicontinuous topology form—at least two in the DMPC/MA mixture (Pn3m, Im3m), and at least three in the DLPC/LA mixture (Ia3d, Pn3m, Im3m). Hence, the Ia3d phase becomes favourable with decreasing hydrocarbon chain length. The order of appearance of the bicontinuous cubic phases with increasing temperature varies with the PC/FA ratio. These cubic phases exist either as single phases or concurrently to the hexagonal H_{II} phase. At 75 mol% MA (the eutectic composition for the DMPC/MA mixture), the only liquid crystalline mesophase present is the hexagonal phase. At 67 mol% LA (the eutectic composition for the DLPC/LA mixture), the liquid crystalline phase sequence is: $L_\alpha \rightarrow Ia3d \rightarrow Ia3d + H_{II} \rightarrow Pn3m + H_{II} \rightarrow Im3m + H_{II} \rightarrow H_{II}$. At higher FA content (85 mol%), micellar cubic phase of space group Fd3m is observed in both mixtures. Pure fatty acids form isotropic phase at temperatures above the melting transition. Thus, with increasing FA

concentration, the non-lamellar phases typical for the studied PC/FA mixtures arrange in the sequence: bicontinuous cubic phases (Ia3d, Pn3m, Im3m) → hexagonal phase (H_{II}) → micellar cubic phase (Fd3m) → isotropic phase (I). This sequence is in principle consistent with the average mean curvature of the polar/non-polar interface becoming more negative with increasing fatty acid content.

Acknowledgements

We thank the European Union for support of the work at EMBL Hamburg through the HCMP Access to Large Installations Project, Contract Number CHGE-CT93-0040. RK and BT acknowledge support from the Bulgarian National Science Foundation, grants K-402/94 and K-407/94.

References

Boulin, C., Kempf, R., Koch, M.H.J., Mc Laughlin, S.M., 1986. Data appraisal and display for synchrotron radiation experiments: Hardware and software. Nucl. Instrum. Methods. A249, 399–407.

Boulin, C., Kempf, R., Gabriel, A., Koch, M.H.J., 1988. Data acquisition systems for linear and area X-ray detectors using delay line readout. Nucl. Instrum. Methods. A269, 312–320.

Erbes, J., Winter, R., Rapp, G., 1996. Rate of phase transformations between mesophases of the 1:2 lecithin/fatty acid mixtures DMPC/MA and DPPC/PA — a time-resolved synchrotron X-ray diffraction study. Ber. Bunsenges. Phys. Chem. 100, 1713–1722.

Finegold, L., Shaw, W., Singer, M., 1990. Unusual phase properties of dilauroyl phosphatidylcholine (C12PC). Chem. Phys. Lipids 53, 177–184.

Gabriel, A., 1977. Position sebnsitive X-ray detector. Rev. Sci. Instrum. 48, 1303–1305.

Hatta, I., Matuoka, S., Singer, M.A., Finegold, L., 1994. A new liquid crystalline phase in phosphatidylcholine bilayers as studied by X-ray diffraction. Chem. Phys. Lipids 69, 129–136.

Heimburg, T., Ryba, N.J.P., Wurz, U., Marsh, D., 1990. Phase transition from a gel to a fluid phase of a cubic symmetry in dimyristoylphosphatidylcholine/myristic acid (1:2, mol/mol) bilayers. Biochim. Biophys. Acta 1025, 77–81.

Hendrix, J., Koch, M.H.J., Bordas, J., 1979. A double focusing X-ray camera for use with synchrotron radiation. Appl. Cryst. 12, 467–472.

Huang, Z., Seddon, J.M., Templer, R.H., 1996. An inverse micellar Fd3m cubic phase formed by hydrated phosphatidylcholine/fatty alcohol mixtures. Chem. Phys. Lipids 82, 53–61.

Kasper, J.S., Lonsdale, K. (Eds.), 1985. International Tables for X-Ray Crystallography, vol. 2. Reidel, Dordrecht.

Kantor, H.L., Prestegard, J.H., 1978. Fusion of phosphatidylcholine bilayer vesicles: Role of free fatty acids. Biochemistry 17, 3592–3597.

Koynova, R.D., Boyanov, A.I., Tenchov, B.G., 1987. Gel-state metastability and nature of the azeotropic points in mixtures of saturated pholphatidylcholines and fatty acids. Biochim. Biophys. Acta 903, 186–196.

Koynova, R.D., Tenchov, B.G., Quinn, P.J., Laggner, P., 1988. Structure and phase behaviour of hydrated mixtures of L-dipalmitoylphosphatidylcholine and palmitic acid. Corresations between structrual rearrangements, specific volume changes and endothermic events. Chem. Phys. Lipids 48, 205–214.

Mabrey, S., Sturtevant, J.M., 1977. Interaction of saturated fatty acids into phosphatidylcholine bilayers. Biochim. Biophys. Acta 486, 444–450.

Marsh, D., Seddon, J.M., 1982. Gel-to-inverted hexagonal (L_β-H_{II}) phase transitions in phosphatidylethanolamines and fatty acid-phosphatidylcholine mixtures, demonstrated by ^{31}P NMR spectroscopy and X-ray diffraction. Biochim. Biophys. Acta 690, 117–123.

NIST Standard Reference Database 34. 1994. Lipid Thermotropic Phase Transition Database (LIPIDAT), Version 2.0.

Privalov, P.L., Plotnikov, V.V., Filimonov, V.V., 1975. Scanning microcalorimeters for studying macromolecules. J. Chem. Thermodyn. 7, 41–47.

Rama Krishna, Y.V.S., Marsh, D., 1990. Spin label ESR and ^{31}P NMR studies of the cubic and inverted hexagonal phases of dimyristoylphosphatidylcholine/myristic acid (1:2, mol/mol) mixtures. Biochim. Biophys. Acta 1024, 89–94.

Rapp, G., Rappolt, M., Laggner, P., 1993. Time-resolved simultaneous small- and wide-angle X-ray diffraction on dipalmitoylphosphatidylcholine by laser temperature-jump. Prog. Colloid Polymer Sci. 93, 25–29.

Rapp, G., Gabriel, A., Dosiere, M., Koch, M.H.J., 1995. A dual detector single readout system for simultaneous small- (SAXS) and wide-angle (WAXS) scattering. Nucl. Instrum. Meth. Phys. Res. A 357, 178–182.

Rappolt, M., Rapp, G., 1996. Simultaneous small- and wide-angle X-ray diffraction during the main transition of dimyristoylphosphatidylethanolamine. Ber. Bunsenges. Phys. Chem. 100, 1153–1162.

Schullery, S.E., Seder, T.A., Weinstein, D.A., 1981. Differential thermal analysis of dipalmitophosphatidylcholine-fatty acid mixtures. Biochemistry 20, 6818–6824.

Seddon, J.M., 1990. Structure of the inverted hexagonal (H_{II}) phase, and non-lamellar phase transitions of lipids. Biochim. Biophys. Acta 1031, 1–69.

Seddon, J.M., Hogan, J.L., Warrender, N.A., Pebay-Peyroula, E., 1990. Structural studies of phospholipid cubic phases. Prog. Colloid Polymer Sci. 81, 189–197.

von Sydow, E., 1956. Ark. Kemi 9, 231–254.

ELSEVIER

Chemistry and Physics of Lipids
88 (1997) 63–71

CPL
CHEMISTRY AND PHYSICS OF LIPIDS

FT–IR study on microscopic structures and conformations of POP–PPO and POP–OPO molecular compounds

Akiyoshi Minato [a,*], Junko Yano [a], Satoru Ueno [a], Kevin Smith [b], Kiyotaka Sato [a]

[a] *Faculty of Applied Biological Science, Hiroshima University, Higashi-Hiroshima, 739, Japan*
[b] *Colworth Laboratory, Unilever Research, Bedford, MK44 1LQ, UK*

Received 3 March 1997; accepted 16 June 1997

Abstract

The microscopic structures and conformations of the molecular compounds of POP–PPO and POP–OPO were examined using microprobe polarized Fourier transform infrared (FT–IR) spectroscopy. The two molecular compounds are formed in a double chain length structure due to specific acyl–acyl interactions through oleic acid moieties, yet peculiar differences were observed between the two molecular compounds. The subcell structure of β form of the POP–PPO compound was $T_{\parallel}$, whose b_s-axis was approximately parallel to the unit cell b-axis. The olefinic conformation were neither of skew-*cis*-skew′ type nor of skew-*cis*-skew type. On the other hand, two subcell structures were assumed for β form of the POP–OPO compound: (a) the palmitoyl leaflet forms the $T_{\parallel}$ subcell and the oleoyl leaflet $O'_{\parallel}$, or (b) the two leaflets are both of $T_{\parallel}$ subcell in which the directions of subcell axes of the palmitoyl and oleoyl chains are different. The olefinic conformation of the β form of the POP–OPO compound revealed the skew-*cis*-skew′ type. It was assumed that steric hindrance between the palmitoyl and oleoyl chains resulted in the formation of the molecular compounds of two types of double chain length structure: (a) complete separation of the palmitoyl and oleoyl chain leaflets as revealed in the POP–OPO compound, and (b) one leaflet of the palmitoyl chains and other leaflet of the palmitoyl-oleoyl mixed acid chains in the POP–PPO compound. The olefinic conformation of the POP–PPO compound was largely deformed compared to that in the PPO–OPO compound. © 1997 Elsevier Science Ireland Ltd.

Keywords: FT–IR spectroscopy; Molecular compound; Saturated-oleoyl mixed acid triacylglycerol; Phase behavior; Polymorphism

1. Introduction

Triacylglycerols (TAGs) are the major components of fat, whose macroscopic properties, such

* Corresponding author. Tel.: +81 824 247935; fax: +81 824 227062; e-mail: kyosato@ipc.hiroshima-u.ac.jp

PII S0009-3084(97)00045-5

as texture and plasticity, are influenced by the physical properties of their TAG components. The physical properties of TAGs are in turn influenced by microscopic structures and conformations of the TAG molecules present in the fat products (Formo, 1979; Small, 1986; Sato, 1996).

The X-ray diffraction (XRD) crystal structure analysis is the best approach to clarify the molecular level structure. However, it is difficult to obtain high quality single crystals of TAGs. Therefore, only a few reports have been presented on the molecular structure of the most stable polymorphs of TAGs using the single crystal XRD method: trilaurin (Larsson, 1964), tricaprin (Jensen and Mabis, 1966) and 1,2-dipalmitoyl-3-acetyl-*sn*-glycerol (Goto et al., 1992). As for many TAG crystals, in particular for their metastable forms, the information about subcell and lamellar structures have been assessed by powder XRD measurements. However, local structural information such as molecular conformation and orientation of functional groups is not available by the powder XRD.

Vibrational (infrared or Raman) spectroscopy can obtain information on the molecular structure and conformation of lipids by utilizing oriented specimens or tiny crystals in conjunction with a microprobe (Kobayashi, 1988). A good correspondence between the single crystal XRD and IR analyses have been demonstrated for the molecular structures of *cis*-unsaturated fatty acids (Sato, 1996; Kaneko et al., 1996). Studies of binary mixture systems of unsaturated fatty acids have revealed quite diversified phase behavior including the existence of miscible phases (Sato et al., 1997), eutectic phases (Yoshimoto et al., 1991; Inoue et al., 1993; Ueno et al., 1994) and molecular compound formation (Inoue et al., 1992). Thus FT–IR analysis has been quite powerful in elucidating the molecular structures and interactions of the unsaturated fatty acids.

In this paper, we describe the microscopic structures and the molecular conformations of the molecular compounds of POP–PPO (Minato et al., 1997a) and POP–OPO (Minato et al., 1997b) (POP; *sn*-1,3-dipalmitoyl-2-oleoylglycerol, PPO; *rac*-1,2-dipalmitoyl-3-oleoylglycerol and OPO; *sn*-1,3-dioleoyl-2-palmitoylglycerol) using the microprobe polarized FT–IR technique. These three TAGs are the main constituents of vegetable fats such as palm oil and cocoa butter. The implication of the structural analysis of the molecular compounds of POP–PPO and POP–OPO may stand on two aspects, (a) the formation of the molecular compounds in the binary mixtures of TAGs is revealed in such special cases of SOS–SSO (Engstrom, 1992), SOS–OSO (Koyano et al., 1992), POP–PPO (Minato et al., 1997a) and POP–OPO (Minato et al., 1997b) (SOS; *sn*-1,3-distearoyl-2-oleoylglycerol, SSO; *rac*-1,2-distearoyl-3-oleoylglycerol, OSO; *sn*-1,3-dioleoyl-2-stearoylglycerol), and (b) the specific molecular interactions are operating between the component TAGs to form the molecular compounds. Therefore, the precise information of the microscopic structures of the molecular compounds may give rise to deep insights of the molecular interactions operating between the TAGs. In particular, all the mixed systems examined in the prior and present work involve a common fatty acid moiety; the oleoyl chain.

In our previous report, the quite complicated polymorphic behavior of SOS and POP were unveiled with the microprobe FT–IR method (Yano et al., 1993), which provided structural information of the saturated acyl and oleoyl chains in a separate manner. The present experiments specifically aimed at clarifying the subcell structures, the olefinic conformations, and the glycerol group conformations of the most stable β forms of the molecular compounds of POP–PPO and POP–OPO.

2. Materials and methods

Three TAG samples, POP, PPO, and OPO, were employed. POP and PPO were provided from Unilever (UK) and OPO was purchased from Sigma (USA). The purity of the samples was more than 99%. No further purification was carried out. The molecular compounds were prepared by mixing the component TAGs of POP–PPO and POP–OPO at a 1:1 ratio, melting above 50°C, crystallizing and incubating at 29°C over 1 week. The complete mixing was confirmed by the extinction of the exo- and endo-thermic peaks arising

from each pure TAG component by means of the DSC measurement. The powder XRD spectra (Rigaku Geigerflex, $\lambda = 0.1542$ nm, Tokyo, Japan) were taken at 18°C to confirm the occurrence of the most stable β forms for the two mixtures studied. Microprobe polarized FT–IR measurements were performed with a Spectrum 2000 instrument (Perkin-Elmer, USA). The resolution was set at 2 cm^{-1} for the two β forms, which were slowly crystallized between KBr plates below their melting temperatures. Tiny crystals with a needle shape were grown. The previous study on SOS β crystals showed that the needle axis is parallel to the crystallographic b-axis (Yano et al., 1993). The same geometry was applied to a present case. The directions of the crystal axis and the polarization of the incident IR beam were set so that the b-axis of the crystal and the 0° polarization direction makes an angle of 90°. The polarization angle was changed by 5° step from 0 to 180° as shown in the top right of Fig. 1.

3. Results

Table 1 summarizes the XRD long and short spacings of POP–PPO and POP–OPO compounds in the most stable β forms, which will be referred as β_C. Both forms are of a double chain length structure according to their long spacing values. Very strong short spacings of 0.460 and 0.457 nm are characteristic of triclinic parallel ($T_{\parallel}$) subcell structures (Harnqvist, 1988). The polarized absorption spectra taken for β_C(POP–PPO) and β_C(POP–OPO) are shown in Figs. 1 and 2, respectively.

Fig. 1a and b show the CH_2 scissoring and the CH_2 rocking bands of β_C(POP–PPO), which are sensitive to the subcell packing of the polymethylene chain. The 0° polarization is perpendicular to the b–axis of the unit cell. A single spectrum was observed at 1471 cm^{-1}, indicating a subcell structure of parallel type (Fig. 1a). The intensity of this spectral band showed a clear dichroism with respect to the polarization direction; e.g. maximum at the 90° polarization, and minimum at the 0° polarization. The single CH_2 rocking band at 717 cm^{-1} (Fig. 1b), which is also characteristic of parallel type subcell, showed a clear dichroism. In contrast to the polarization property of the scissoring bands, the rocking band exhibited maximum absorbance at the 0° polarization. This means that the dipole moments of the scissoring and rocking modes make a right angle as shown in Fig. 3.

As to the olefinic conformation, it was concluded that the –HC=CH– out-of-plane bending (γ(=CH)) band around 690 cm^{-1} and the =CH asymmetric stretching (ν(=CH))around 3010 cm^{-1} are sensitive to a local conformation of skew-*cis*-skew′ at the *cis* double bond (Kobayashi, 1988). However, no absorbance of the =CH out-of-plane bending band was observed around

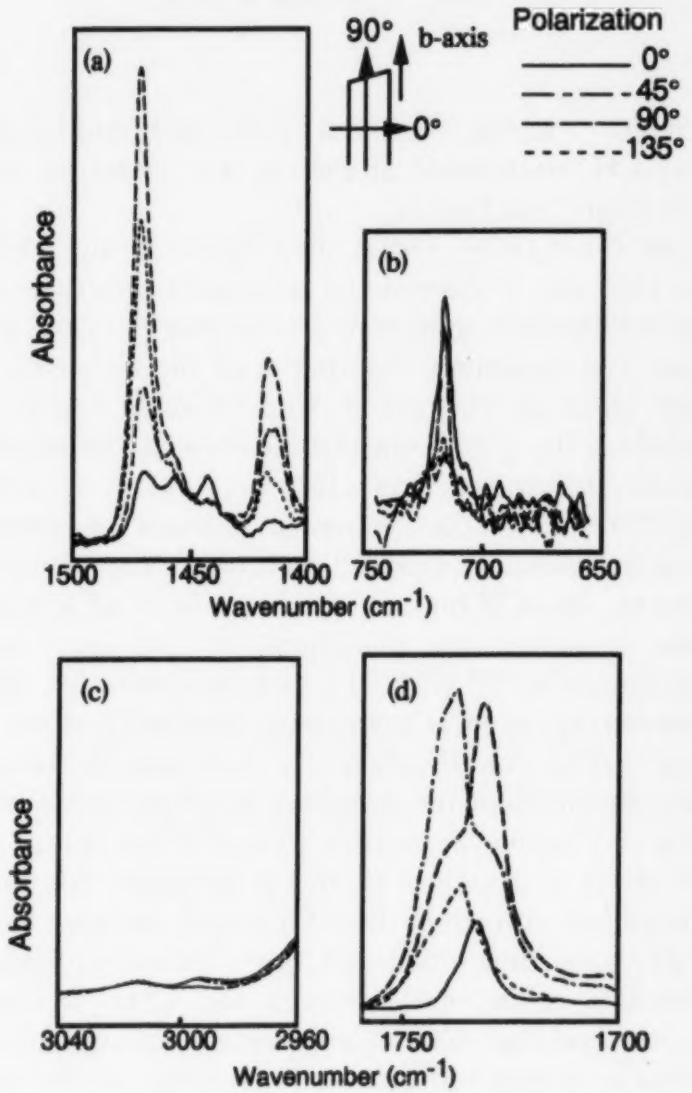

Fig. 1. Polarized microprobe FT–IR spectra of β_C(POP–PPO): (a) CH_2 scissoring, (b) CH_2 rocking and =CH out-of-plane bending, (c) =CH stretching, (d) C=O stretching of glycerol group.

Table 1
X-ray diffraction spectra of POP–PPO and POP–OPO compounds in the most stable β form

POP–PPO (nm)	POP–OPO (nm)
40.1 (vs)	4.21 (vs)
1.38 (s)	1.43 (s)
0.537 (m)	0.527 (m)
0.521 (m)	0.521 (m)
0.506 (w)	0.509 (w)
0.460 (vs)	0.457 (vs)
0.442 (m)	0.442 (m)
0.397 (s)	0.413 (s)
0.337 (m)	0.397 (m)
	0.380 (m)
	0.375 (s)
	0.363 (m)

vs, very strong; s, strong; m, medium; w, weak.

690 cm^{-1} in Fig. 1b, and a small and broad band of =CH asymmetric stretching was observed at 3012 cm^{-1} in Fig. 1c.

As for β_C(POP–OPO), the CH_2 scissoring band at 1470 cm^{-1} showed the maximum absorbance at 105° and the minimum absorbance at 15° (Fig. 2a). The maximum absorbance of the CH_2 rocking band at 717 cm^{-1} was obtained at 15°, whereas the 105° polarization showed the minimum absorbance (Fig. 2b). In contrast to the β_C(POP–PPO), the intensity changes of these spectra showed a reduced dichroism. The olefinic group, the =CH out-of-plane bending band at 675 cm^{-1} showed the maximum at 150° and the minimum at 60° (Fig. 2b), and vice versa for the absorbance of =CH asymmetric stretching at 3007 cm^{-1} (Fig. 2c). This behavior is reasonable, since the directions of the transition dipole moments of the two modes are normal to each other (Fig. 3). There is a deviation in the polarization for the maximum directions by 45 or 135° between the CH_2 scissoring mode and the =CH out-of-plane bending mode, and between the CH_2 rocking mode and the =CH asymmetric stretching mode. This deviation indicates a discrepancy in the vibrational directions of carbon and hydrogen atoms between the polymethylene groups of the oleoyl and palmitoyl chains and the olefinic group of the oleoyl chain.

Fig. 1d and 2d show the C=O stretching bands of the carbonyl group, ν(=CO), which revealed rather complicated polarization dependence, as discussed in the next section.

4. Discussion

The present discussion will be focused on the molecular structures of β_C(POP–PPO) and β_C(POP–OPO). For convenience, the basic structural models which have been proposed based on

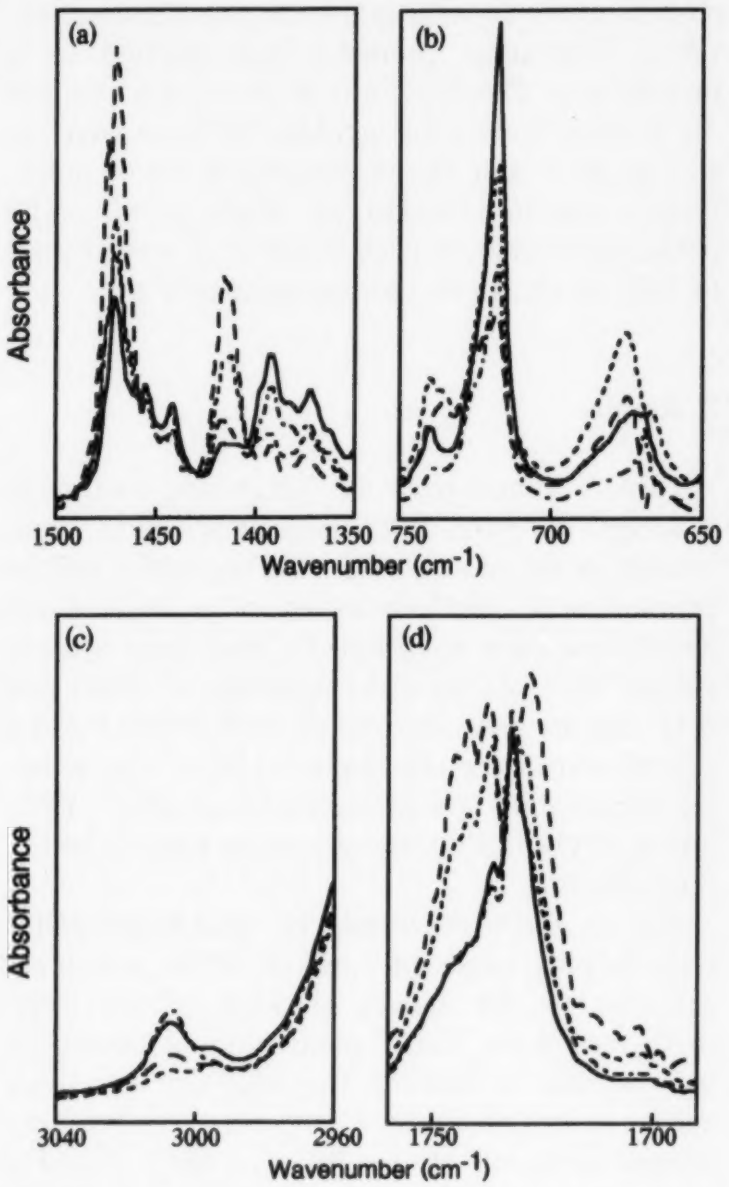

Fig. 2. Polarized microprobe FT–IR spectra of β_C(POP–OPO): (a) CH_2 scissoring, (b) CH_2 rocking and =CH out-of-plane bending, (c) =CH stretching, (d) C=O stretching of glycerol group. The polarization directions with respect to the crystal shape is the same as that in Fig. 1.

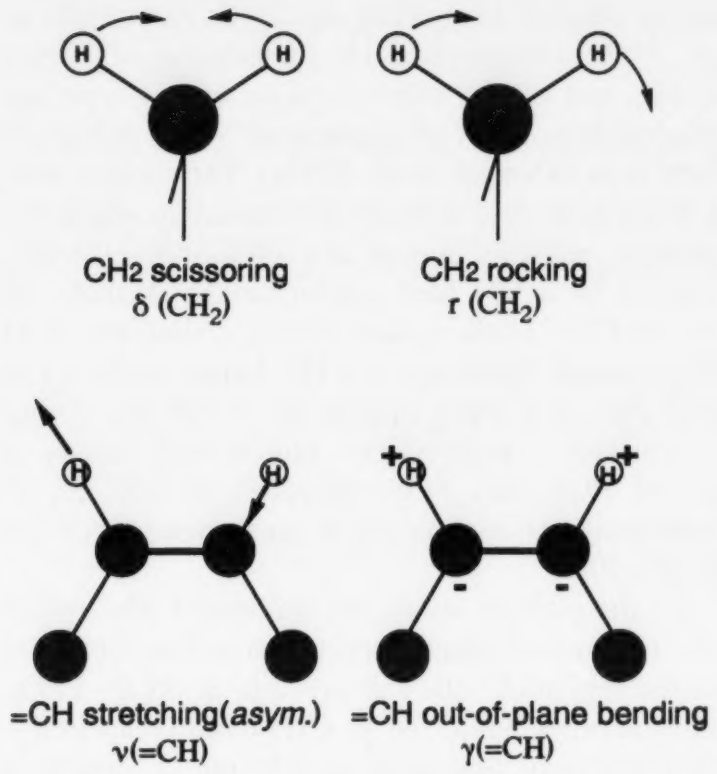

Fig. 3. Vibrational modes of the methylene and olefin groups.

the XRD and DSC studies are illustrated in Fig. 4a and b (Minato et al., 1997a,b). The major point is that the three component TAGs are stacked in a triple chain length structure (Fig. 4c and d), whereas the double chain length structure is formed in the two molecular compounds. This must be ascribed to specific acyl chain interactions. In the two compounds POP–OPO and POP–PPO, the common nature is that one leaflet is composed of the palmitoyl chains. However, the second leaflet is composed singly of the oleoyl chains for the POP–OPO compound, whereas the oleoyl and palmitoyl chains are coexisting in the POP–PPO compound. Thus, it is interesting to discuss the possible structures of the crystallographic subcell, and of the olefinic and glycerol groups, in each molecular compound.

4.1. Subcell structure

The subcell structures of the two β_C forms are of parallel type, because the absorbance of the CH_2 scissoring band and the CH_2 rocking band showed the single peaks. The subcell of orthorhombic type gives rise to splitting in the two spectral bands (Kobayashi, 1988). Then, a problem arises on the detailed subcell structure of parallel type, typically $T_\parallel$ and $O'_\parallel$, and their geometric relations with respect to the crystal axis.

The well-defined polarization properties of the all characteristic bands were observed in an almost complete manner for β_C(POP–PPO), but incompletely for β_C(POP–OPO) (Fig. 1a,b and Fig. 2a,b). From these FT–IR data combined with the XRD short spacing data, one may conclude that the palmitoyl and oleoyl chains of β_C(POP–PPO) are packed according to the triclinic parallel ($T_\parallel$) subcell, with the arrangement of the subcell axes of the two chains in the same directions (Fig. 5). On the other hand, the incomplete polarization of β_C(POP–OPO) indicates the presence of two types of subcell structure. One is due to a geometrical deviation in the direction of the transition dipole moments between the palmitoyl chain leaflet and oleoyl chain leaflet (see Fig. 4a) caused by a contribution of the glycerol group. The other possibility is that the subcell of the oleoyl chains is $O'_\parallel$. However, the XRD of β_C(POP–OPO) did not show the short spacing of

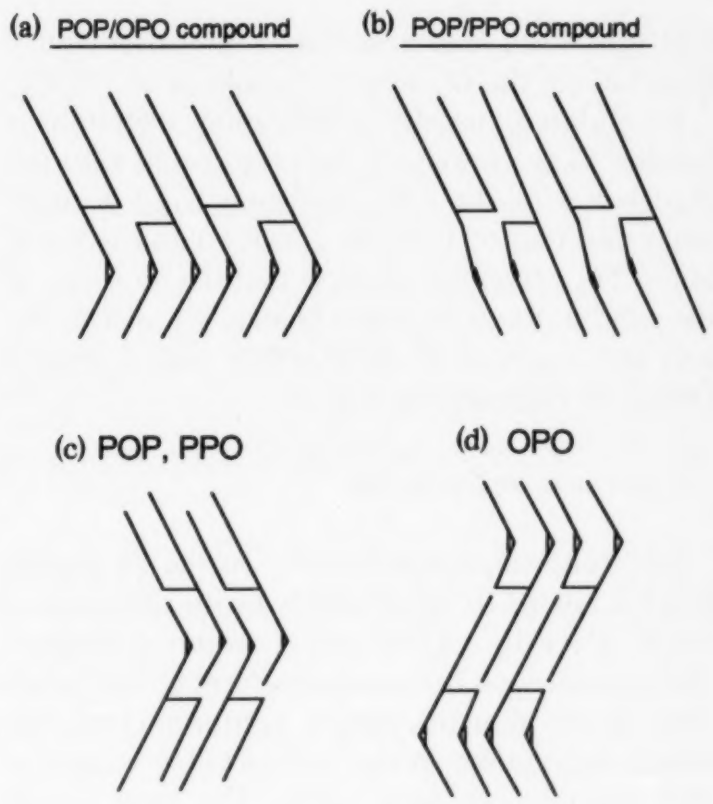

Fig. 4. Structure models of (a) POP–OPO compound, (b) POP–PPO compound, (c) POP and PPO, and (d) OPO.

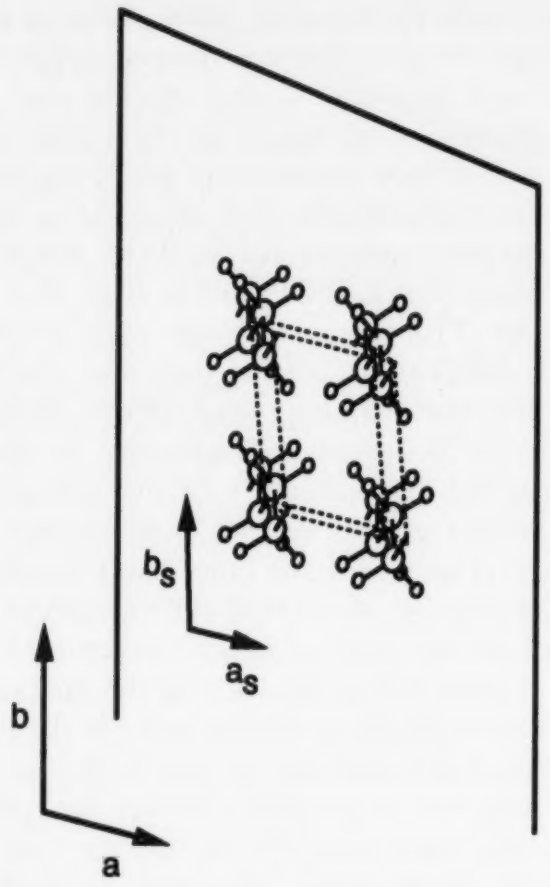

Fig. 5. The relative directions of the $T_{\parallel}$ subcell axes (a_s, b_s) and the unit cell axes (a, b).

0.47 nm which was observed in the oleic acid γ form having the $O'_{\parallel}$ subcell (Suzuki et al., 1985).

In addition, as the polarization direction is parallel to the b-axis of the crystal unit cell, the absorbance of the CH_2 scissoring band is minimum and that of the CH_2 rocking band is maximum. Therefore, we conclude that the direction of the subcell b-axis is approximately parallel to the unit cell b-axis of β_C(POP–PPO) and β_C(POP–OPO), as illustrated in Fig. 5.

4.2. Olefinic conformation

The conformational diversity of the *cis*-double bond is related to the flexibility of the unsaturated lipids. Recently, XRD and vibrational spectroscopic studies on the monounsaturated fatty acids have shown that the olefinic conformations vary widely depending on the polymorphic structures (for example, see Sato, 1996). The most typical conformations are of the skew-*cis*-skew′ (s-*c*-s′) type with a bent geometry, which is revealed in γ forms of oleic (Suzuki et al., 1985; Kobayashi et al., 1986) and erucic acids (Kaneko et al., 1993, 1994), and of the skew-*cis*-skew (s-*c*-s) type appearing in γ_1 form of erucic acid, which is also of bent type (Kaneko et al., 1992a). Petroselinic acid LM form showed a peculiar structure in which the internal rotation angles are (160, *cis*, −158°), leading to a less bent conformation (Kaneko et al., 1992b). These studies indicate that the =CH out-of-plane bending (γ(=CH)) bands of the s-*c*-s′ and the s-*c*-s types appear at ~ 700 cm^{-1} and ~ 730 cm^{-1}, respectively. The γ(=CH) bands of β_1 of POP and SOS appeared at 690 cm^{-1}, indicating the olefinic s-*c*-s′ conformation (Yano et al., 1993).

In the present study, no significant absorption of =CH out-of-plane bending band was observed in the region of 750–650 cm^{-1} in β_C(POP–PPO). On the other hand, the γ(=CH) band of β_C(POP–OPO) clearly appeared at 675 cm^{-1}, which is similar to the frequency of the γ(=CH) band observed in β forms of SOS and POP (Yano et al., 1993). Therefore, we conclude that the olefinic conformation of the β_C(POP–OPO) is of the s-*c*-s′ type. As for β_C(POP–PPO), however, olefinic conformations may be neither of s-*c*-s′ type nor of s-*c*-s type. This means that the steric hindrance between the oleoyl and palmitoyl chains might give rise to the deviation in the olefinic conformation from the s-*c*-s′ and s-*c*-s types.

In this regard, it is interesting to observe the progression bands of the CH_2 wagging and twisting–rocking combination modes, which are very sensitive to the chain length of the acyl moiety and to molecular conformation (Snyder, 1960; Fischmeister, 1974). Fig. 6 shows the CH_2 progression bands of tripalmitin (PPP) β (polarized) and β_C(POP–PPO) (not polarized) measured at 78 K. The progression bands of β_C(POP–PPO) are quite similar to that of PPP β. The same spectra denoted by dotted lines are observed in two samples, caused by the contribution of the palmitoyl chains. This result indicates that the palmitoyl chains of β_C(POP–PPO) must have the same conformation as that of palmitoyl chain of PPP β. Therefore, the oleoyl chains of β_C(POP–PPO) are markedly influenced by the palmitoyl chains, and thereby a deviation in the olefinic

conformation of β_C(POP–PPO) from s-*c*-s′ type or s-*c*-s type is caused.

4.3. Glycerol conformation

The C=O stretching bands, ν(=CO), due to the glycerol groups exhibited quite complicated behavior, and the details in the vibrational assignments are still open to future studies. However, some indicative information was available for the two β_C forms of the POP–PPO and POP–OPO compounds.

The ν(=CO) bands of β_C(POP–PPO) and β_C(POP–OPO) were remarkably different from each other as shown in Fig. 1d and 2d. However, remarkable similarity was observed between β_C(POP–PPO) and PPP β (not shown here), and between β_C(POP–OPO) and POP β (Yano et al., 1993). This means that the local molecular structures close to the glycerol carbonyl groups may be similar in the above two combinations. However, further studies of the conformation of the glycerol group are necessary.

4.4. Comparison with β_C(SOS–SSO) and β_C(SOS–OSO)

It is interesting to compare the IR spectra of the two β forms of the POP–PPO and POP–OPO compounds with those of β_C(SOS–SSO) and β_C(SOS–OSO), whose phase behavior was already clarified (Engstrom, 1992; Koyano et al., 1992). This is because the four compounds may reveal common structural behavior by sharing the oleoyl moieties and also by slightly differing in the saturated acid moieties.

A perfect correspondence in various FT–IR spectra of β_C(SOS–SSO) and β_C(SOS–OSO) could be observed for each spectral band between the two combinations of β_C(POP–PPO) and β_C(SOS–SSO), and β_C(POP–OPO) and β_C(SOS–OSO). This dictates that the molecular structures are almost identical in the two pairs of these molecular compounds.

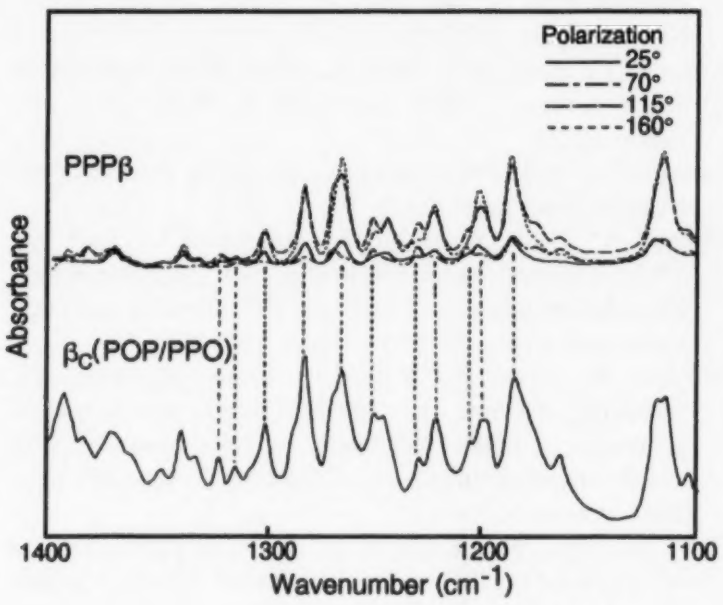

Fig. 6. The progression bands of wagging mode and twisting–rocking mode of the POP–PPO compound and PPP β form taken at 78K.

4.5. Steric hindrance and molecular compound structures

The present work has given the molecular level information of the compound structures comprised of the 1:1 mixtures of POP–OPO and POP–PPO, as illustrated in Fig. 4. Since the molecular forces operating in the present molecules are of a van der Waals type, it is quite interesting how the molecular interactions can enable the formation of the stable compounds.

The structure of β_C(POP–OPO) looks more stable compared to that of β_C(POP–PPO), since each molecule of POP and OPO is arranged upside down alternatively in the former as shown in Fig. 4a. In this structure, the palmitoyl and oleoyl leaflets are separated, and no coexistence of the two chains in the same leaflet occurs. Thus, the steric hindrance between the palmitoyl and oleoyl chains is minimized. In addition, the olefinic IR spectra, γ(=CH) (Fig. 5) of β_C(POP–OPO) indicates the existence of the s-*c*-s′ conformation, meaning the least influence of the palmitoyl chains on the olefinic conformation.

In the structure of β_C(POP–PPO), the number of oleoyl and palmitoyl chains of β_C(POP–PPO) are not balanced. Therefore, the separation of palmitoyl chain leaflet and palmitoyl–oleoyl mixed acid chain leaflet must occur as in Fig. 4b.

Dynamic analysis on the polymorphic transformations from α-β'-β of the POP–PPO compound with a time-resolved synchrotron radiation XRD study also supports this model (Minato et al., 1997a). The present FT–IR results indicate that the oleoyl chains of β_C(POP–PPO) are remarkably deviated from the usual olefinic conformations of s-*c*-s′ and s-*c*-s types, because of the steric hindrance caused by the adjacent palmitoyl chains. This result is different from the structure model proposed for β_C(SOS–SSO), where stearoyl chains are bent due to the presence of the oleoyl chains in stearoyl–oleoyl mixed acid chain leaflet (Engstrom, 1992).

More precise structures of these molecular compounds are left for future works, although the structural models in Fig. 4a and b are the most plausible. An elucidation of the structures of mixed acid leaflet in terms of precise subcell packing and conformation, glycerol structures, and methyl end packing will be required. In this regard, we stress again that the *cis*-unsaturated fatty acids exhibit quite diverse molecular structures. This diversity may be seen in the subcell structures and precise conformations of the oleoyl moiety, particularly in β_C(POP–PPO). The elucidation of these properties may be valuable to assess the lateral chain packing in liquid crystalline phases of amphiphilic lipids containing oleic acid and saturated acid moieties (Small, 1984).

References

Engstrom, L., 1992. Triglyceride systems forming molecular compounds. J. Fat Sci. Technol. 94, 173–181.

Fischmeister, I., 1974. Infrared absorption spectroscopy of normal and substituted long-chain fatty acids and esters in the solid state. Prog. Chem. Fats Lipids 24, 93–162.

Formo, M.W., 1979. Physical properties of fats and fatty acids, In: Swern, D. (Ed.), From Bailey's Industrial Oil and Fat Products, vol. 1. Wiley, New York, pp. 177–232.

Goto, M., Kodali, D.R., Small, D.M., Honda, K., Kozawa, K., Uchida, T., 1992. Single crystal structure of a mixed-chain triglycerol: 1,2-Dipalmitoyl-3-acetyl-*sn*-glycerol. Proc. Natl. Acad. Sci. USA. 89, 8083–8086.

Harnqvist, H., 1988. Crystal structures of fats and fatty acids. In: Garti, N., Sato, K. (Eds.), From Crystallization and Polymorphism of Fats and Fatty Acids, Marcel Dekker, New York, pp. 97–137.

Inoue, T., Motoda, I., Hiramatsu, N., Suzuki, M., Sato, K., 1992. Phase behavior of binary mixtures of *cis*-monounsaturated fatty acids with different ω-chain length. Chem. Phys. Lipids 63, 243–250.

Inoue, T., Motoda, I., Hiramatsu, N., Suzuki, M., Sato, K., 1993. Phase behavior of binary mixture of palmitoleic acid (*cis*-9-hexadecenoic acid) and asclepic acid (*cis*-11-octadecenoic acid). Chem. Phys. Lipids 66, 209–214.

Jensen, L.H., Mabis, A.J., 1966. Refinement of the structure of β-tricaprin. Acta Cryst. 21, 770–781.

Kaneko, F., Kobayashi, M., Kitagawa, Y., Matsuura, Y., Sato, K., Suzuki, M., 1992a. Structure of the γ_1 phase of erucic acid. Acta Cryst. C48, 1060–1063.

Kaneko, F., Kobayashi, M., Kitagawa, Y., Matsuura, Y., Sato, K., Suzuki, M., 1992b. Structure of the low-melting phase of petroselinic acid. Acta Cryst. C48, 1054–1057.

Kaneko, F., Yamazaki, K., Kobayashi, M., Kitagawa, Y., Matsuura, Y., Sato, K., Suzuki, M., 1993. Structure of the γ phase of erucic acid. Acta Cryst. C49, 1232–1234.

Kaneko, F., Yamazaki, K., Kobayashi, M., Sato, K., Suzuki, M., 1994. Vibrational spectroscopic study on polymorphism of erucic acid and palmitoleic acid: γ_1-α_1 and γ-α reversible solid state phase transition. Spectrochimica Acta 50A, 1589–1603.

Kaneko, F., Kobayashi, M., Sato, K., Suzuki, M., 1996. Martensitic phase transition of petroselinic acid: influence of polytypic structure. J. Phys. Chem. 101, 285–292.

Kobayashi, M., Kaneko, F., Sato, K., Suzuki, M., 1986. Vibrational spectroscopic study on polymorphism and order–disorder phase transition in oleic acid. J. Phys. Chem. 90, 6371–6378.

Kobayashi, M., 1988. Vibrational spectroscopic aspects of polymorphism and phase transition of fats and fatty acids. In: Garti, N., Sato, K. (Eds.), From Crystallization and Polymorphism of Fats and Fatty Acids. Marcel Dekker, New York, pp. 139–187.

Koyano, T., Hachiya, I., Sato, K., 1992. Phase behavior of mixed systems of SOS and OSO. J. Phys. Chem. 96, 10514–10520.

Larsson, K., 1964. The crystal structure of the β form of the trilaurin. Ark. Kemi. 23, 1–15.

Minato, A., Ueno, S., Smith, K., Amemiya, Y., Sato, K., 1997a. Thermodynamic and kinetic study on phase behavior of binary mixtures of POP and PPO forming molecular compound systems. J. Phys. Chem. 101, 3498–3505.

Minato, A., Ueno, S., Yano, J., Smith, K., Seto, H., Amemiya, Y., Sato, K., 1997b. Thermal and structural properties of POP–OPO binary mixtures examined with synchrotron radiation X-ray diffraction. J. Am. Oil Chem. Soc., in press.

Sato, K., 1996. Polymorphism of pure triacylglycerols and natural fats. In: Padley, F. (Ed.), From Advances in Applied Lipid Research, vol. 2. JAI Press, New York, pp. 213–268.

Sato, K., Yano, J., Kawada, I., Kawano, M., Kaneko, F., Suzuki, M., 1997. Polymorphic behavior of gondoic acid

and phase behavior of binary mixtures of gondoic acid/asclepic acid and gondoic acid/oleic acid. J. Am. Oil Chem. Soc., in press.

Small, D.M., 1984. Lateral chain packing in lipids and membranes. J. Lipid Res. 25, 1490–1499.

Small, D.M., 1986. The Physical Chemistry of Lipids. Plenum, New York, pp. 345–395.

Snyder, R.G., 1960. Vibrational spectra of crystalline *n*-paraffins part I. Methylene rocking and wagging modes. J. Mol. Spectrosc. 4, 411–434.

Suzuki, M., Ogaki, T., Sato, K., 1985. Crystallization and transformation mechanisms of α, β and γ polymorphs of ultra-pure oleic acid. J. Am. Oil Chem. Soc. 62, 1600–1604.

Ueno, S., Suetake, T., Yano, J., Suzuki, M., Sato, K., 1994. Structure and polymorphic transformations in elaidic acid (*trans*-ω9-octadecenoic acid). Chem. Phys. Lipids 72, 27–34.

Yano, J., Ueno, S., Sato, K., Arishima, T., Sagi, N., Kaneko, F., Kobayashi, M., 1993. FT–IR study of polymorphic transformations in SOS, POP and POS. J. Phys. Chem. 97, 12967–12973.

Yoshimoto, N., Nakamura, T., Suzuki, M., Sato, K., 1991. Physical properties of binary mixtures of petroselinic acid/oleic acid and asclepic acid/oleic acid. J. Phys. Chem. 95, 3384–3390.

ELSEVIER

Chemistry and Physics of Lipids
88 (1997) 73–82

CPL
CHEMISTRY AND PHYSICS OF LIPIDS

Structure of stratum corneum lipids characterized by FT-Raman spectroscopy and DSC. III. Mixtures of ceramides and cholesterol

Matthias Wegener [a], Reinhard Neubert [a,*], Willi Rettig [a], Siegfried Wartewig [b]

[a] *Department of Pharmacy, Martin-Luther-University Halle-Wittenberg, Wolfgang-Langenbeck-Str. 4, D-06120 Halle, Germany*
[b] *Institute of Applied Dermatopharmacy, Wolfgang-Langenbeck-Str. 4, D-06120 Halle, Germany*

Received 6 March 1997; received in revised form 5 June 1997; accepted 25 June 1997

Abstract

The thermotropic and lyotropic phase behaviour of mixtures of ceramides type IV and cholesterol was investigated using Fourier transform (FT) Raman spectroscopy and differential scanning calorimetry (DSC). In the dry and in the fully hydrated state of these mixtures the DSC-curves exhibit an eutectic melting followed by the melting of the residual solid component. The Raman spectrum of the mixtures is complex, nevertheless, the appearance of the conformationally dependent bands indicates the ordered structure of the hydrocarbon chains. The temperature dependence of the conformationally sensitive bands in the CH_2 stretching region (2800–2975 cm^{-1}) and in the chain C–C stretching region (1050–1150 cm^{-1}) was used to estimate the degree of order in terms of the relative population of *trans* and *gauche* conformers. The spectrum of the pure cholesterol shows only a weak temperature dependence in the CH_2 stretching region and, therefore, the decrease of the intensity of the asymmetric CH_2 stretching mode at 2880 cm^{-1} can be attributed to the melting of the alkyl chains of ceramides. The temperature and width of the phase transition, derived from Raman data, are similar to those of the DSC study. © 1997 Elsevier Science Ireland Ltd.

Keywords: Raman spectroscopy; DSC; Ceramides; Cholesterol; Stratum corneum; Phase behaviour

1. Introduction

Stratum corneum, the outermost layer of the human skin, is responsible for the permeability of human skin to dermally and transdermally delivered drugs. The stratum corneum consists of 10–15 layers of relatively impermeable corneocytes, which are embedded in lipids arranged in a lamellar structure. The most important diffusional pathway through the stratum corneum is the intercellular pathway which is influenced by the

* Corresponding author. Tel.: +49 345 5525000; fax: +49 345 5527021.

PII S0009-3084(97)00050-9

stratum corneum lipids. A variety of techniques have been used to study the structure of stratum corneum and these lipids. Increasing interest is currently focusing on the molecular structure of the stratum corneum lipids. The Fourier transformed infrared spectroscopy (FTIR) technique was applied to study the molecular nature of stratum corneum (Golden et al., 1985; Ongpipattanakul et al., 1994). In recent years the Fourier transform (FT) Raman spectroscopy is also being used to collect vibrational spectra of the human stratum corneum (Williams et al., 1992; Barry et al., 1992; Anigbogu et al., 1995).

Stratum corneum lipid bilayers consist mainly of three fractions namely, ceramides (35%), fatty acids (25%) and cholesterol (20%) and its derivates (Elias, 1990). Ceramides are *N*-acyl linked sphingolipids and have been suggested to have a central role for the barrier function of stratum corneum (Holleran et al., 1991). The free hydroxyl groups and the amide group can form an extensive hydrogen bonded network. The phase behaviour of ceramides and the influence of the hydration have been investigated only in few studies (Wiedmann and Salmon, 1991; Han et al., 1995; Tanikawa and Miyajima, 1995; Wegener et al., 1996). The physico-chemical properties of ceramides and their role with regard to the function of the barrier as well as their interactions with stratum corneum lipids are not yet sufficiently understood.

Cholesterol, another major component of stratum corneum, is required for the permeability barrier homeostasis (Menon et al., 1985; Feingold et al., 1990). Although the interactions of cholesterol with phospholipids (de Kruyff et al., 1973; Demel and de Kruyff (1976), McMullen et al., 1994) and cerebrosides have attracted much interest (Johnston and Chapman, 1988; Jackson et al., 1988), the effect of cholesterol on the thermotropic phase transition of hydrated natural hydroxyceramides was studied by Wiedmann and Salmon (1991) using solely differential scanning calorimetry (DSC).

In a previous paper, we discussed ceramides type IV as a model substance for the fraction of ceramides and reported the temperature dependence of their physical properties by applying FT-Raman spectroscopy and DSC (Wegener et al., 1996). Examining conformationally sensitive Raman bands, we have shown that the hydrocarbon chains of ceramides type IV exhibit a highly ordered structure in the crystalline state and that the melting process can be characterized in terms of the relative population of the *trans* and *gauche* conformers of alkyl chain residues.

The aim of this work is directed above all to investigate the molecular interactions between well-defined stratum corneum lipids and understand the complex function of the stratum corneum lipids. Thus, in the present study, the influence of cholesterol on both phase transition and hydrocarbon ordering of ceramides type IV by using differential scanning calorimetry and FT Raman spectroscopy is reported. In addition, the behaviour of the hydrated systems has been investigated. In a previous communication, we have briefly discussed both aspects (Wartewig et al., 1997). Additionally, continuing this concept, the thermotropic phase behaviour of mixtures of ceramides type IV/stearic acid has been elucidated in an other paper (Neubert et al., 1997)

2. Materials and methods

2.1. Samples

Polycrystalline samples of ceramides type IV and cholesterol were obtained from Sigma (Sigma, St. Louis, MO) and were used as received. Ceramides type IV contain α-hydroxy fatty acids mainly composed of $C_{18:0}$, $C_{22:0}$, $C_{24:0}$, and $C_{24:1}$. The mixtures were casted from chloroform solution and dried under vacuum. Excess bidistilled water was added to obtain fully hydrated lipid mixtures. Uniform hydration was achieved by heating the sample in a water bath (85°C) for 30 min. Stable samples were prepared by annealing the lipids at 40°C for 24 h. The sample was placed in a cylindrical glass tube for Raman scattering experiments and in an aluminium pan for DSC measurements.

2.2. Differential scanning calorimetry

Calorimetric scans were performed at 5 K min^{-1} on a DSC-2 (Perkin-Elmer, Norwalk, USA) differential scanning calorimeter. The extrapolated onset temperature, T_O, was determined by extrapolating to the baseline of the most rapid rise of the peak as a function of temperature using Perkin-Elmer software. The extrapolated peak completion temperature, T_C, was determined in an analogous procedure using the dropping part of the peak after maximum (Hemminger, 1994). Both extrapolated onset and completion temperatures of the mixtures were corrected for the contributions to the total transition width which are due to the finite width of the transition peaks of the pure lipids using the empirical procedure according to Maybrey and Sturtevant, 1976. The enthalpy was obtained by integrating the area under the peak of the phase transition by comparison with that of a known standard (In).

2.3. Fourier transform Raman spectroscopy

FT-Raman spectra were recorded with a FTIR spectrometer IFS 66 (Bruker, Karlsruhe, Germany) equipped with the Raman module FRA 106 using a diode pumped Nd:YAG laser at an operating wavelength of 1064 nm. The scattered radiation was collected at 180° to the source. Typical spectra were recorded at a laser power of 300 mW at sample location and a resolution of 4 cm^{-1}. In order to obtain a good signal to noise ratio, typically, 400 scans were co-added for the spectra, corresponding to a measurement time of 10 min. Using the temperature control accessory R 495 the temperature dependence of the Raman spectra were studied in the range 40 to 100°C (stability ± 0.2 K). The sample was allowed to equilibrate for 15 min to stabilize the temperature before recording each spectrum. The manipulation and evaluation of the spectra were carried out using the Bruker OPUS software package, as described elsewhere (Wegener et al., 1996). Generally, Raman intensities were determined as integrated band intensities.

3. Results and discussion

3.1. Ceramides type IV

The DSC curve of anhydrous ceramides type IV shows a relatively broad endothermic phase transition at 89°C (Fig. 1a) with an enthalpy change of 112 J g^{-1} (Wegener et al., 1996). This transition is reversible and reproducible in repeated scans.

In the case of full hydration, the transition temperature is lowered to 74°C, which agrees with previous studies of fully hydrated hydroxyceramides (Han et al., 1995; Tanikawa and Miyajima, 1995; Shah et al., 1995). A repeated scan of the fully hydrated sample shows a broad exothermic peak, which is attributed to a transition from

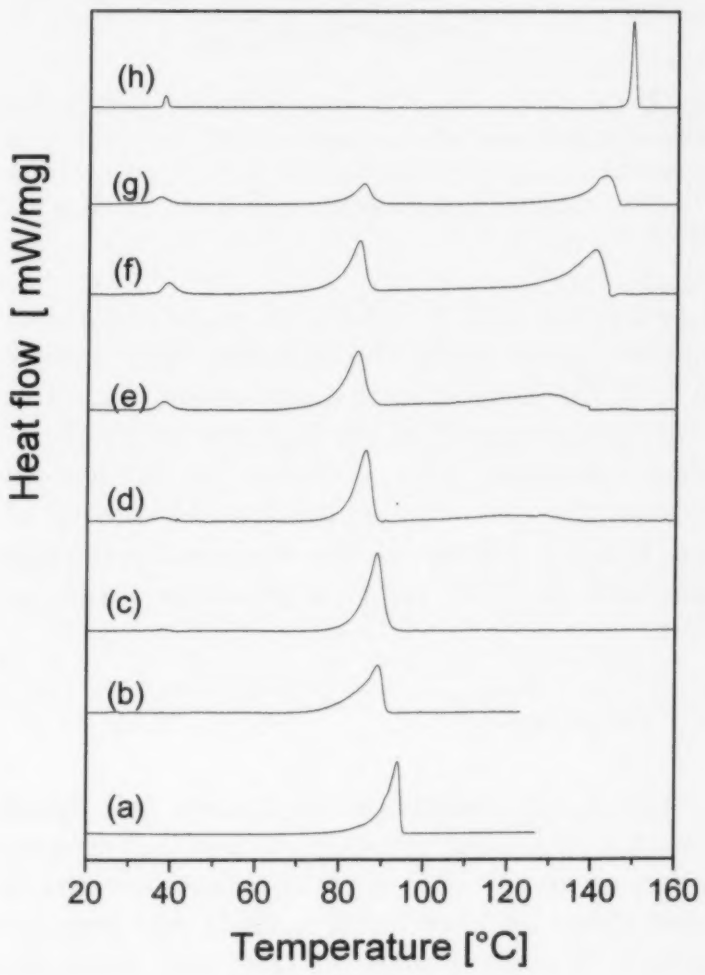

Fig. 1. Calorimetric scans of ceramides IV/cholesterol mixtures after storage at 40°C for 24 h with %cholesterol being: (a) 0 mol%; (b) 25 mol%; (c) 45 mol%; (d) 60 mol%; (e) 70 mol%; (f) 85 mol%; (g) 90 mol%; and (h) 100 mol%.

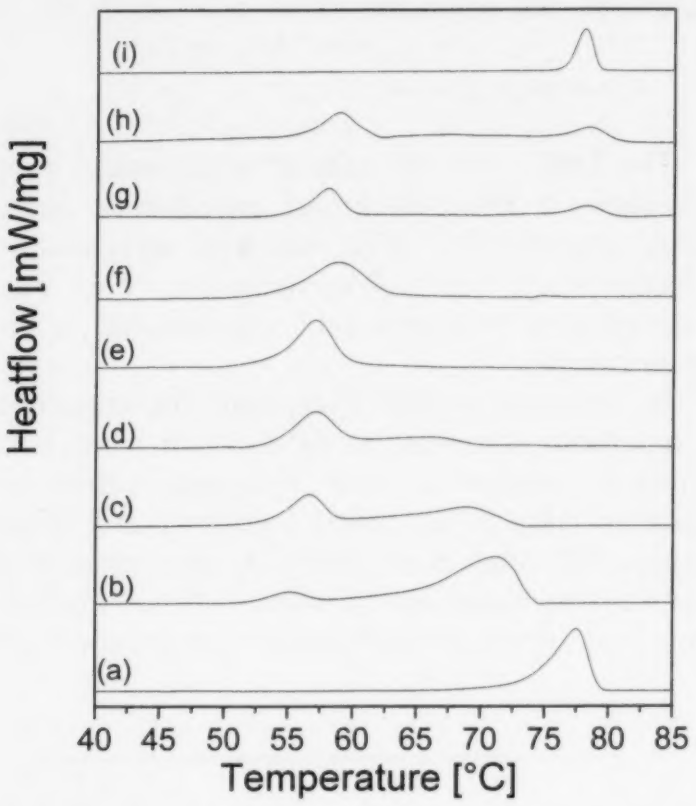

Fig. 2. Calorimetric scans of fully hydrated ceramides IV/cholesterol mixtures after storage at 40°C for 24 h with %cholesterol being: (a) 0 mol%; (b) 25 mol%; (c) 38 mol%; (d) 47 mol%; (e) 63 mol%; (f) 73 mol%; (g) 84 mol%; (h) 90 mol%; and (i) 100 mol%.

a metastable state to a stable gel phase (Tanikawa and Miyajima, 1995). The annealing of the sample at 40°C for 24 h results in a conversion to a stable state, demonstrated by the fact that no exotherm phase transition was observed by subsequent heating (Fig. 2a). The temperature dependence of the Raman spectra of the hydrated ceramides annealed at 40°C yields a phase transition at 72°C.

3.2. Cholesterol

Anhydrous cholesterol undergoes two phase changes on heating from 0°C to 160°C. The transition at about 37°C (Fig. 1h), first reported in 1965 (Spier and van Senden, 1965), has been the subject of many studies on DSC and X-ray diffraction. The crystalline structure of the two relevant polymorphs of anhydrous cholesterol has been described elsewhere (Hsu and Nordman, 1983). According to these studies, one of the major changes occuring in side chains of the two molecules of the unit cell is the conformational change from *gauche-trans* to the energetically more stable *trans-trans* conformation. These conformational transitions can also be observed in the Raman spectrum as a small decrease of the band position of the symmetric CH_2 stretching mode (Fig. 3).

Hydrated cholesterol (monohydrate) undergoes a phase transition at 78°C (Fig. 2i). This is a transition from the hydrated to the anhydrous state (Loomis et al., 1979; Small, 1986) and can be seen both in the DSC curve and in the temperature dependence of the Raman spectrum in the methylene stretching region (Fig. 4). The differences in the Raman spectra of the anhydrous and hydrated cholesterol are described in the literature (Bulkin and Krishan, 1971; Faiman, 1977) and our investigations conform to this data.

3.3. Mixtures of ceramides type IV and cholesterol

Representative DSC curves of mixtures of anhydrous ceramides type IV/cholesterol are given in Fig. 1. It is evident, that the addition of ceramides type IV induces distinct effects on the thermal behaviour of cholesterol.

First of all, like in the scans of the pure cholesterol (Fig. 1h) a thermal event appears at nearly

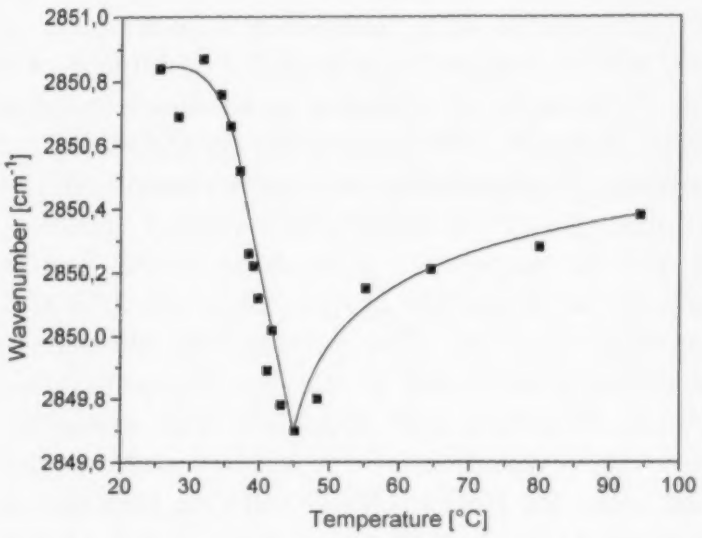

Fig. 3. Band position of the symmetric CH_2 stretching mode versus temperature for anhydrous cholesterol.

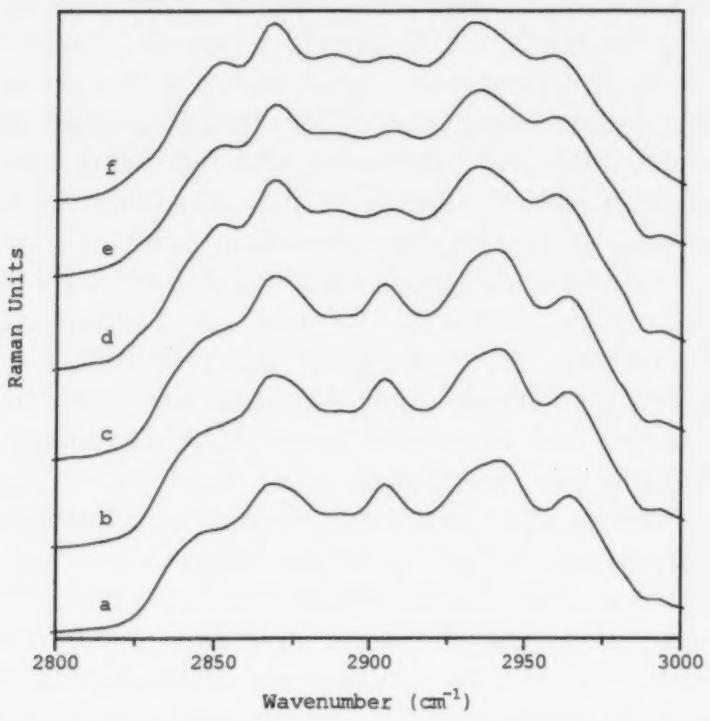

Fig. 4. Temperature dependence of the Raman spectra in the CH_2 stretching region of hydrated cholesterol at $T = 25°C$ (a); $T = 43°C$ (b); $T = 65°C$ (c); $T = 76°C$ (d); and $T = 90°C$ (e) in comparison to the Raman spectrum of anhydrous cholesterol (f).

the same temperature of 37°C (Fig. 1b–g). This peak in the scans of the mixtures is due to the solid-solid transition of cholesterol because the intensity of this peak can be simply correlated to the amount of anhydrous cholesterol. The appearance of this specific transition of cholesterol in all mixtures indicates the existence of free cholesterol in the solid state mixtures. This is the first strong indication of the immiscibility of cholesterol with ceramides type IV in the solid phase. This finding is in accordance with the eutectic type phase diagram (Fig. 5) derived from the measured DSC curves of the mixtures (Fig. 1b–g). The phase diagram suggests the second argument that the components are immiscible in the solid state but miscible in the molten state. The measured DSC curves of the mixtures with a cholesterol content of 60 mol% and more (Fig. 1d-g) show at higher temperatures a distinct eutectic behaviour. Therefore, the peaks at about 82°C are due to the melting of the eutectic and the immediately following broad event is caused by the melting of the residual solid cholesterol. This assumption is supplemented by polarizing optical microscopy studies, which demonstrate that there are cholesterol crystals after melting of the eutectic mixture. The peak again at 82°C in the curve given in Fig. 1c represents the melting of the almost eutectic composition.

For samples with a cholesterol content of 25 mol% and lower, the low temperature transition of cholesterol can also be detected using an enhanced sensitivity. In the high temperature region the distinct eutectic melting compared to the curves of the cholesterol-rich mixtures cannot be observed. However, in accordance with the constructed phase diagramm in Fig. 5, we assume that the shoulder of the transition peak in Fig. 1b is caused by the eutectic melting process. A peak shape analysis reveals that there are two thermal events.

The DSC experiments with fully hydrated mixtures of ceramides type IV/cholesterol show that hydration leads to a further decrease in the temperature of the eutectic melting to about 54°C. The scans of the different mixtures are given in

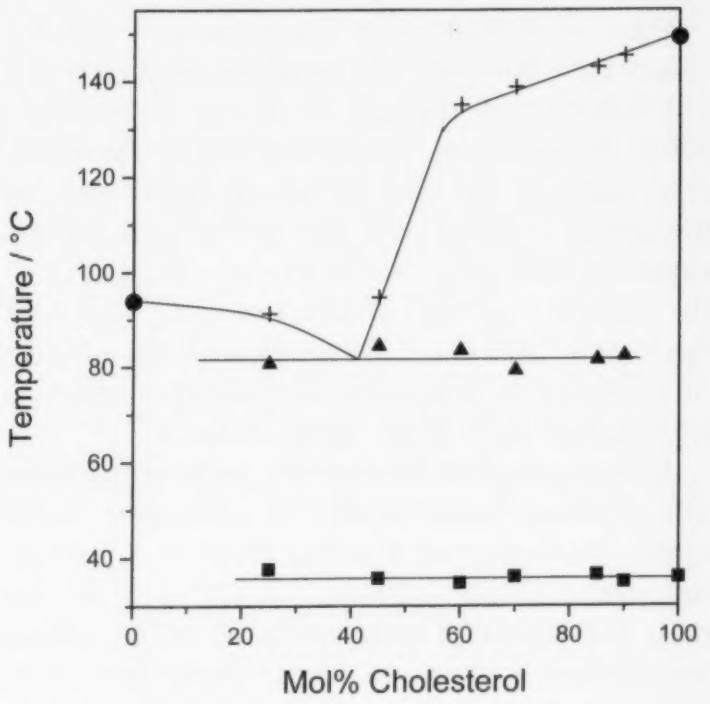

Fig. 5. Phase diagram of dry mixtures of ceramides type IV and cholesterol: ■, extrapolated onset temperature; T_O, due to the solid-solid transition of pure cholesterol; ●, maximum transition temperature; ▲, corrected extrapolated onset temperature of the eutectic peak; and +, corrected extrapolated completion temperature.

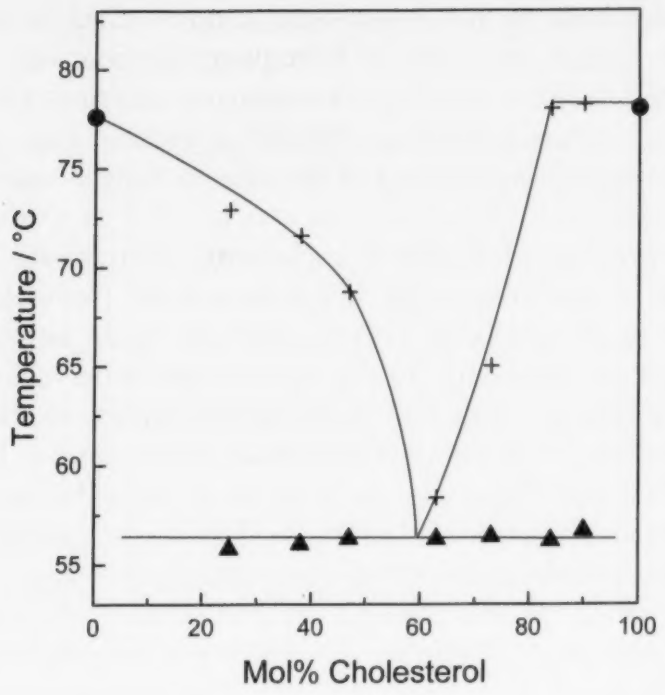

Fig. 6. Phase diagram of fully hydrated mixtures of ceramides type IV and cholesterol: ●, maximum transition temperature; ▲, corrected extrapolated onset temperature of the eutectic peak; +, corrected extrapolated completion temperature.

Fig. 2. The phase diagram of the fully hydrated samples is shown in Fig. 6.

The Raman spectra of the ceramides type IV/cholesterol mixtures are complex owing to the superposition of the spectra of the two components. Nevertheless, the conformationally dependent bands in the CH_2 stretching region indicate the highly ordered structure of the hydrocarbon chains at 40°C (Fig. 7). As can be seen in Fig. 7, the intensity of the asymmetric CH_2 stretching mode near 2880 cm^{-1} decreases with the addition of cholesterol, indicating decreasing number of *trans* conformers of the alkyl chains.

The temperature dependence of conformationally sensitive bands in the CH_2 stretching region (2800–3000 cm^{-1}) and in the chain C–C stretching region (1050–1150 cm^{-1}) was used to estimate the degree of order in terms of the relative population of *trans* and *gauche* conformers. Fortunately, the Raman spectrum of cholesterol exhibits only a weak temperature dependence in the range from 20 to 100°C. Therefore, it can be assumed that the temperature-induced changes in the Raman spectra of the mixtures are related to structural alterations of the ceramides part. As an example, these changes in the CH_2 stretching region for the 75 mol% ceramides type IV/25 mol% cholesterol sample are shown in Fig. 8. The intensity of the asymmetric CH_2 stretching band at about 2880 cm^{-1} decreases with increasing temperature and disappears in the underlying background above the phase transition point.

In order to determine the integrated intensity of the $\nu_s(CH_2)$ and $\nu_{as}(CH_2)$ lines, the overlapping bands were decomposed by using the OPUS fit procedure taking into consideration both ceramides and cholesterol bands. The 'Levenberg-Marquardt' algorithm was used for this procedure. To reduce the number of adjustable parameters, a pure Gaussian function was supposed as line shape for each band and the position of the broad 'Fermi resonance' band was fixed. Fig. 9 shows an example of the results of this decomposition for the 40 mol% ceramides type IV/60 mol% mixture at 40 and 60°C, respectively.

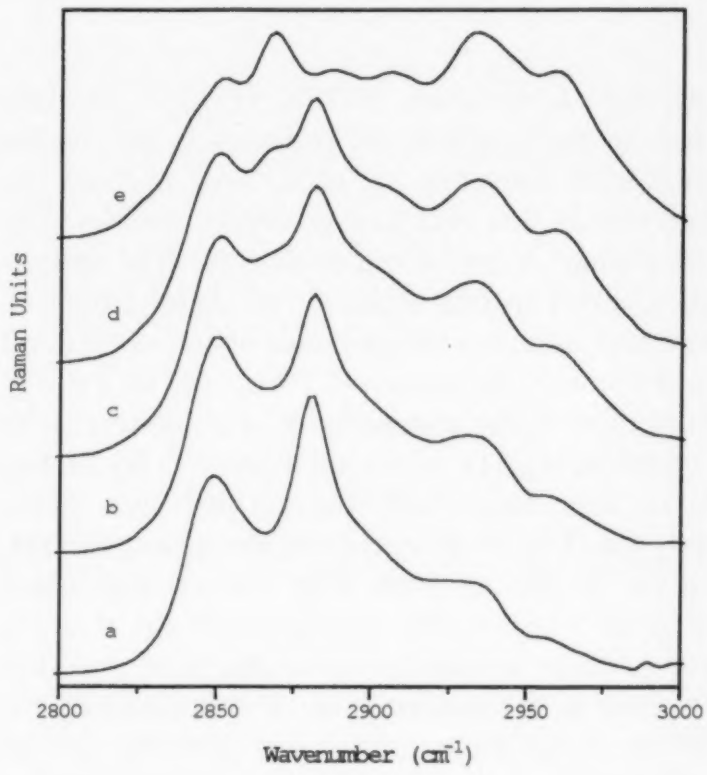

Fig. 7. Raman spectra of various anhydrous ceramides type IV/cholesterol mixtures at 40°C: (a) 100 mol% ceramides type IV; (b) 75 mol% ceramides type IV/25 mol% cholesterol; (c) 40 mol% ceramides type IV/60 mol% cholesterol; (d) 25 mol% ceramides type IV/75 mol% cholesterol; and (e) 100 mol% cholesterol.

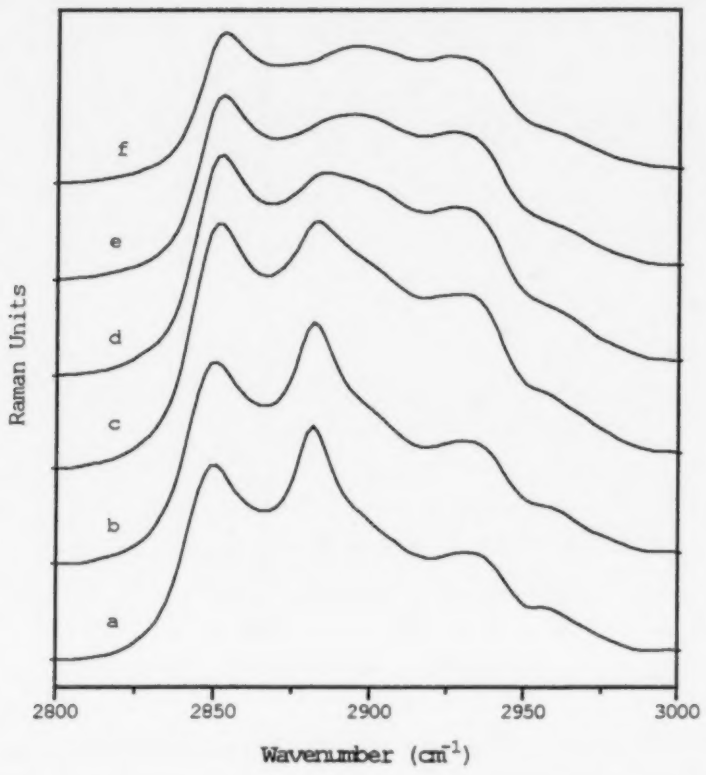

Fig. 8. Temperature dependence of the Raman spectra in the CH_2 stretching region for the 75 mol% ceramides/25 mol% cholesterol mixture: (a) $T = 40°C$; (b) $T = 60°C$; (c) $T = 70°C$; (d) $T = 75°C$; (e) $T = 80°C$; and (f) $T = 86°C$.

As shown in Fig. 10, with increasing temperature the intensity ratio $I[(\nu_{as}(CH_2))/I(\nu_s(CH_2))]$, as a measure of the relative population of the *trans* and *gauche* conformers, continuously decreases for all mixtures and tends to approach zero after the melting of the eutectic mixture. Another possibility for characterizing the phase transition is the temperature dependence of the band position of the symmetric CH_2 stretching mode (Fig. 11). The point of inflection of such a curve can be compared with the phase transition temperature of the DSC curve.

In the region of the skeletal stretching vibrations the asymmetric (at 1063 cm^{-1}) and symmetric (at 1130 cm^{-1}) C–C stretching modes of the alkyl chains in *trans* conformation are to be seen in all mixtures at 40°C. The temperature dependence of these integrated intensities to a reference band (2727 cm^{-1}, ν(CH) aliphatic, overtones CH bending) yields the same curve as the temperature dependence of the CH_2 stretching region and confirms to the validity of these results.

The longitudinal acoustic modes (LAM) of weak intensity in the low frequency region below 300 cm^{-1}, as observed in anhydrous (Wegener et al., 1996) and hydrated ceramides type IV, can be only seen in mixtures with low cholesterol content. Unfortunately, it was not possible to quantify the disturbance of the extended all-*trans* hydrocarbon chain due to the addition of cholesterol, because the intensities of the LAM in the pure ceramides are rather low and in mixtures with high cholesterol content the interference with cholesterol bands is too high for a detailed analysis.

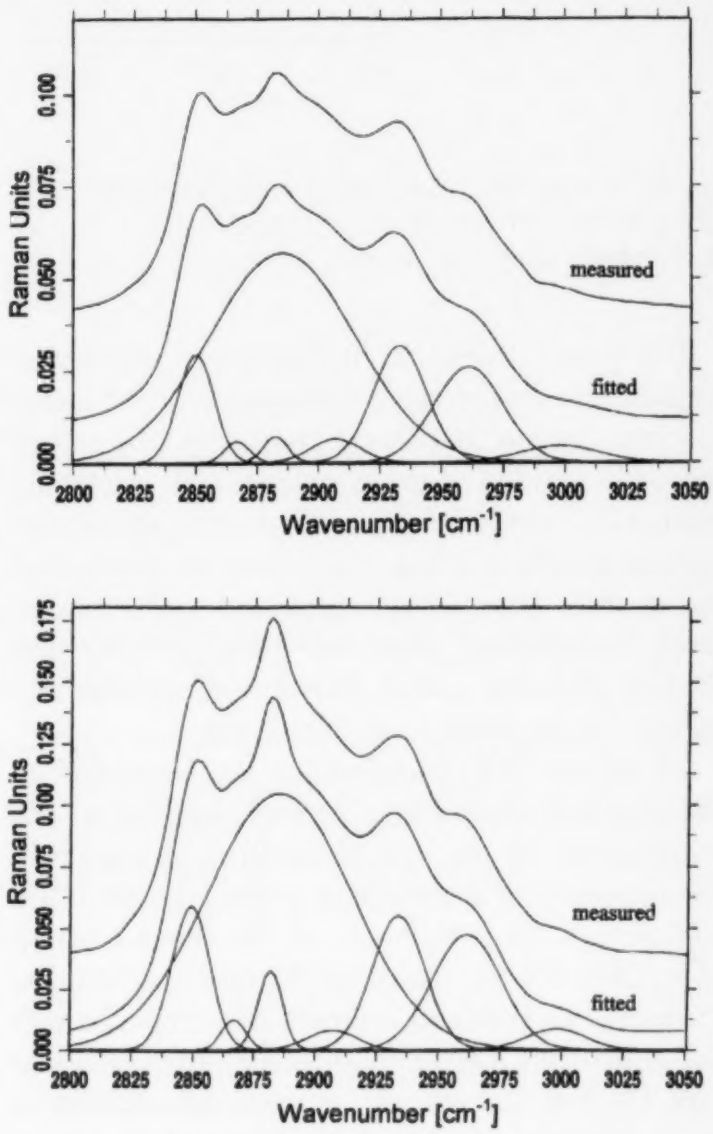

Fig. 9. Decomposition of the CH stretching band for 40 mol% ceramides type IV/60 mol% cholesterol mixture. Top: $T = 60°C$. Bottom: $T = 40°C$. The bands around 2850 and 2882 cm^{-1} are attributed to the symmetric and asymmetric stretching vibrations of the CH_2 goups, respectively.

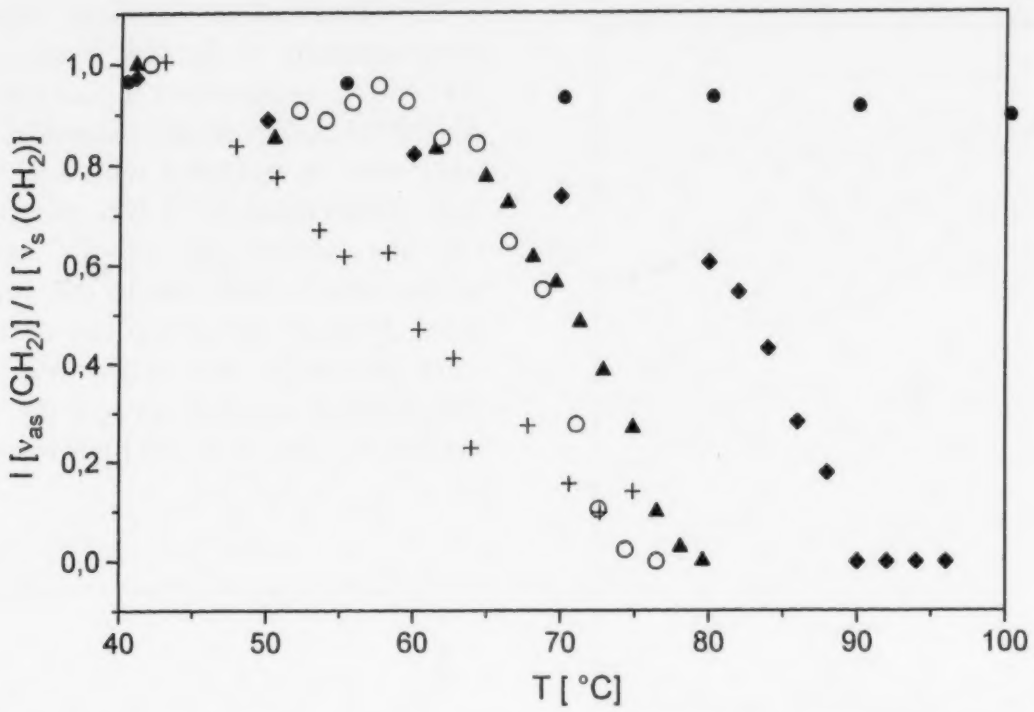

Fig. 10. Temperature dependence of the intensity ratio I [$\nu_{as}(CH_2)$]/I[$\nu_s(CH_2)$] of the ceramides type IV/cholesterol mixtures after storage at 40°C for 24 h: ●, 100 mol% cholesterol; ○, 75 mol% cholesterol; +, 60 mol% cholesterol; ▲, 25 mol% cholesterol; and ◆, 100 mol% ceramides type IV.

The phase transition temperature determined by using the temperature dependence of the intensity ratio $I[(\nu_{as}(CH_2))/I(\nu_s(CH_2))]$ (Fig. 10) and of the band position of the symmetric CH_2 stretching mode (Fig. 11) is nearly equivalent to the transition temperature of the DSC curve. In the case of the mixture 40 mol% ceramides/60 mol% cholesterol, a significant difference between DSC and Raman data was found. For elucidating this fact further investigations are in progress.

As in the DSC experiments, the hydration of the mixtures results in a further decrease of the temperature of the eutectic melting as shown in the temperature dependence of the intensity ratio $I[(\nu_{as}(CH_2))/I(\nu_s(CH_2)]$ and of the band position of $\nu_s(CH_2)$ for the hydrated (75 mol% ceramides/25 mol% cholesterol) mixture in comparison to the anhydrous mixture and to the pure ceramides type IV (Fig. 12). As can be seen, the addition of both cholesterol and water results in lowering of the temperature of the phase transition. The hydration of the mixtures of ceramides type IV and cholesterol shifts the eutectic melting to the lowest temperature of 55°C.

In conclusion, DSC and FT-Raman spectroscopy have been used to investigate the thermotropic and lyotropic phase behaviour of ceramides type IV and of mixtures of ceramides type IV and cholesterol. Solid ceramides type IV in the anhydrous and hydrated state exhibit a highly ordered conformation of the alkyl chains. The hydration of ceramides type IV induces a marked effect on the main transition, detected by both DSC and Raman scattering. On the other hand, the Raman spectrum of the hydrated ceramides type IV at room temperature exhibits no differences in comparison to that of the anhydrous sample, particularly alterations in the head group of ceramides (amid I at 1628 cm^{-1} and 1654 cm^{-1}) were not observed. Otherwise, the effect of water on the lipid can be clearly observed in the temperature dependence of the conformationally sensitive bands of the hydrocarbon chain.

The mixing of cholesterol and ceramides type IV also causes a decrease of the phase transition temperature. The DSC investigations show an eutectic melting of the cholesterol/ceramides type IV mixtures in the anhydrous and hydrated state, indicating immiscibility of the lipids. Using the

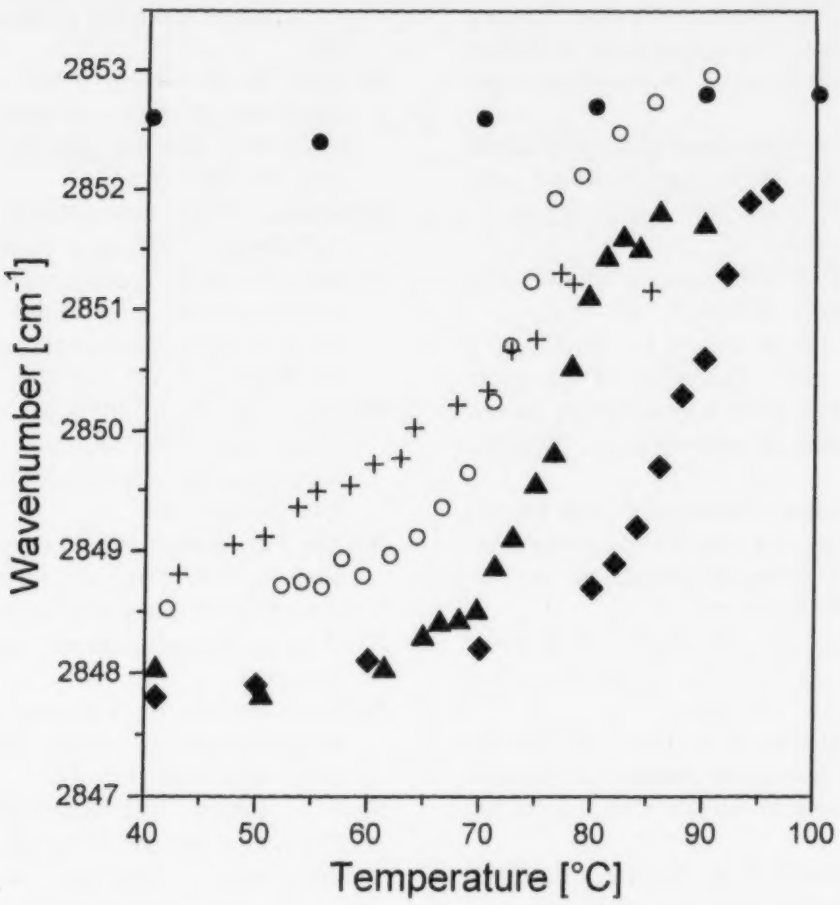

Fig. 11. Temperature dependence of the band position of the symmetric CH_2 stretching mode of the ceramides IV/cholesterol mixtures after storage at 40°C for 24 h: ●, 100 mol% cholesterol; ○, 75 mol% cholesterol; +, 60 mol% cholesterol; ▲, 25 mol% cholesterol; and ◆, 100 mol% ceramides type IV.

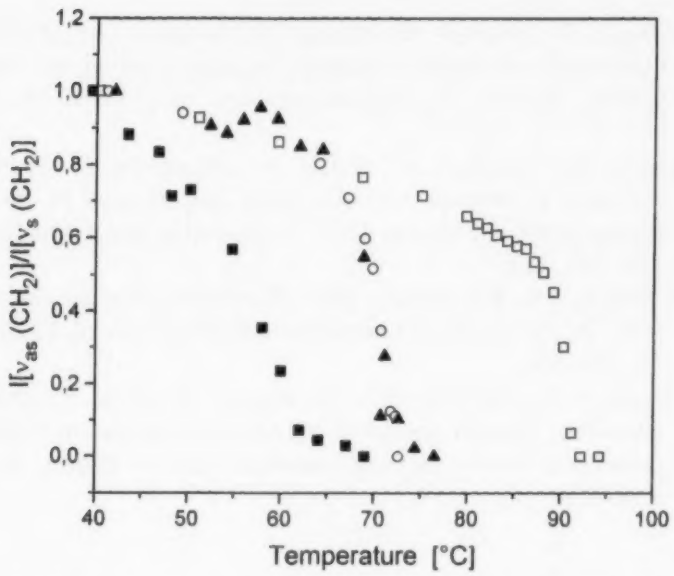

Fig. 12. Influence of cholesterol and water on the temperature dependence of the intensity ratio $I[\nu_{as}(CH_2)]/I[\nu_s(CH_2)]$: □, ceramides Type IV (dry); ○, ceramides type IV (hydrated); ▲, 75 mol% ceramides/25 mol% cholesterol (dry); ■, 75 mol% ceramides/25 mol% cholesterol (hydrated).

temperature dependence of the Raman band intensities and band positions of conformationally sensitive bands the melting process on the molecular level has been described and these investigations confirm to the DSC measurements.

Acknowledgements

This work was supported by the Deutsche Forschungsgemeinschaft (DFG), Sonderforschungsbereich 197, Project A8.

References

Anigbogu, A.N.C., Williams, A.C., Barry, B.W., Edwards, H.G.M., 1995. Fourier transform Raman spectroscopy of interactions between the penetration enhancer dimethyl sulfoxide and human stratum corneum. Int. J. Pharm. 125, 265–282.

Barry, B.W., Edwards, H.G.M., Williams, A.C., 1992. Fourier transform Raman and infrared vibrational study of human skin: Assignment of spectral bands. J. Raman Spectrosc. 23, 641–645.

Bulkin, B.J., Krishan, K., 1971. Vibrational spectra of liquid crystals. III. Raman spectra of crystal, cholestric, and isotropic cholesterol esters, 2800–3100 cm^{-1} region. J. Am. Chem. Soc. 93, 5998–6004.

Demel, R.A., de Kruyff, B., 1976. The function of sterols in membranes. Biochim. Biophys. Acta 457, 109–132.

de Kruyff, B., Demel, R.A., Slotboom, A.J., van Deenen, L.L.M., Rosenthal, A.F., 1973. The effect of the polar headgroup on the lipid–cholesterol interaction: A monolayer and differential scanning calorimetry study. Biochim. Biophys. Acta 307, 1–19.

Elias, P.M., 1990. The importance of epidermal lipids for the stratum corneum barrier. In: Osborne, D.W., Amann, A. H. (Eds.), Topical Drug Delivery Formulations, vol. 42. Marcel Dekker, New York, Basel, pp. 13–18.

Faiman, R., 1977. Raman spectroscopic studies of different forms of cholesterol and its derivates in the crystalline state. Chem. Phys. Lipids 18, 84–104.

Feingold, K.R., Man, M.Q., Menon, G.K., Cho, S.S., Brown, B.E., Elias, P.M., 1990. Cholesterol synthesis is required for cutaneous barrier function in mice. J. Clin. Invest. 86, 1738–1745.

Golden, G.M., Guzek, D.B., Harris, R.R., McKie, J.E., Potts, R.O., 1985. Lipid thermotropic transitions in human stratum corneum. J. Invest. Dermatol. 86, 255–259.

Han, C.-H., Sanftleben, R., Wiedmann, T.S., 1995. Phase properties of mixtures of ceramides. Lipids 30, 121–128.

Hemminger, W., 1994. Calorimetric methods. In: Mathot, V.B.F. (Ed.), Calorimetry and Thermal Analysis of Polymers. Hanser, Munich.

Holleran, W.M., Mao-Qiang, M., Gao, W.N., Menon, G.K., Elias, P.M., Feingold, K.R., 1991. Spingolipids are required for mammalian epidermal barrier function. J. Clin. Invest. 88, 1338–1345.

Hsu, L.-Y., Nordman, C.E., 1983. Phase transition and crystal structure of the 37°C form of cholesterol. Science 220, 604–606.

Jackson, M., Johnston, D.S., Chapman, D., 1988. Differential scanning calorimetric and Fourier transform infrared spectroscopic investigations of cerebroside polymorphism. Biochim. Biophys. Acta 944, 497–506.

Johnston, D.S., Chapman, D., 1988. A calorimetric study of the thermotropic behaviour of mixtures of brain cerebrosides with other brain lipids. Biochim. Biophys. Acta 939, 603–614.

Loomis, C.R., Shipley, G.G., Small, D.M., 1979. The phase properties of hydrated cholesterol. J. Lipid Res. 20, 525–535.

Maybrey, S., Sturtevant, J.M., 1976. Investigation of phase transitions of lipids and lipid mixtures by high sensitivity differential scanning calorimetry. Proc. Natl. Acad. Sci. USA 73, 3862–3866.

McMullen, T.P.W., Lewis, R.N.A.H., McElhaney, R.N., 1994. Comparative differential scanning calorimetric and FTIR and ^{31}P-NMR spectroscopic studies of the effects of cholesterol and androstenol on the thermotropic phase behavior and organization odf phosphatidylcholine bilayers. Biophys. J. 66, 741–752.

Menon, G.K., Feingold, K.R., Moser, A.H., Brown, B.E., Elias, P.M., 1985. De novo sterolgenesis in the skin. II. Regulation by cutaneous barrier requirements. J. Lipid Res. 26, 418–427.

Neubert, R., Rettig, W., Wartewig, S., Wegener, M., Wienhold, A., 1997. Structure of stratum corneum lipids characterized by FT-Raman spectroscopy and DSC. II Mixture of ceramides and saturated fatty acids. Chem. Phys. Lipids (accepted).

Ongpipattanakul, B., Francoeur, M.L., Potts, R.O., 1994. Polymorphism in stratum corneum lipids. Biochim. Biophys. Acta 1190, 115–122.

Shah, J., Atienza, J.M., Rawlings, A.V., Shipley, G.G., 1995. Physical properties of ceramides: effect of fatty acid hydroxylation. J. Lipid Res. 36, 1945–1955.

Small, D., 1986. Sterols and sterol esters. In: Handbook of Lipid Research, vol. 4. Plenum, New York, pp. 395–406.

Spier, H.L., van Senden, K.G., 1965. Phase transition of cholesterol. Steroids 6, 871–873.

Tanikawa, S., Miyajima, K., 1995. Calorimetric and infrared spectroscopic study of phase behavior of hydroxyceramides/cholesterol-3-sulfate system. Chem. Phys. Lipids 77, 121–130.

Wartewig, S., Neubert, R., Rettig, W., Wegener, M., 1997. Ceramides/ cholesterol mixtures as characterized by FT Raman spectroscopy. Mikrochim. Acta (Suppl.) 14, 263–264.

Wegener, M., Neubert, R., Rettig, W., Wartewig, S., 1996. Structure of stratum corneum lipids characterized by FT-Raman spectroscopy and DSC: I. ceramides. Int. J. Pharm. 128, 203–213.

Wiedmann, T.S., Salmon, A., 1991. Thermotropic phase properties of the hydroxyceramides/cholesterol system. Lipids 26, 364–368.

Williams, A.C., Edwards, H.G.M., Barry, B.W., 1992. Fourier transform Raman spectroscopy: A novel application for examining human stratum corneum. Int. J. Pharm. 81, R11–R14.

INFORMATION FOR AUTHORS

Submission of Manuscripts

The original and two copies, typed double-spaced with 4-cm margins, should be sent *(i) from Europe to:* Professor F. Paltauf, Institut für Biochemie und Lebensmittelchemie, Technische Universität Graz, Petersgasse 12, A 8010 Graz, Austria, and *(ii) from other parts of the world to*: Professor H.H.O. Schmid, The Hormel Institute, University of Minnesota, 801 16th Avenue N.E., Austin, MN 55912, USA.

A submission letter should always accompany the submitted paper providing the following information:

a) The full name and address of the corresponding author (including telephone and fax numbers, and e-mail addresses).

b) Any known changes of address within a period of six months after submission of the paper.

c) The full title of the submitted paper.

d) The names and addresses of at least three suitable potential reviewers. If there are compelling reasons for excluding some individuals as potential reviewers, these can be mentioned. However, choice of reviewers is at the editors' discretion.

Electronic Manuscripts

Electronic manuscripts have the advantage that there is no need for the rekeying of text, thereby avoiding the possibility of introducing errors and resulting in reliable and fast delivery of proofs.

For the initial submission of manuscripts for consideration, hardcopies are sufficient. After *final acceptance*, your disk plus two final and exactly matching printed versions should be submitted together. Double density (DD) or high density (HD) diskettes ($3^1/_2$ or $5^1/_4$ inch) are acceptable. It is important that the file saved is in the native format of the wordprocessor program used. Please do not save your text as ASCII or similar as this will cause all special formatting codes to be lost. Label the disk with the name of the computer and wordprocessing package used, your name, and the name of the file on the disk. Further information may be obtained from the Publisher.

Organization of Manuscripts

(a) *Title page*. The title should be concise, descriptive and informative. The names of the authors should be followed by their addresses and indicated by corresponding letters. Changes in address should be indicated by footnotes. The author(s) to whom correspondence and proofs should be sent should be indicated, giving a full address (including fax number and e-mail address). Authors are requested to select a maximum of six key words and to present them on the title page of the typescript. These key words will be used for indexing and abstracting. Indicate also if the paper is a "Review" or "Short Communication".

(b) *Abstract*. An abstract not exceeding 150 words should summarize the objectives, procedures, results and conclusions of the research. It should be typed on a separate page and will appear at the beginning of the article.

(c) *Presentation of material*. The text should be concise and organized in the conventional manner. An *Introduction* should state the purpose of the work in the context of current knowledge. *Experimental Procedures* should be brief but sufficiently detailed to allow for potential repetition of the work by others. *Results* may include tables and figures, and a *Discussion* should primarily deal with the interpretation of the results. When appropriate, especially in Short Communications, *Results* and *Discussion* sections may be combined.

(d) *Acknowledgements*. Financial support, technical assistance, and other help or advice should be acknowledged in a separate paragraph at the end of the text.

References

1. Quote references in the text by first author's name and year. For two authors quote both names; for three or more authors, quote first author's name, et al.

2. At the end of the article, list references alphabetically by first author; include all authors' names, followed by initials and include full titles of publications.

Examples of references: (a) to Journal articles: Hupfer, B., Ringsdorf, H., 1983. Spreading and polymerization behavior of diacetylene phospholipids at the gas-water interface. Chem. Phys. Lipids 33, 263–282. *(b) to books:* Dahlén, G., 1990. Clinical significance of Lp[a] lipoprotein. In: Berg, K., Rettersøl, N., Refsum, F. (Eds.), From Phenotype to Gene in Common Disorders. Munksgaard, Copenhagen, pp. 163–178. The names of the journals should be abbreviated according to the list of serial title word abbreviations (ISDS. Paris, 1985. ISBN 2-904938-02-8). Unpublished results should not be listed in the References section. In the text they are mentioned as follows "(Tervoort, M.V. , Glimcher, J., unpublished data)". When unpublished results are cited, the data should be provided for the Editors' information when essential for proper evaluation, or if requested. A personal communication should be mentioned in the text as follows: "(Tervoort, M.V. personal communication)". Authors should not make unauthorized use of personal communications. Personal communications are not to be included in the References section.

Tables and Figures

(a) Tables should be numbered separately in Arabic numerals (Table 1, 2, 3. . . .) and must have a title.

(b) Figures should be numbered in Arabic numerals (Fig. 1, 2, 3. . . .). Illustrations will not be redrawn by the Publisher and therefore they should be submitted as either original ink drawings, computer generated prints (laser printer), or sharp, high contrast, unmounted photographs on glossy paper with the lettering proportional to the size of the illustrations taking reduction in size into account. Each illustration should be clearly marked on the reverse side with the name of the author(s), the number of the illustration and its orientation (top); use a soft pencil or preferably a felt-tipped pen. Illustrations should be designed for use in either a single column (7.5 cm) or a double column (16 cm). Actual magnification of all photomicrographs should be indicated. Reproduction in colour will have to be approved by the Editors. The extra costs of colour reproduction will be charged to the author(s).

(c) The appropriate position of each table and figure should be indicated in the margin of the manuscript.

(d) Legends to figures should be typed, double spaced, beginning on a separate page.

Nomenclature and Abbreviations

Standard nomenclature should be used throughout; unfamiliar or new terms, arbitrary abbreviations, and trade names should be defined when first used. Unnecessary symbols and abbreviations should be avoided.

Proofreading

Since acceptance is based upon the submitted version of the paper, it is essential that no new material be inserted in the text at the time of proofreading; furthermore, no alteration to style or meaning will be permitted at this stage. Any new material that the authors wish to introduce for reasons of scientific accuracy will be checked by the Editors, and a charge may be made for corrections. Authors are encouraged to return their proofs by fax.

Reprints

Fifty reprints of each article will be supplied free of charge to the author(s). Additional reprints can be ordered at the prices shown on the reprint order accompanying proofs. Later orders cannot be filled since reprints are made at the time the journal is printed. There is no page charge.

CHEMISTRY AND PHYSICS OF LIPIDS

Vol. 88, No. 1 CONTENTS August 8th 1997

Cited/abstracted in: Current Awareness in Biological Sciences; Current Contents/Life Sciences; Chemical Abstracts; Excerpta Medica; Index Medicus

Published and Printed in Ireland
© The paper used in this publication meets the requirements of ANSI/NISO Z39.48-1992 (Permanence of Paper)
Library of Congress Catalog Number: 68-26533

0009-3084(19970808)88:1;1-W

08008